Characterization of Amorphous Solid Dispersions of AMG 517 in HPMC-AS

and Crystallization using Isothermal Microcalorimetry

By

Copyright 2011

Julie L. Calahan

Submitted to the graduate degree program in Pharmaceutical Chemistry and the Graduate Faculty of the University of Kansas in partial fulfillment of the requirements for the degree of Master of Science.

Chairperson	John F. Stobaugh
Committee Members	Fernando Alvarez-Nunez
	Eric J. Munson

Date Defended: April 4, 2011

The Thesis Committee for Julie L. Calahan

certifies that this is the approved version of the following thesis:

CHARACTERIZATION OF AMORPHOUS SOLID DISPERSIONS OF AMG 517 IN HPMC-AS AND CRYSTALLIZATION USING ISOTHERMAL MICROCALORIMETRY

_____

Chairperson John F. Stobaugh

Date approved: April 4, 2011

Acknowledgements

First, I want to acknowledge my Lord Jesus Christ and dedicate this paper to him. For giving me the ability and desire to pursue this degree program, for directing me in every decision, for being present with me at every step and for providing some great friends and scientists to help make this possible. An old proverb says "Plans fail for lack of counsel, but with many advisors they succeed." Well, I have had many advisors and am privileged to list and acknowledge them here:

1- Roger – As my original advisor, this project would not have existed without you, the feasibility studies and training on the TAM. Thank you for working with me to design and present the original project proposal. Even though you weren't able to officially continue as my thesis advisor, I am grateful for your continued support & encouragement and look forward to discussing the results with you.

2- Fernando – Thank you for being willing to step in as an advisor partway through my research project, for pointing me to some important resources on ASDs, for your direction and encouragement and for great advice on scientific writing and editing.

3- Dr Eric Munson – I feel fortunate to have been part of your group (even from a distance) and especially enjoyed visiting with you in Kansas and meeting your other students. Thank you for the important discussions at key points of the project, for the support from the academic side and for continuing with my project through your move to Kentucky.

4- Karthik – The scientific discussions on modulated DSC, solid state kinetics and SSNMR have been invaluable to my understanding of amorphous solid dispersions. Thank you for providing me with flexible time to work on the research and all that you have done to make this process easier.

5- Darren - Thank you for the important scientific discussions about thermodynamics and kinetics, and more importantly for your friendship, support and encouragement and for waiting with me during the defense.
6- Special thanks to Abe Germansderfer for help with the DOE design and to Lei Zhou for much needed help evaluating the crystallization data and interpreting the results.
7- Special thanks to Mike Kennedy for training on Buchi spray dry system, Gianni Toccara and Peter Quan for training on SEM, Jack Hu for training on GC, Dominick Daurio for help using JMP program and Tian Wu for an introduction to solid state kinetics.
8- Special thanks to Darren Reid and Stephanie Davis for proofreading the paper.
9- Thank you to Nancy Helm, Prof. Christian Schoenich, Prof. John Stobaugh, all the Pharm Chem staff at University of Kansas, as well as Dave Brems, Janan Jona and Drazen Ostovic for supporting the KU Distance Learning Masters program at Amgen.

Finally, thank you to my mom who taught me how to write, my dad who was a chemistry major, to Mike Jones for reminding me that I am more than my data and to all my family and friends for the many prayers and encouraging words to trust God and not give up when it was hard to continue. My love and thanks to you all. ☺

Table of Contents

Chapter 1. Introduction

The Importance of Amorphous Materials

Historically, pharmaceutical companies have focused on developing crystalline forms of drug molecules and much effort has gone toward discovering and developing the most stable crystalline form of a given drug molecule. Crystalline solids are those that demonstrate regular long-range packing order of the molecules, while amorphous solids are disordered at the molecular level, with some short-range packing order but lacking the long-range order of a crystalline form. (1, 2) Each crystalline form has specific physical properties that may affect manufacturing and/or dosing requirements, so it is of great importance to understand and control the crystallinity of the drug material during the development process. (3) Developing the most stable form will prevent changes in the formulation after manufacture and helps to ensure a reliable drug product.

The most stable crystalline form is the lowest energy state for a solid. In contrast, the amorphous state of a material represents the highest free energy form of that solid system, and the amorphous form of a material therefore has the highest crystallization potential. (4) With changes in condition, and over time, the amorphous or meta-stable material will always move toward the lowest energy state, which is the most stable crystalline form. (3) For this reason, understanding the relationship between the crystallization and amorphous states is of great interest to pharmaceutical science.

Amorphous vs. Crystalline Materials

Over the past several years there has been increasing interest in the development of amorphous materials, particularly on developing low solubility drugs as amorphous materials. Along with having higher energy, the amorphous state of a material will have higher solubility than its crystalline state. (5) The low solubility of many crystalline drug materials can affect not only the bioavailability of the drug, but also presents problems for manufacturing and development of the material. Insoluble drug materials are difficult to work with and the effect in vivo may be limited by dissolution as well. Developing the amorphous form of a drug has the potential to offer solubility and bioavailability advantages over the development of a crystalline form, provided the stability liability can be overcome. (5, 6)

BCS Classification

The Biopharmaceutics Classification System is used by the FDA (7, 8) to classify drugs into categories according to solubility and permeability, to predict whether bioavailability will be a potential issue for drug delivery. As shown in Figure 1, drug molecules are assigned a box based on having high or low solubility and high or low permeability or low metabolism. (7) Low solubility drugs with high permeability are often considered to have "solubility-limited" bioavailability and formulation strategies are often used to increase the apparent solubility of such drugs. The pie chart in Figure 2 (9) illustrates the relative percentages of different types of drugs being developed recently. The large percentage of Class II drugs with solubility-limited bioavailability underscores the importance of developing new manufacturing strategies to increase the apparent solubility of potential drug molecules. Class II drugs, with low solubility

but high permeability, are the most likely BCS class of drugs to benefit from solubility enhancement through development of the amorphous form. (10)

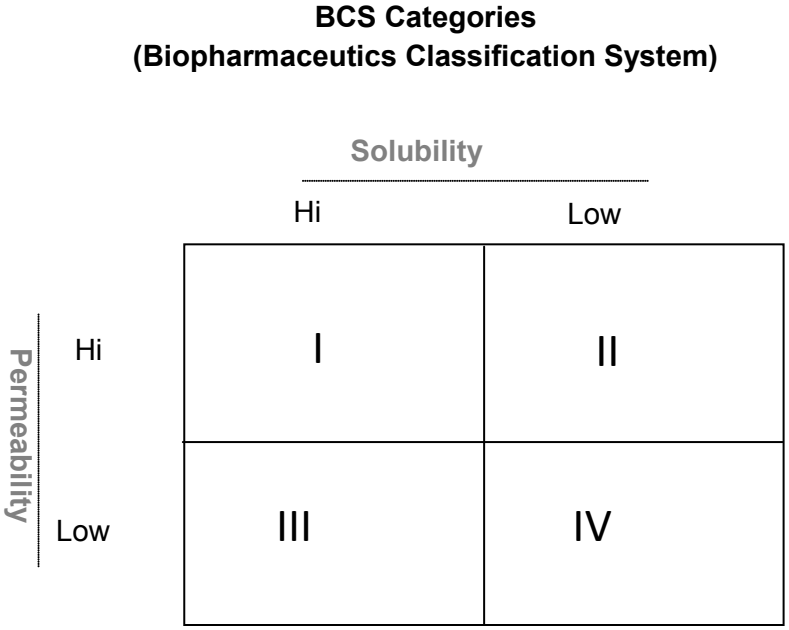

Figure 1. BCS Classification System. (8, 9)

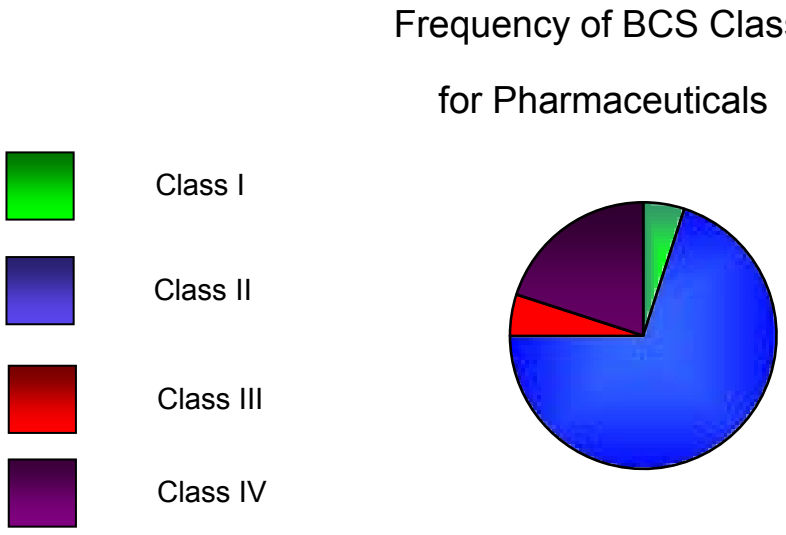

Figure 2. The frequency of pharmaceutical drugs found in each class of the different classes of BCS chart. (10)

Amorphous Solid Dispersions

Introduction to Amorphous Solid Dispersions

One of the techniques being developed for development of drugs in the amorphous state is amorphous solid dispersion technology. (11-15) Amorphous Solid Dispersions (ASDs) have been shown to help stabilize amorphous materials and enhance dissolution and bioavailability of drugs with low solubility. The first to report enhanced stability using solid dispersions were Chiou & Riegelmann. (11, 16) Solid dispersions are used to improve the solubility of the drug, increase bioavailability and stabilize the amorphous form of the drug. (17)

Definition of ASDs

There are several definitions of amorphous solid dispersion found in the literature (15-18), each describing the solid dispersion in a manner specific to the application being studied. Chiou defines ASD as a mixture of amorphous API with an amorphous polymer. (11, 19) For this present discussion, a general definition is used: Amorphous solid dispersion (ASD) is defined as a molecular level dispersion of a hydrophobic drug, such as AMG 517, within an amorphous matrix material, such as HPMC-AS polymer.

Recent examples and uses of ASDs

In 1983, Hiroyuki Imaizumi made solid dispersions of indomethacin in PVPP from acetone solution and found that indomethacin was stabilized against heat and moisture. (20) In

2001, Ping Tong et al. made ASDs of indomethacin and its Na salt by mixing and by co-precipitation. They observed phase separation of the physical mixture, but only one Tg for the co-precipitated ASD. (21) There was inhibition of crystallization in the dispersion, which they believe is due to interaction between the acid and the salt. A more recent example of a solid dispersion is from Jingjun Huang et al. where dispersions of nifedipine in various polymer blends were prepared. They found an increase in Tg from 50°C for amorphous nifedipine to 115°C for the ASD, as well as enhanced physical stability. H-bonding was observed between nifedipine and polymer, leading to the conclusion that stability is not only due to increased Tg, but is also a result of chemical interactions between drug and polymer. (22)

Other recent literature on the subject includes details on preparation methods for amorphous solid dispersions, (23-25) characterization of solid dispersions, (26), (27) using solid dispersions to increase dissolution and enhance bioavailability, (15, 17, 28) excipient selection for solid dispersions (29, 30), crystallization observations (31-34), understanding how drug-polymer solubility and miscibility affects stability, (14, 19, 35-37) and prediction of crystallization kinetics. (19, 38, 39) The recent explosion of literature dealing with all aspects of amorphous solid dispersions shows that this technology has potential for great benefit to the drug development process, and that there is still much to be learned about amorphous solid dispersions.

ASD Preparation by Spray Drying

A primary goal of preparing ASDs is to prepare the drug in such a way that it is completely miscible with the polymer. (40, 41) There are several techniques available for ASD

preparation, (23, 42) including hot melt extrusion (43-45), melt quenching (46), melt granulation (47), solvent evaporation (12) and spray drying (27, 48-52). Figure 3 illustrates the process of spray drying ASDs out of solution. The "molecularly dispersed solution" contains solvent, polymer and drug dissolved together in solution. The solution is sprayed through a nozzle and rapidly dried. If the drying temperature is below both the crystallization temperature and separation temperature, then the solid particles collected are mixed at the molecular level and an amorphous solid dispersion results. If the drying temperature is above the separation temperature, then the drug molecules will phase separate and/or crystallize out of the polymer carrier.

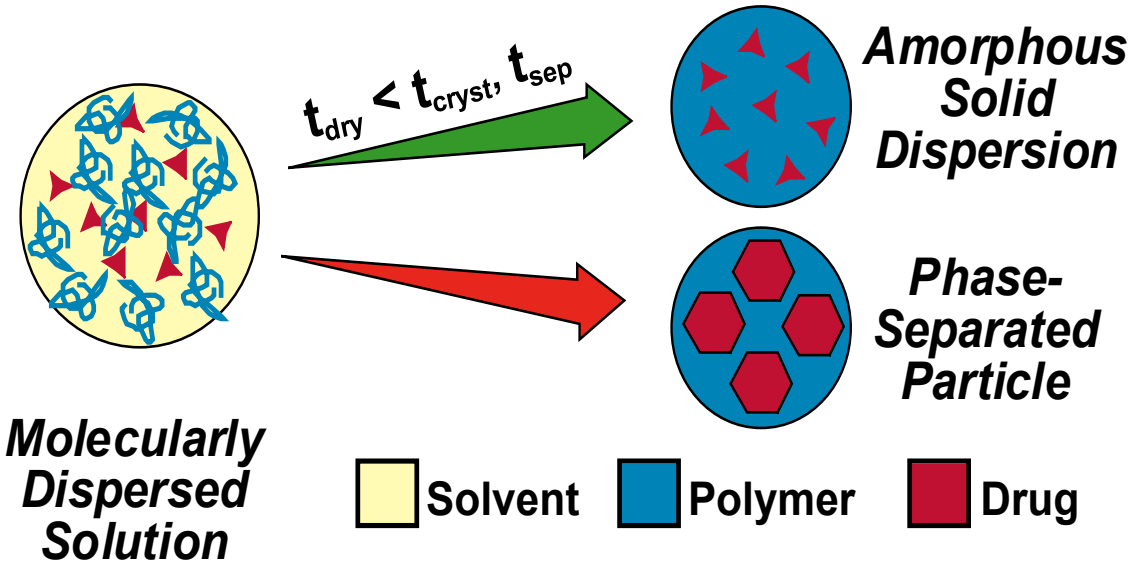

Figure 3. Spray drying of ASDs (53)

Miscibility & Phase Separation

Phase separation can happen before or simultaneous with crystallization. The degree of phase separation varies based on factors such as preparation technique, % drug v polymer and

drying (annealing) time. Figure 4 illustrates the phase separation which can result when an ASD goes through the process of crystallizing the amorphous drug out of the dispersion. (54)

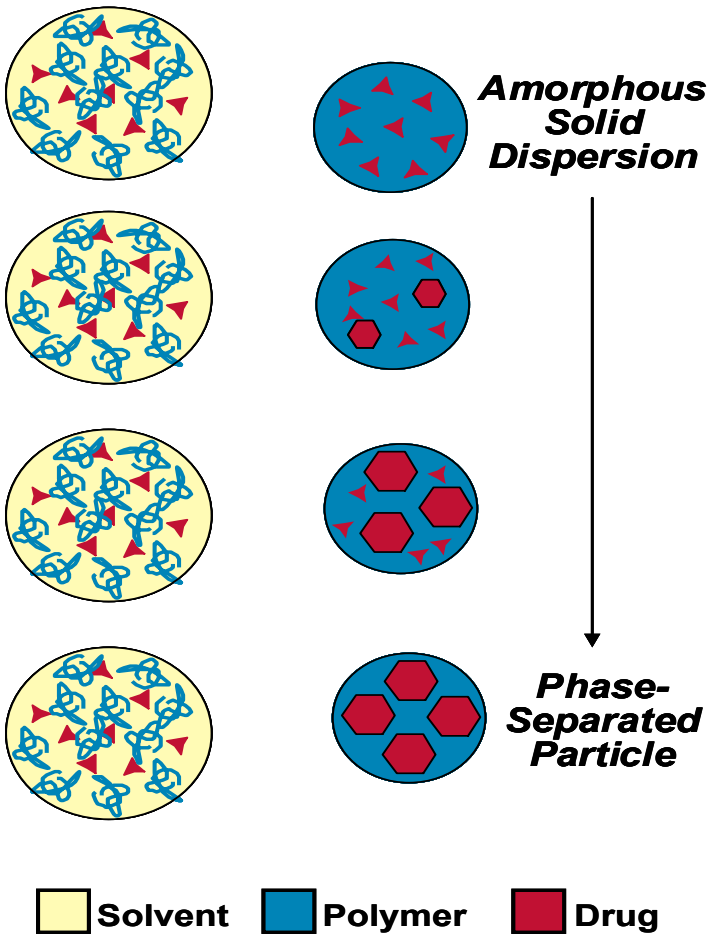

Figure 4. Illustration of ASD phase separation process

The left side of Figure 4 illustrates the situation with drug and polymer dissolved in a solvent. Although it is not the focus of this project, it has also been observed that polymers can enhance stability in the solution state. (55) The right side illustrates the composition of the spray dried ASD. An ideal ASD is a uniform dispersion of drug molecules in polymer. Moving from

top to bottom, the circles represent drug molecules in coming together to form larger particles which are phase separated from the polymer. The particles of an ASD may undergo phase separation prior to crystallization. The phase separated particle is more likely to crystallize since it has become less kinetically stable. A drug in a solid dispersion may exist in an amorphous state due to the carrier (the polymer) acting to inhibit crystallization. (56)

In contrast to a physical mixture, the drug and polymer phases in an amorphous solid dispersion are indistinguishable. Individual drug molecules are interspersed between chains of polymer, allowing for interaction between drug and polymer. The latter case, with drug and polymer phases indistinguishable, has been demonstrated to provide kinetic stability to a drug-polymer system. In this situation, the drug and polymer are distinct phases and there will be little, if any, interaction between drug and polymer. In order to provide the most stability to the dispersion, the polymer must mix homogeneously with the drug. (2)

Miscibility of ASDs is analogous to aqueous solubility. Aqueous solubility studies suggest increased solubility in aqueous systems can be a result of binding interactions between the polymer and drug, (55) with drug molecules bound to polymer. Polymers have been found to increase the solubility of aqueous drug solutions due to molecular interactions such as electrostatic bonding (ionic and dipole interactions). Polymer-drug binding affects the physicochemical properties of the dispersion and the choice of appropriate polymer used to make ASDs can have a significant effect on physical stability. For some systems, when polymer concentration increases, polymer-polymer bonds decrease their ability to form drug complexes. Polymer molecules tend to form electrostatic bonds with themselves, limiting their ability to

form complexes. (55) Dispersions prepared below the solid solubility limit are more physically stable. (54)

Glass Transition & mDSC

The glass transition is the primary thermal event associated with amorphous material as it undergoes transition from solid to a rubbery liquid phase. The glass transition temperature (T_g) is the temperature at which an amorphous "glass" turns into a metastable "supercooled liquid" and is commonly measured using modulated DSC technique. (57) Molecular level mixing of ASDs is indicated by miscibility, as observed by spectroscopy and a single T_g in DSC. (58) In a phase mixed system, dispersed at the molecular level, only one amorphous phase (only one T_g) is observed using mDSC. More than one T_g indicates more than one amorphous phase. (58, 59) A polymer blend may be considered miscible when only one T_g is observed. If the components are immiscible, a separate T_g is observed for each component. (59) In this way, the presence of a single T_g is an indication of miscibility between drug and polymer.

The glass transition is a kinetic event influenced by molecular weight (MW), additives and thermal history including preparation technique, cooling rate and degree of cure (2, 59) and is usually approximately 2/3 to 4/5 of the melting point, T_m (using Kelvin units). (2) If the ASD is phase separated, it will show a separate T_g corresponding to each components being mixed. A phase separated system with particle domains < 15-30 nm will also result in a single T_g being observed, since the domains are so small as to be virtually indistinguishable from individual molecules. (58, 60)

Phase Diagram

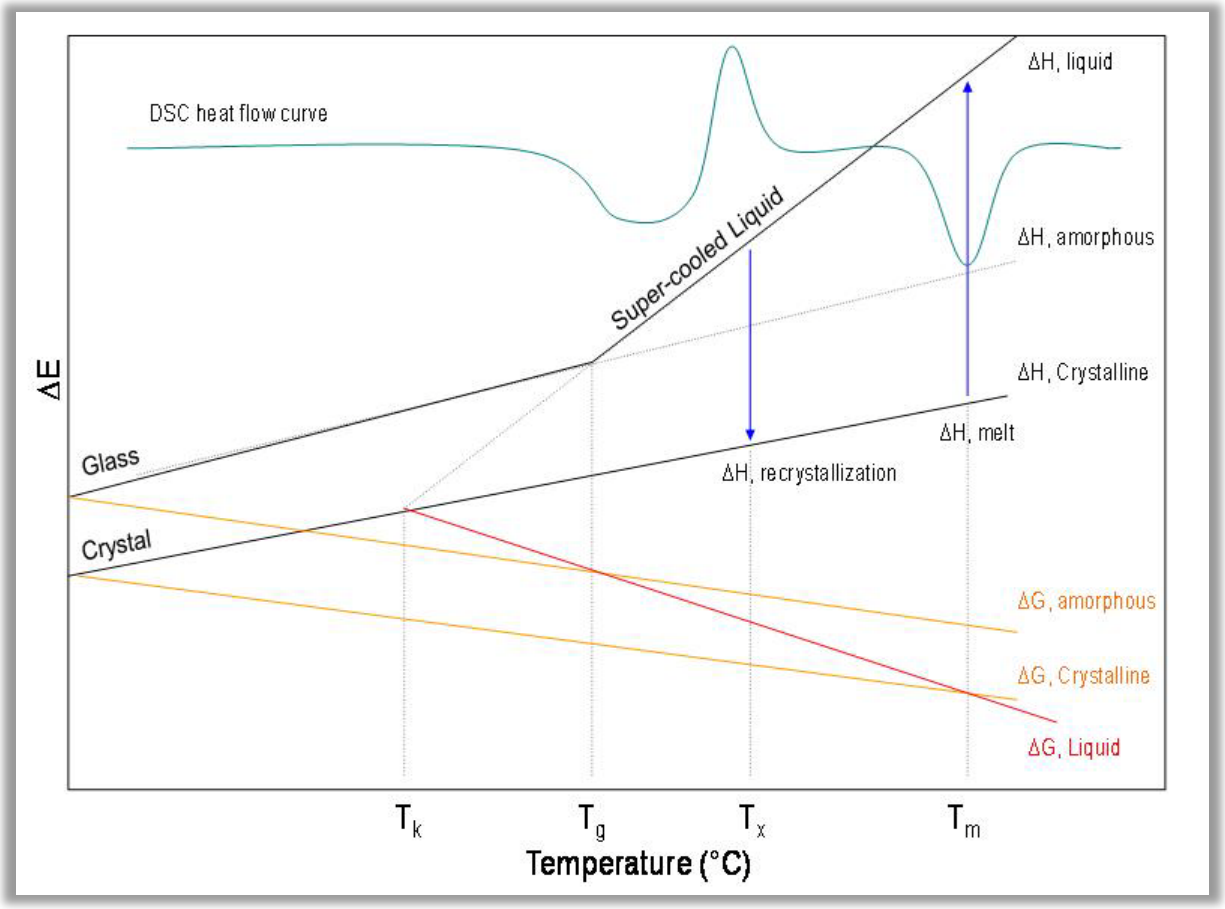

Figure 5. Phase diagram

An energy diagram for amorphous and crystalline states is shown in Figure 6 and can be used to illustrate glass transition in relation to other thermal parameters. (5) Starting from a point on the "glass" (or amorphous) line and increasing temperature, the material increases in Volume/ Enthalpy/ Entropy until the T_g is reached. At the T_g, the slope of the line changes in the super-cooled liquid zone as the amorphous glass becomes more mobile and reaches the liquid phase as

it melts, at T_m. As energy is decreased at T_m, the stable crystal state is reached. If the amorphous glass material is subjected to annealing conditions, a vertical line can be drawn at the annealing temperature indicating the energy change associated with structural relaxation. As temperature is increased, this relaxation energy is recovered when the temperature reaches T_g. Understanding the energy diagram is important when considering the storage temperature for ASDs. Moving left along the curve away from the T_g, the material (such as an ASD) becomes more stable.

Storage Temperature

"The difference between storage temperature and T_g is critical for stability of amorphous materials." (61) High reduced temperature (the difference between T_g and storage temperature) is beneficial for stabilizing ASD above 120 ºC. (37) Differences in crystallization rate are not explained exclusively by reduced temperature. (62) Glassy solids have molecular mobility up to at least 50ºC below T_g. For this reason, amorphous solid dispersions are recommended to be stored below T_g-50ºC. (63) The T_g-50 Rule is dependent on the fragility of the system and relaxation behavior. (2) Relaxation of an ASD can also be observed using mDSC, aging, annealing or conditions. Relaxation enthalpy decreases with higher annealing or storage temperature. (64)

Gordon – Taylor Equation

Several equations have been developed to predict the T_g of solid mixtures, the Gordon-Taylor equation being the most well known. The Gordon-Taylor equation is used to predict T_g for amorphous mixtures and for miscible blends of drug and polymer. Water is known to cause a decrease in the T_g of amorphous materials. The Gordon-Taylor equation (1952) can be used to predict the T_g of amorphous drug in the presence of water. (65) The Gordon-Taylor equation assumes perfect volume additivity with no specific interactions between the components. (66)

$$T_{g_{mix}} = \frac{(w_1 T_{g1}) + (K w_2 T_{g2})}{w_1 + (K w_2)}$$ Gordon-Taylor, 1952 Equation 1

The Gordon-Taylor equation was designed to elucidate the effect of water content on T_g and can be extended to tertiary form for ASDs with 3 components and a tertiary form of the G-T equation used with a third component such as water or solvent. (32) Combined with the Simha Boyer rule, the extended version of the Gordon - Taylor equation for a ternary system with solvent or water-containing dispersions is:

$$T_g = \frac{w_1 T_{g1} + K_2 w_2 T_{g2} + K_3 w_3 T_{g3}}{w_1 + K_2 w_2 + K_3 w_3}$$ Equation 2

with $K_2 = Q_1 Tg_1 / Q_2 Tg_2$ Equation 3

and $K_3 = Q_1 Tg_1 / Q_3 Tg_3$ Equation 4

where Q is density, where w_1 is the lowest T_g material and w_3 is the higher T_g material. (23, 61) Other T_g models can be compared with the traditional Gordon-Taylor model, such as the Couchman-Karazc equation: (23, 67, 68)

$$T_g = \frac{w_1 dC_{p1} \ln T_{g1} + w_2 dC_{p2} \ln T_{g2}}{w_1 dC_{p1} + w_2 dC_{p2}}$$ Equation 5

All of these T_g prediction models assume no interaction between components of the mixture (Truong, 31) "For complete miscibility, interactions between the two components are necessary. A miscible system can phase separate and become unstable if specific interactions between the components are adversely affected by a 3rd component like water." (54) Deviation from Gordon-Taylor and other T_g prediction models indicates some type of interaction in the system. Studies of drug-excipient interactions in dispersions can be evaluated using thermodynamic phase diagrams such as a graph of temperature versus % drug. (69-71) Another study has reported mixed phase T_g analysis (23) with TGA being used to determine % water, drug content measured by HPLC and the polymer fraction is determined from the difference (100-H_2O-drug). (23)

Examples of both positive and negative deviation from Gordon-Taylor ideality have been reported. One list of polymer T_g values (69) shows, among other things, that T_g was depressed more with higher % PVP. (62, 72) Depression of the T_g with respect to Gordon-Taylor predictions has also been observed for itraconazole-HPMC melt extrusions. (25) Negative deviation from Gordon-Taylor prediction indicates that the level of drug-polymer interaction is

less than the drug-drug or polymer-polymer interactions. (73) A study with BMS488043 is an example of a higher T_g being observed for ASD compared with drug alone and indicates strong interactions between drug and polymer. (61)

The intermolecular interactions and self-associations determine the extent of deviation from Gordon-Taylor ideality and it has been suggested that miscibility is mainly the result of the balance between adhesion and cohesion forces. (23, 66) Self-association among any of the components results in higher free volume than expected from ideal mixing, leading to higher molecular mobility, and lower T_g values. On the other hand, interaction between components results in lower free volume and higher T_g values. (66, 70)

Possible explanations for negative T_g deviation are: 1) Undetected phase separation, although this is unlikely if a single Tg is observed, 2) ASDs produced using slower cooling rates have lower T_g than quickly cooled ASDs, configurational entropy being stored in the glass after cooling or 3) if molecular forces between drug and polymer are weaker than self-associating interactive drug-drug or polymer-polymer forces. (23) It is well known that T_g is depressed and broadened in the presence of moisture, increasing molecular mobility and decreasing the activation energy for crystallization. (62) In order for negative deviation, or T_g depression, to happen, the free volume in the homogeneous mixture must be larger than for the phase mixed material. (25)

An explanation of broad T_g regions is related to drug-polymer mixing, aided by water evaporation. Water may block drug-polymer H-bonding if it is sorbed onto the polymer. (25) Water is a plasticizer for many amorphous materials. (74) Stability against crystallization is

consistent with degree of supersaturation and it can be said that increased RH decreases T_g. Following adsorption of water, T_g is reduced and systems are described as plasticized. Increased water sorption leads to reduced T_g, relative to dry material. (62)

In summary, the presence of a single Tg is a commonly used and important, though not an infallible, indicator of miscibility, since it provides an indication of phase mixing and miscibility, but no information about the thermodynamics of mixing. (75) Deviation from ideal G-T behavior can be due to: 1) water competing with drug for interaction with polymer, 2) interaction between drug and polymer causing increased free volume of the homogeneous phase, or 3) formation of a polymer-rich phase. (25)

Crystallization Kinetics

Traditional Solid State Stability

It is necessary to identify stable conditions of a drug in development. Traditional solid state experiments are carried out at accelerated stability conditions using elevated temperatures and/or high humidity conditions. Stability results are typically reported as < or > over a specified time during which the sample is held at the specified condition. The common reporting non-specific stability results is due to difficulty in obtaining more specific crystallization rate data on solids, and because crystallization rate models are sometimes difficult to fit. However, crystallization rate models do exist, and isothermal microcalorimetry can provide continuous crystallization data for accelerated conditions which can be compared with the various models, then extrapolated back to determine room temperature stability for the materials.

Both thermodynamic and kinetic factors are involved in stabilization of solid dispersions. (37) Miscibility between a drug and polymer reduces the chemical potential of the drug, which reduces the thermodynamic driving force for crystallization. (62) A completely miscible system will produce the most thermodynamically stable situation for an ASD. The phase separation process will usually happen before nucleation and crystal growth occur for an ASD but may also occur simultaneously. The extent of phase mixing and phase separation for an ASD impacts the ability of the ASD to stabilize the amorphous drug against crystallization. (60) Understanding the crystallization rate of miscible and partially miscible ASDs is critical for the development of amorphous drugs as solid dispersions.

Nucleation and Crystal Growth

Crystallization, the "process by which a super-cooled liquid (glass) undergoes a first order phase transition to form the thermodynamically more stable crystallization phase," involves nucleation and growth. (19) "The nucleation-growth model recognizes two distinct steps in crystallization that have different temperature dependence: the lower temperature favors nucleation and the higher temperature favors growth." Crystallization involves nucleation and crystal growth and is governed by the diffusion rate of molecules. (72)

Nucleation rate is governed by the activation energy, E_a, required to develop stable nuclei and molecule diffusion. (76) The nucleation-growth model says that nucleation is preferred by low temperature, where growth is preferred by high temperatures and rapid cooling can prevent nucleation. (2) Slow cooling allows more time for nucleation to occur, whereas fast cooling can

prevent full nucleation, stabilizing the amorphous state of the dispersion. Excess energy "along with surface tension gives the work necessary to form a nucleus of critical size." (2) From a simulation of crystal nucleation in suspensions of colloid spheres with varying PS distribution, it was determined that the probability of critical nuclei forming goes through a maximum as super-saturation increases. (77)

Kinetic Models

The rate of crystallization can be determined using equations derived from crystallization theory, such as the Johnson-Mehl-Avrami (or JMA) equation. Kinetic models include those developed by Avrami (1939, 1940, 1941), Sheridan/Anwar (1996), Supaphol/Spruiell (2001), Wellen/Rabello (2005), Yang (2005), Khawam/Flanagan (2006), Ziaee/Supaphol (2006) and Prout/Tompkins (1944). (16) The general kinetic equation for crystallization is

$$d\alpha/dt = k(T)f(\alpha) \qquad \text{Equation 6}$$

where $d\alpha/dt$ is the fraction crystallized, $k(T)$ is a rate constant function and $f(\alpha)$ is the reaction model equation. (32) Johnson-Mehl-Avrami (JMA) theory is the most commonly used for the determination of crystallization rate constants of amorphous materials, (78) with the following equation being used to determine isothermal induction time and rate constants.

$$\alpha = 1-\exp[-Kt^m], \qquad \text{Equation 7}$$

where α is the fraction crystallized, K is crystallization rate, t is time of crystallization and m is the reaction order which depends on the nucleation mechanism (m=2 for rods, m=3 for plates). (78) Differentiation of the above equation gives (79)

$$d\alpha/dt = Km(1-\alpha)[-\ln(1-\alpha)]^{1-1/m} \qquad \text{Equation 8}$$

For the JMA equation to be valid, the growth rate of the new phase must be 1) controlled by temperature, 2) independent of time and 3) have low anisotropy of crystals. (79) The Avrami equation is based on a couple assumptions: 1) that the nucleation rate is constant with respect to time and 2) that crystallization grows linearly with respect to crystallization time. These assumptions lead to an over-prediction of crystallization rate because the nucleation rate decreases when the nucleation sites are used up. (16) However, the JMA equation is valid in isothermal conditions for nucleation at randomly dispersed second phase particles, such as would be found in a molecularly dispersed ASD. The growth rate of the new phase should be controlled by temperature and independent of time. (79)

After calculating the rate constant K using the JMA equation for each crystallization condition, the Arrhenius equation (below) can be applied to the crystallization data:

$$\ln k = \ln A - E_a/RT \qquad \text{Equation 9}$$

where k is the crystallization rate, A is a constant, E_a is the activation energy, R is the gas constant and T is temperature. A plot of ln k v 1/T (in Kelvin units) has slope of E_a/R, giving

activation energy E_a for the material. (80) The Arrhenius equation can also be extrapolated to predict the rate constant at extended temperature.

The kinetic crystallization equation may not strictly follow Arrhenius behavior because activation energies (E_a) of nucleation and growth can have different temperature dependencies. Therefore the overall rate won't usually follow Arrhenius behavior. (32). The different apparent E_a from isothermal and non-isothermal experiments can tell something about the underlying mechanisms of crystallization (78) and at least one study has been reported where nucleation and crystal growth were studied separately to establish the crystallization mechanism." (32)

The Role of Water

Residual water can have an effect on physical and chemical properties of drugs in the solid state. (81) There is a competing effect between the polymer increasing hygroscopicity and the thermodynamic effect of combining drug with polymer. (62) "Water acts as a plasticizer to produce significant increase in molecular mobility" (81) which lowers the T_g and increases the crystallization rate. However, water sorbed to the amorphous glass can also inhibit the rearrangement needed for crystallization, inhibiting crystallization. (32) Water sorbed between drug and excipient can facilitate interactions to catalyze degradation or stabilize the amorphous state. (81-83) Water sorption may also increase defects and disrupt the crystallization process. (32)

The effect of water on solid state properties depends on regions of higher energy, higher molecular disorder and higher mobility. Water brought in by the excipient can also distribute

into the vapor phase. This becomes important if the excipient water escapes into the headspace. Sorbed water between the drug and excipient can facilitate interaction. If the drug molecules move into the structure of the plasticized polymer, this could help stabilize the amorphous phase. High RH conditions would affect this interaction. (81) Plasticizing effects of residual solvent, absorbed water and additives can be significant to the stability of amorphous materials and are difficult to quantify or control. (63) High temperature and high RH are expected to accelerate any drug-excipient interactions, so it is important to monitor T_g at elevated conditions. (81) Overall, we conclude that there may be many different contributing factors for the enhanced physical stability provided to amorphous materials by making amorphous solid dispersions.

Overview of Thesis Work

Kennedy presents a case study of the AMG 517-HPMC-AS amorphous solid dispersion system which sets the background for the present work. (84)

AMG 517

AMG 517 is a BCS Class II drug molecule with low bioavailability with solubility-limited absorption. The structure of AMG 517 is shown below. (85) The molecule is no longer in development at Amgen, Inc. The solubility is ~ 0.05 μg/ml and calculated logP = 5.1 for this lipophilic molecule. The freebase has a pK_a ~1.8 on the basic nitrogen, and it readily forms salts, hydrates, solvates and multiple crystalline forms. The melting point of the crystalline freebase is

229°C, and an amorphous glass transition (T_g) is found around 110°C. The CF_3 group attached to the benzyl ring on the end is useful in SS-NMR studies. The combined properties of AMG 517 have made it an attractive molecule for investigation of amorphous solid dispersion technology. (84)

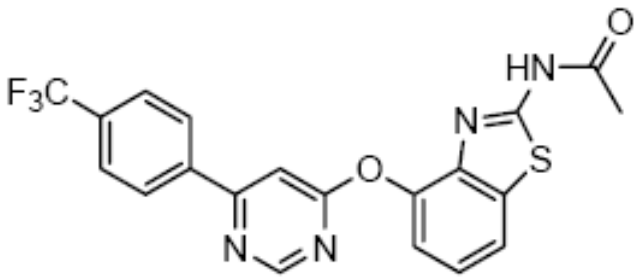

$C_{20}H_{13}F_3N_4O_2S$
Mol. Wt.: 430.40

Figure 6. Chemical structure of AMG 517.

ASDs of AMG 517 with HPMC-AS and HPMC were prepared by spray drying and physical stability and in vivo exposure were evaluated. SEM showed solid, collapsed, corrugated particles. Particle size was 29-40µm. Dissolution was improved for spray dried amorphous AMG 517 compared with crystallized AMG 517 and pharmcokinetic studies with the solid dispersion gave 163% AUC compared to the control suspension formulation. (84)

HPMC-AS

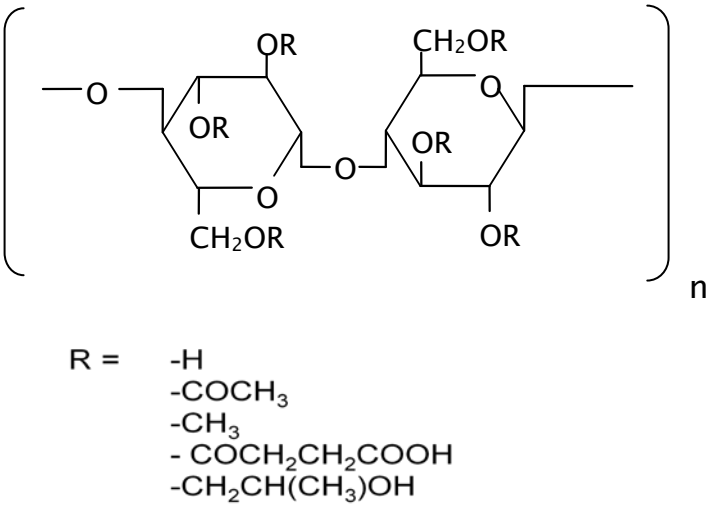

Figure 7. Chemical structure of HPMC-AS (Shin-Etsu)

HPMC-AS (Hydroxypropyl methylcellulose acetate succinate) is a water-soluble polymer with weight-average MW between 17,000 and 20,000 (86) and T_g approximately 117°C. (87) HPMC-AS has been found to be an effective polymer for use with amorphous solid dispersions of low solubility drugs in studies with several drugs including griseofulvin, nifedipine and AMG 517. (84, 88) The effect of PVP v HPMC-AS on kinetics of solid dispersions with felodipine was also studied and the physical stability of ASDs was found to be highly dependent on the choice of polymer used, and HPMC-AS was specifically found to be better than PVP. (19)

HPMC-AS absorbs moisture from the atmosphere, the amount absorbed being dependent on the initial moisture content, the temperature and humidity, (25) so controlling crystallization humidity conditions is expected to be important. Additionally, increasing HPMC-AS content

increased the induction time for solid dispersion with naproxen, (76) so it should be expected that higher drug load ASDs will crystallize faster.

Project Overview

This project focuses on examining the solid state properties of AMG 517, a BCS Class II drug, manufactured by spray drying as amorphous solid dispersions with HPMC-AS polymer, and stability using isothermal microcalorimetry and solid state NMR.

Chapter 2 describes several techniques used to evaluate ASDs and what information each technique or method provides. The techniques include X-ray powder diffraction (XRPD), HPLC, gas chromatography (GC), thermal gravimetric analysis (TGA), modulated differential scanning calorimetry (mDSC), scanning electron microscopy (SEM), particle size distribution analysis (PS), vapor sorption (DVS), isothermal microcalorimetry (TAM), and solid state nuclear magnetic resonance spectroscopy (SSNMR).

Chapter 3 presents the initial ASD characterization data. Focus is on the importance of phase mixing, residual solvent drying and glass transition.

In Chapter 4, a series of ASDs is crystallized using TAM isothermal microcalorimetry, with crystallinity evaluation using 19F SSNMR and rate constant determination using the JMA/Avrami model. Stability predictions are made by applying statistical analysis to the crystallization data using JMP design software and compared with traditional solid state stability results.

References

1. Shalaev E, Zografi, George. The Concept of 'Structure' in Amorphous Solids from the Perspective of the Pharmaceutical Sciences. In: Levine H, editor. Amorphous Food and Pharmaceutical Systems. Cambridge UK: The Royal Society of Chemistry; 2002. p. 11-30.
2. Yu L. Amorphous pharmaceutical solids: preparation, characterization and stabilization. Advanced Drug Delivery Reviews2001;48(1):27-42.
3. Byrn SR, Ralph R. Pfeiffer, Joseph G. Stowell. Solid-State Chemistry of Drugs. 2nd Edition ed. West Lafayette, Indiana: SSCI, Inc.; 1999.
4. Fukuoka E, Makita M, Nakamura Y. Glassy state of pharmaceuticals. V. Relaxation during cooling and heating of glass by differential scanning calorimetry. Chem Pharm Bull1991;39(8):2087-90.
5. Hancock BC, George Zografi. Characteristics and Significance of the Amorphous State in Pharmaceutical Systems. Journal of Pharmaceutical Sciences1997 August 1, 1996;86(1):1-12.
6. Murdande SB, Pikal MJ, Shanker RM, Bogner RH. Solubility advantage of amorphous pharmaceuticals: I. A thermodynamic analysis. Journal of Pharmaceutical Sciences2009;99(3):1254-64.
7. Wu C-Y, Benet LZ. Predicting Drug Disposition via Application of BCS: Transport/Absorption/ Elimination Interplay and Development of a Biopharmaceutics Drug Disposition Classification System. Pharmaceutical Research2005;22(1):11-23.
8. Amidon GL, Lennernas H, Shah VP, Crison JR. A theoretical basis for a biopharmaceutic drug classification: the correlation of in vitro drug product dissolution and in vivo bioavailability. Pharm Res FIELD Full Journal Title:Pharmaceutical research1995;12(3):413-20.
9. Avdeef A. Absorption and Drug Development, Solubility, Permeability, and Charge State. Hoboken N.J.: Wiley; 2003.
10. Marchaud D, Permutt, R. Lipid School: Understanding Lipid Excipients. Gattefosse Lipid School Short Course; Sept 17, 2008: Gattefosse; 2008. p. Slide 23.
11. Chiou WL, Sidney Riegelmann. Pharmaceutical Applications of Solid Dispersion Systems. Journal of Pharmaceutical Sciences1971 September 1971;60(9):1281-302.
12. Doherty C, York P. Evidence for solid- and liquid-state interactions in a furosemide-polyvinylpyrrolidone solid dispersion. J Pharm Sci FIELD Full Journal Title:Journal of Pharmaceutical Sciences1987;76(9):731-7.
13. Janssens S, Van den Mooter G. Review: physical chemistry of solid dispersions. J Pharm Pharmacol FIELD Full Journal Title:Journal of Pharmacy and Pharmacology2009;61(12):1571-86.
14. Qian F, Huang J, Hussain MA. Drug-polymer solubility and miscibility: Stability consideration and practical challenges in amorphous solid dispersion development. Journal of Pharmaceutical Sciences2010;99(7):2941-7.
15. Tiwari R, Tiwari G, Srivastava B, Rai AK. Solid dispersions: an overview to modify bioavailability of poorly water soluble drugs. Int J PharmTech Res FIELD Full Journal Title:International Journal of PharmTech Research2009;1(4):1338-49.
16. Ghaste RP, Chougule DD, Shah RR, Ghodake DS. Solid dispersions: an overview. Pharm Rev FIELD Full Journal Title:Pharmaceutical Reviews2009;7(5):No pp given.

17. Craig DQM. The mechanisms of drug release from solid dispersions in water-soluble polymers. Int J Pharm FIELD Full Journal Title:International Journal of Pharmaceutics2002;231(2):131-44.
18. Greenhalgh DJ, ADRIAN C. WILLIAMS, PETER TIMMINS, AND PETER YORK. Solubility Parameters as Predictors of Miscibility in Solid Dispersions. Journal of Pharmaceutical Sciences1999 November 11, 1999;88(11).
19. Rumondor ACF, Stanford LA, Taylor LS. Effects of Polymer Type and Storage Relative Humidity on the Kinetics of Felodipine Crystallization from Amorphous Solid Dispersions. Pharmaceutical Research2009;26(12):2599-606.
20. Imaizumi H, Naoki Nambu, Tsuneji Nagai. Stabilization of Amorphous State of Indomethacin by Solid Dispersion in Polyvinylpolypyrrolidone. Chemical Pharmaceutical Bulletin1983 1983;31(7):2512-.
21. Tong P, George Zografi. A Study of Amorphous Molecular Dispersions of Indomethacin and Its Sodium Salt. Journal of Pharmaceutical Sciences2001 2001;90:1991-2004.
22. Huang J, Wigent Rodney J, Schwartz Joseph B. Drug-polymer interaction and its significance on the physical stability of nifedipine amorphous dispersion in microparticles of an ammonio methacrylate copolymer and ethylcellulose binary blend. Journal of Pharmaceutical Sciences2008;97(1):251-62.
23. Janssens S, De Zeure A, Paudel A, Van Humbeeck J, Rombaut P, Van den Mooter G. Influence of Preparation Methods on Solid State Supersaturation of Amorphous Solid Dispersions: A Case Study with Itraconazole and Eudragit E100. Pharm Res FIELD Full Journal Title:Pharmaceutical Research2010;27(5):775-85.
24. Patel RC, Masnoon S, Patel MM, Patel NM. Formulation strategies for improving drug solubility using solid dispersions. Pharm Rev FIELD Full Journal Title:Pharmaceutical Reviews2009;7(6):No pp given.
25. Six K, Berghmans H, Leuner C, Dressman J, Van Werde K, Mullens J, et al. Characterization of Solid Dispersions of Itraconazole and Hydroxypropyl methyl cellulose Prepared by Melt Extrusion, Part II. Pharmaceutical Research2003;20(7):1047-54.
26. He C, Zhang G, Xiang B, Cao D. Research progress in identification of solid dispersion. Hebei Yike Daxue Xuebao2009;30(12):1354-7.
27. Al-Obaidi H, Brocchini S, Buckton G. Anomalous properties of spray dried solid dispersions. J Pharm Sci FIELD Full Journal Title:Journal of Pharmaceutical Sciences2009;98(12):4724-37.
28. Sinha S, Baboota S, Ali M, Kumar A, Ali J. Solid Dispersion: An Alternative Technique for Bioavailability Enhancement of Poorly Soluble Drugs. J Dispersion Sci Technol FIELD Full Journal Title:Journal of Dispersion Science and Technology2009;30(10):1458-73.
29. Bley H, Fussnegger B, Bodmeier R. Characterization and stability of solid dispersions based on PEG/polymer blends. Int J Pharm FIELD Full Journal Title:International Journal of Pharmaceutics2010;390(2):165-73.
30. Nand P, Nikore RL, Drabu S. Differential scanning calorimetry studies of solid dispersion of indomethacin using mixed carriers. Asian J Chem FIELD Full Journal Title:Asian Journal of Chemistry2009;21(9):6715-8.

31. Ghebremeskel AN, Chandra Vemavarapu, Mayur Lodaya. Use of surfactants as plasticizers in preparing solid dispersions of poorly soluble API: Selection of polymer-surfactant combinations using solubility parameters and testing the processability. International Journal of Pharmaceutics2007 2007;328:119-29.
32. Kawakami K, Miyoshi K, Tamura N, Yamaguchi T, Ida Y. Crystallization of sucrose glass under ambient conditions: evaluation of crystallization rate and unusual melting behavior of resultant crystals. Journal of Pharmaceutical Sciences2006;95(6):1354-63.
33. Rumondor ACF, Taylor LS. Effect of Polymer Hygroscopicity on the Phase Behavior of Amorphous Solid Dispersions in the Presence of Moisture. Mol Pharmaceutics FIELD Full Journal Title:Molecular Pharmaceutics2010;7(2):477-90.
34. Thybo P, Pedersen BL, Hovgaard L, Holm R, Mullertz A. Characterization and Physical Stability of Spray Dried Solid Dispersions of Probucol and PVP-K30. Pharm Dev Technol FIELD Full Journal Title:Pharmaceutical Development and Technology2008;13(5):375-86.
35. Marsac PJ, Shamblin SL, Taylor LS. Theoretical and Practical Approaches for Prediction of Drug-Polymer Miscibility and Solubility. Pharmaceutical Research2006;23(10):2417-26.
36. Pajula K, Taskinen M, Lehto V-P, Ketolainen J, Korhonen O. Predicting Formation and Stability of Amorphous Small Molecule Binary Mixtures from Computationally Determined Flory-Huggins Interaction Parameter and Phase Diagram. Mol Pharmaceutics FIELD Full Journal Title:Molecular Pharmaceutics2010;7(3):795-804.
37. Yoo S-u, Krill SL, Wang Z, Telang C. Miscibility/stability considerations in binary solid dispersion systems composed of functional excipients towards the design of multi-component amorphous systems. J Pharm Sci FIELD Full Journal Title:Journal of Pharmaceutical Sciences2009;98(12):4711-23.
38. Ito A, Watanabe T, Yada S, Hamaura T, Nakagami H, Higashi K, et al. Prediction of recrystallization behavior of troglitazone/polyvinylpyrrolidone solid dispersion by solid-state NMR. Int J Pharm FIELD Full Journal Title:International Journal of Pharmaceutics2010;383(1-2):18-23.
39. Yang J, Grey K, Doney J. An improved kinetics approach to describe the physical stability of amorphous solid dispersions. Int J Pharm FIELD Full Journal Title:International Journal of Pharmaceutics2010;384(1-2):24-31.
40. Dahlberg C, Millqvist-Fureby A, Schuleit M, Furo I. Polymer-drug interactions and wetting of solid dispersions. Eur J Pharm Sci FIELD Full Journal Title:European Journal of Pharmaceutical Sciences2010;39(1-3):125-33.
41. Punitha S, Karthikeyan D, Devi P, Vedha Hari BN. Enhancement of solubility and dissolution of celecoxib by solid dispersion technique. J Pharm Sci Technol FIELD Full Journal Title:Journal of Pharmaceutical Science & Technology2009;1(2):63-8.
42. Broman E, Khoo C, Taylor LS. A comparison of alternative polymer excipients and processing methods for making solid dispersions of a poorly water soluble drug. Int J Pharm FIELD Full Journal Title:International Journal of Pharmaceutics2001;222(1):139-51.
43. Andrews GP, AbuDiak OA, Jones DS. Physicochemical characterization of hot melt extruded bicalutamide-polyvinylpyrrolidone solid dispersions. J Pharm Sci FIELD Full Journal Title:Journal of Pharmaceutical Sciences2009;99(3):1322-35.

44. Nollenberger K, Gryczke A, Meier C, Dressman J, Schmidt MU, Bruehne S. Pair distribution function X-ray analysis explains dissolution characteristics of felodipine melt extrusion products. J Pharm Sci FIELD Full Journal Title:Journal of Pharmaceutical Sciences2009;98(4):1476-86.
45. Roth W, Setnik B, Zietsch M, Burst A, Breitenbach J, Sellers E, et al. Ethanol effects on drug release from Verapamil Meltrex, an innovative melt extruded formulation. Int J Pharm FIELD Full Journal Title:International Journal of Pharmaceutics2009;368(1-2):72-5.
46. Lin C-W, Cham T-M. Effect of particle size on the available surface area of nifedipine from nifedipine-polyethylene glycol 6000 solid dispersions. Int J Pharm FIELD Full Journal Title:International Journal of Pharmaceutics1996;127(2):261-72.
47. Shimpi SL, Mahadik KR, Paradkar AR. Study on mechanism for amorphous drug stabilization using gelucire 50/13. Chem Pharm Bull FIELD Full Journal Title:Chemical & Pharmaceutical Bulletin2009;57(9):937-42.
48. Ambike AA, Mahadik KR, Paradkar A. Spray-Dried Amorphous Solid Dispersions of Simvastatin, a Low Tg Drug: In Vitro and in Vivo Evaluations. Pharm Res FIELD Full Journal Title:Pharmaceutical Research2005;22(6):990-8.
49. Friesen DT, Shanker R, Crew M, Smithey DT, Curatolo WJ, Nightingale JAS. Hydroxypropyl Methylcellulose Acetate Succinate-Based Spray-Dried Dispersions: An Overview. Mol Pharmaceutics2008;5(6):1003-19.
50. Paradkar A, Ambike AA, Jadhav BK, Mahadik KR. Characterization of curcumin-PVP solid dispersion obtained by spray drying. Int J Pharm FIELD Full Journal Title:International Journal of Pharmaceutics2004;271(1-2):281-6.
51. Salama R, Hoe S, Chan H-K, Traini D, Young PM. Preparation and characterisation of controlled release co-spray dried drug-polymer microparticles for inhalation 1: Influence of polymer concentration on physical and in vitro characteristics. European Journal of Pharmaceutics and Biopharmaceutics2008;69(2):486-95.
52. Yoshihashi Y, Iijima H, Yonemochi E, Terada K. Estimation of physical stability of amorphous solid dispersion using differential scanning calorimetry. J Therm Anal Calorim FIELD Full Journal Title:Journal of Thermal Analysis and Calorimetry2006;85(3):689-92.
53. Kennedy MT. Production and Application of the Amorphous Form of Amgen Small Molecules: Review of collaborative research and process technology. Internal presentation2008.
54. Vasanthavada M, Tong W-Q, Joshi Y, Kislalioglu MS. Phase Behavior of Amorphous Molecular Dispersions I: Determination of the Degree and Mechanism of Solid Solubility. Pharm Res FIELD Full Journal Title:Pharmaceutical Research2004;21(9):1598-606.
55. Loftsson T, Fridriksdottir H, Gudmundsdottir TK. The effect of water-soluble polymers on aqueous solubility of drugs. International Journal of Pharmaceutics1996;127(2):293-6.
56. Muela S, Escalera B, Pena MA, Bustamante P. Influence of temperature on the solubilization of thiabendazole by combined action of solid dispersions and co-solvents. Int J Pharm FIELD Full Journal Title:International Journal of Pharmaceutics2010;384(1-2):93-9.
57. Sichina WJ. Measurement of Tg by DSC. Thermal Analysis, Perkin Elmer Instruments. [Application Note]. 2000;Application Note:1-5.

58. Rumondor ACF, Ivanisevic I, Bates S, Alonzo DE, Taylor LS. Evaluation of Drug-Polymer Miscibility in Amorphous Solid Dispersion Systems. Pharm Res FIELD Full Journal Title:Pharmaceutical Research2009;26(11):2523-34.
59. Coleman NJ, Craig DQM. Modulated temperature differential scanning calorimetry: a novel approach to pharmaceutical thermal analysis. International Journal of Pharmaceutics1996;135(1,2):13-29.
60. Ivanisevic I, Bates S, Chen P. Novel methods for the assessment of miscibility of amorphous drug-polymer dispersions. J Pharm Sci FIELD Full Journal Title:Journal of Pharmaceutical Sciences2009;98(9):3373-86.
61. Tobyn M, Brown J, Dennis AB, Fakes M, Gao Q, Gamble J, et al. Amorphous drug-PVP dispersions: Application of theoretical, thermal and spectroscopic analytical techniques to the study of a molecule with intermolecular bonds in both the crystalline and pure amorphous state. J Pharm Sci FIELD Full Journal Title:Journal of Pharmaceutical Sciences2009;98(9):3456-68.
62. Marsac PJ, Konno H, Rumondor ACF, Taylor LS. Recrystallization of Nifedipine and Felodipine from Amorphous Molecular Level Solid Dispersions Containing Poly(vinylpyrrolidone) and Sorbed Water. Pharmaceutical Research2008;25(3):647-56.
63. Hancock BC, Sheri L. Shamblin, George Zografi. Molecular Mobility of Amorphous Pharmaceutical Solids Below Their Glass Transition Temperature. Pharmaceutical Research1995 1995;12(6):799-806.
64. Kawakami K, Ida Y. Direct Observation of the Enthalpy Relaxation and the Recovery Processes of Maltose-Based Amorphous Formulation by Isothermal Microcalorimetry. Pharmaceutical Research2003;20(9):1430-6.
65. Gordon M, Taylor JS. Ideal copolymers and the second-order transitions of synthetic rubbers. I. Noncrystalline copolymers. J Appl Chem1952;2:493-500.
66. Gupta P, Bansal AK. Molecular interactions in celecoxib-PVP-meglumine amorphous system. J Pharm Pharmacol FIELD Full Journal Title:Journal of Pharmacy and Pharmacology2005;57(3):303-10.
67. Couchman PR, Karasz FE. A classical thermodynamic discussion of the effect of composition on glass-transition temperatures. Macromolecules1978;11(1):117-19.
68. Ambike Anshuman A, Mahadik KR, Paradkar A. Stability study of amorphous valdecoxib. Int J Pharm FIELD Full Journal Title:International journal of pharmaceutics2004;282(1-2):151-62.
69. Giron D. Thermal analysis, microcalorimetry and combined techniques for the study of pharmaceuticals. Journal of Thermal Analysis and Calorimetry1999;56(3):1285-304.
70. Schneider HA. Considerations concerning the glass temperature of blends of miscible polymers. Polym Bull (Berlin) FIELD Full Journal Title:Polymer Bulletin (Berlin)1998;40(2-3):321-8.
71. Schneider HA. The meaning of the glass temperature of random copolymers and miscible polymer blends. J Therm Anal Calorim FIELD Full Journal Title:Journal of Thermal Analysis and Calorimetry1999;56(3):983-9.
72. Miyazaki T, Yoshioka S, Aso Y, Kawanishi T. Crystallization rate of amorphous nifedipine analogues unrelated to the glass transition temperature. International Journal of Pharmaceutics2007;336(1):191-5.

73. Crowley KJ, George Zografi. Water Vapor Absorption into Amorphous Hydrophobic Drug/ Poly(vinylpyrrolidone) Dispersions. Journal of Pharmaceutical Sciences. [Journal Article]. 2002 October 2002;91(10):2150-65.
74. Rabel SR, Jona JA, Maurin MB. Applications of modulated differential scanning calorimetry in preformulation studies. J Pharm Biomed Anal1999;21(2):339-45.
75. Marsac PJ, Li T, Taylor LS. Estimation of Drug-Polymer Miscibility and Solubility in Amorphous Solid Dispersions Using Experimentally Determined Interaction Parameters. Pharm Res FIELD Full Journal Title:Pharmaceutical Research2009;26(1):139-51.
76. Yoshihashi Y, Yonemochi E, Maeda Y, Terada K. Prediction of the induction period of crystallization of naproxen in solid dispersion using differential scanning calorimetry. J Therm Anal Calorim FIELD Full Journal Title:Journal of Thermal Analysis and Calorimetry2010;99(1):15-9.
77. Auer S, Frenkel D. Suppression of crystal nucleation in polydisperse colloids due to increase of the surface free energy. Nature (London, U K)2001;413(6857):711-3.
78. Schmitt EA, Law D, Zhang GGZ. Nucleation and Crystallization Kinetics of Hydrated Amorphous Lactose above the Glass Transition Temperature. Journal of Pharmaceutical Sciences1999;88(3):291-6.
79. Malek J. Crystallization kinetics by thermal analysis. Journal of Thermal Analysis and Calorimetry1999;56(2):763-9.
80. Yoshioka M, Hancock BC, Zografi G. Crystallization of indomethacin from the amorphous state below and above its glass transition temperature. Journal of Pharmaceutical Sciences1994;83(12):1700-5.
81. Ahlneck C, George Zografi. The molecular basis of moisture effects on the physical and chemical stability of drugs in the solid state. International Journal of Pharmaceutics1990 1990;62:87-95.
82. Cotton ML, Wu DW, Vadas EB. Drug-excipient interaction study of enalapril maleate using thermal analysis and scanning electron microscopy. Int J Pharm FIELD Full Journal Title:International Journal of Pharmaceutics1987;40(1-2):129-42.
83. Carstensen JT, Osadca M, Rubin SH. Degradation mechanisms for water-soluble drugs in solid dosage forms. Journal of Pharmaceutical Sciences1969;58(5):549-53.
84. Kennedy M, Hu J, Gao P, Li L, Ali-Reynolds A, Chal B, et al. Enhanced Bioavailability of a Poorly Soluble VR1 Antagonist Using an Amorphous Solid Dispersion Approach: A Case Study. Mol Pharmaceutics2008;5(6):981-93.
85. Balan C, Chen N, Doherty EM, Gore VK, Norman MH, Wang H-l, inventors; (Amgen Inc., USA). assignee. Preparation of 4-heteroaryloxy-6-piperazinopyrimidines and 2-heteroaryloxy-4-piperazinopyridines as vanilloid receptor ligands. Application: US
US patent 2005-56534
20050182067. 2005 20050211.
86. Fukasawa M, S. Obara. Molecular weight determination of hypromellose acetate succinate (HPMCAS) using size exclusion chromatography with a multi-angle laser light scattering detector. Chem Pharm Bull FIELD Full Journal Title:Chemical & Pharmaceutical Bulletin. [Journal Article]. 2004 Nov 2004;52(11):1391-3.

87. Al-Obaidi H, Buckton G. Evaluation of griseofulvin binary and ternary solid dispersions with HPMCAS. AAPS PharmSciTech FIELD Full Journal Title:AAPS PharmSciTech2009;10(4):1172-7.
88. Curatolo W, Nightingale JA, Herbig SM. Utility of Hydroxypropylmethylcellulose Acetate Succinate (HPMCAS) for Initiation and Maintenance of Drug Supersaturation in the GI Milieu. Pharmaceutical Research2009;26(6):1419-31.

Chapter 2. Methods of Characterization for ASDs of AMG 517 in HPMC-AS

Introduction

Many different techniques can be used to understand amorphous solid dispersions. The initial goal of characterization is to confirm the nature of the starting materials which were prepared from the spray drying process. This includes measuring drug load, particle size, surface area, residual solvent drying and amorphous content. Since ASDs are designed to stabilize the drug against crystallization, it is important to understand miscibility and phase separation. The miscibility and phase separation of the drug and polymer components of an ASD directly affect the propensity for crystallization. Methods to track changes in crystallinity are critical when crystallization is being studied, as well as a way to put it all together and "map the crystallization space." This chapter will describe the various analytical techniques used to understand the AMG 517 – HPMC-AS amorphous solid dispersion system.

Techniques to Evaluate Spray Dry Manufacturing

HPLC – confirmation of drug load

High performance liquid chromatography (HPLC) is a commonly used analytical separations technique which can be used to quantify the amount of drug in a solution. A small amount of ASD material must be dissolved in a common solvent, in which both drug and polymer components of the ASD are soluble. The ASD solution is pumped through a column of silica bonded hydrocarbon chains using a high pressure pump. The drug and polymer components pass through and elute from the column at different rates, allowing for separation of the ASD components. The response of a known standard is compared with the response from the drug

passing through the detector, allowing for quantification of the drug in the solution. The presence of impurities and/or degradation products would also be observed in the HPLC chromatograms. This is a common technique in pharmaceutical labs and provides useful confirmation of the drug load in various lots of spray dried ASD materials. (1, 2)

Particle Size Distribution – to measure size of ASDs

Particle size distribution and surface area are important indicators of spray drying control. A common method of particle size analysis uses laser diffraction. (3) Evaluating the size distribution of ASD particles of different lots gives information about the control of the spray drying process. A trend in particle size between lots with varying drug loads may be an indication of significant differences due to drug load and different size particles can behave differently, in terms of stability. The effect of particle size on crystallization has previously been studied, (4, 5) and it is accepted that particle size has an effect on crystallization rate, so ASDs of similar particle size were desired for crystallization studies.

Techniques to Evaluate Residual Solvent

TGA – to measure residual ethyl acetate solvent

Thermogravimetric analysis (TGA) is commonly used to measure water and solvent loss from solid materials. A sample of ~5mg is placed in a hanging pan which is lowered into a temperature controlled furnace. A heating ramp is applied and the weight of the sample is monitored as the temperature is raised, allowing for detection of water and/or solvent loss.

The percent of residual solvent is calculated by the software, comparing the weight of the sample before and after solvent evaporation. For ASDs of AMG 517 with HPMC-AS, the type

of solvent (water, ethyl acetate, etc) and the nature of its bonding to the sample (i.e. residual solvent or hydrate) can be inferred from the temperature at which the solvent comes off the sample. However, TGA is a non-specific method and cannot separate the effects of water versus solvent at a given temperature. Therefore, a more specific method such as GC is used to confirm the amount of residual solvent (ethyl acetate) in the ASDs.

GC – to quantify residual ethyl acetate solvent

Gas chromatography (GC) is a gas separations method used to determine the amount of residual ethyl acetate solvent in the spray dried ASDs. All the components of the spray dried ASDs are soluble in DMSO, making DMSO a practical solvent for GC analysis. The boiling point of ethyl acetate is relatively low, at 77°C, and the boiling point of DMSO is high, at 189°C (6). The ethyl acetate is separated from the DMSO solvent on the GC column using a temperature ramp and flame ionization detector (FID) to detect the different components at different temperatures based on boiling point. The amount of ethyl acetate is determined by comparing the peak area response of the sample with peak area response of standard solutions of known concentration. Using known standards of ethyl acetate allows for quantification of the ethyl acetate in the ASDs, which can be compared with TGA results.

Techniques to Verify Amorphous Nature of ASDs

SEM – to observe surface of ASD particles

Scanning Electron Microscopy (SEM) is a technique to qualitatively observe the surface of particles. An electron source achieves higher resolution than is possible with light microscopy.

The short wavelength of electrons (0.0054 nm) allows for resolution on the order of 1nm or less, compared with 0.2 μm for light microscope and 0.1mm for the unaided eye. (7) With spray dried ASD particles prepared on a micron (μm) scale, light microscopy is not resolved enough to see details about the surface of the particles. SEM provides a definitive way of observing individual crystals growing out of amorphous particles such as the ASDs of AMG 517 in HPMC-AS studied here.

XRD – to verify amorphous nature of ASDs

X-ray powder diffraction (XRD) crystallography is a common analytical tool which gives information about the crystal structure of a material, based on the diffraction of X-rays off the crystal faces. (8, 9) Each crystalline form of a material has a unique pattern of lines or spikes, specific to the packing pattern of that polymorphic form. An amorphous material, including an ASD without a regular packing pattern, will show a broad "halo" instead of a pattern of distinct peaks. This is due to the random ordering of molecules in the amorphous material.

X-ray powder diffraction patterns are used to determine the amorphous or crystalline nature of ASD materials and to verify the crystalline form of AMG 517 as it crystallizes out of the ASD. A partially crystalline ASD will show a few distinct peaks overlaid with a broad amorphous "halo" pattern. The lower limit of detection for crystalline material by XRD in an amorphous dispersion is about 3%. Reference standards of crystalline AMG 517 in HPMC-AS polymer are prepared at various known mixtures in order to determine the detection limit of the system, as well as to compare with partially crystallized ASD samples.

Techniques to Evaluate Miscibility and Phase Separation

Modulated DSC (mDSC) – to measure glass transition

Differential Scanning Calorimetry (DSC) is a useful technique for understanding the thermal properties of a material. Thermal events such as melting, phase changes and recrystallization are routinely detected by DSC measurements. Modulated DSC (mDSC) is especially effective in obtaining glass transition (T_g) values as well as other thermal information about amorphous materials. A sine wave modulation is introduced into the DSC temperature program through the software, which allows for de-convolution of overlapping thermal events, separating the output into three signals: the total heat flow, the nonreversible (kinetic) heat flow and the reversible (heat capacity component) heat flow. (10, 11) It can be used to provide insight into polymorphic transformations and to distinguish between multiple T_gs in a sample if the difference between T_gs is < 15°C. (11) For ASDs, mDSC is needed to evaluate the T_g of the ASDs. A phase mixed ASD has one T_g, and a phase separated solid dispersion has a separate T_g for each component in the system. The T_g of pure amorphous AMG 517 is ~ 110 °C and the T_g of spray dried HPMC-AS polymer is ~125 °C; therefore, the T_g of an ASD of AMG 517 in HPMC-AS should be between 110 – 125 °C.

Figure 1 shows the traditional DSC heat flow curve for an ASD and the modulated DSC (mDSC) curves for the same sample, with thermal events indicated in the different regions of the plots. The normal heat flow plot is shown at the top and the modulated DSC is shown on the bottom, with reversible and non-reversible heat flow curves separated out. In mDSC, the glass

transition is seen in the reversing heat flow curve at ~ 104 °C, and the accompanying endothermic relaxation of 4.66 J/g is seen in the non-reversing heat flow curve.

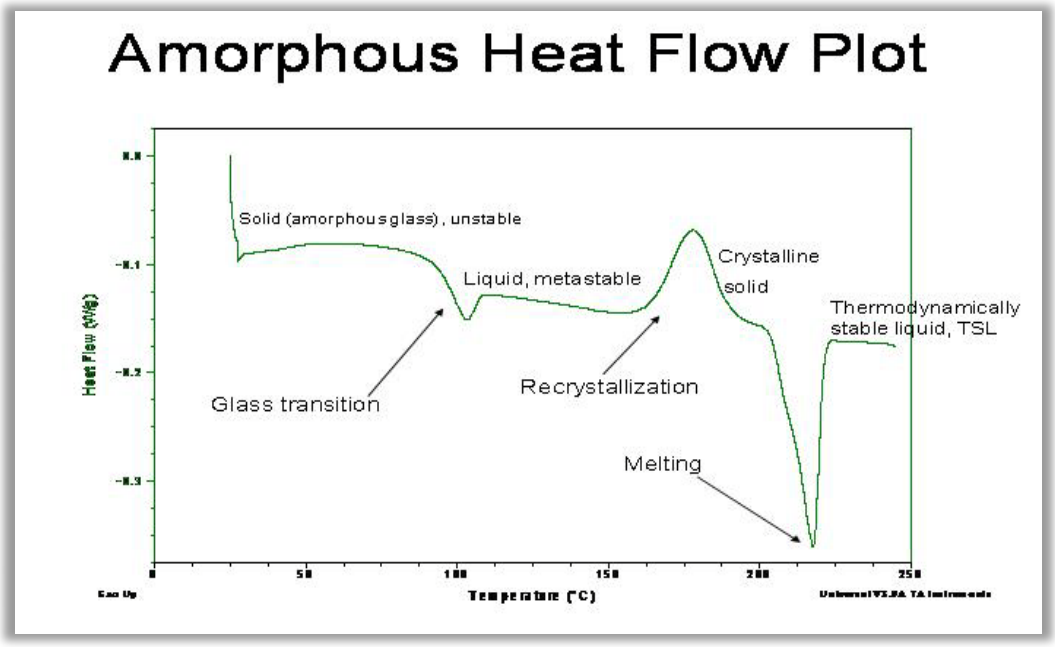

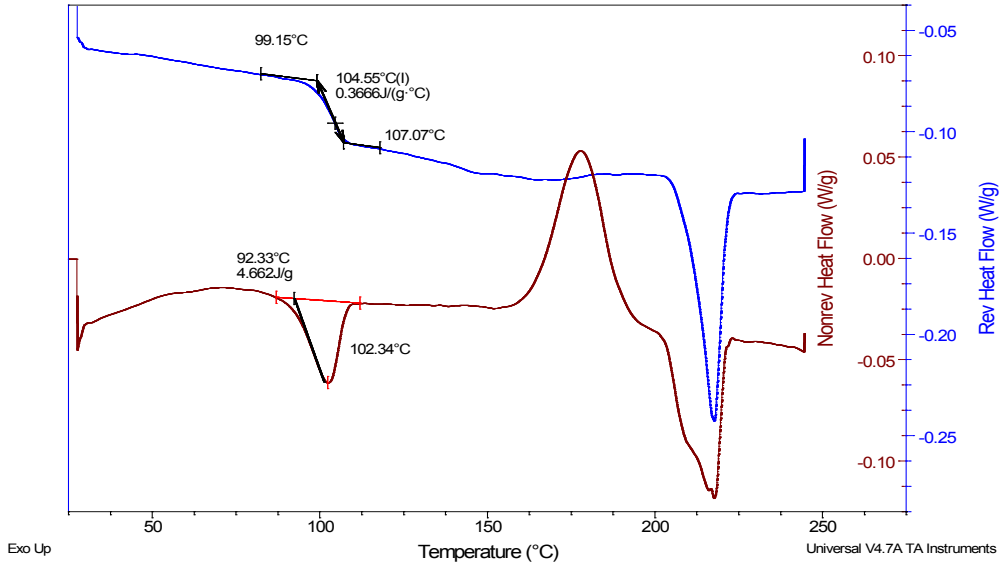

Figure 1. Traditional DSC v mDSC. The top plot shows the traditional DSC heat flow curve for 50% AMG 517 ASD, with thermal events indicated in the different regions of the plot. The modulated DSC is shown below it, with reversible and non-reversible heat flow curves separated out. The glass transition is easily seen in the reversing heat flow curve and the accompanying endothermic relaxation is seen in the non-reversing heat flow curve.

^{19}F SSNMR – to evaluate relaxation

Nuclear Magnetic Resonance (NMR) is a spectroscopic technique based on the magnetic polarization of the spins in the nucleus of atoms in a molecule and is commonly used for compound structure identification based on chemical shifts for liquid samples. Solid State NMR (SSNMR) is emerging as a powerful technique for characterization of solids. Spectral differences between polymorphs reflect the differences in the local environment of the nuclei in the sample. This is useful in detecting differences in crystal packing and even for evaluating differences between amorphous forms.

The classical way to understand NMR is to imagine a vector (a magnetic dipole) precessing about a spinning particle in an external magnetic field, as in Figure 2 below. A nucleus such as ^{1}H, ^{13}C or ^{19}F with spin I = ½, is chosen for NMR analysis. In an externally applied magnetic field B_o, a spinning nucleus with I = ½ charge creates a magnetic field, with the lower energy + ½ spin oriented in the direction of the magnetic field, B_o, and the higher energy – ½ spin state oriented opposite B_o. When a magnetic pulse is applied to the nucleus, the + ½ spin is excited to the higher energy – ½ spin state. As the precessing excited nucleus returns to the equilibrium state, it "relaxes" to give the NMR signal. The free induction decay (FID) is observed and Fourier transformation is used to transform the time domain signal into the frequency domain NMR spectrum. (8, 12, 13)

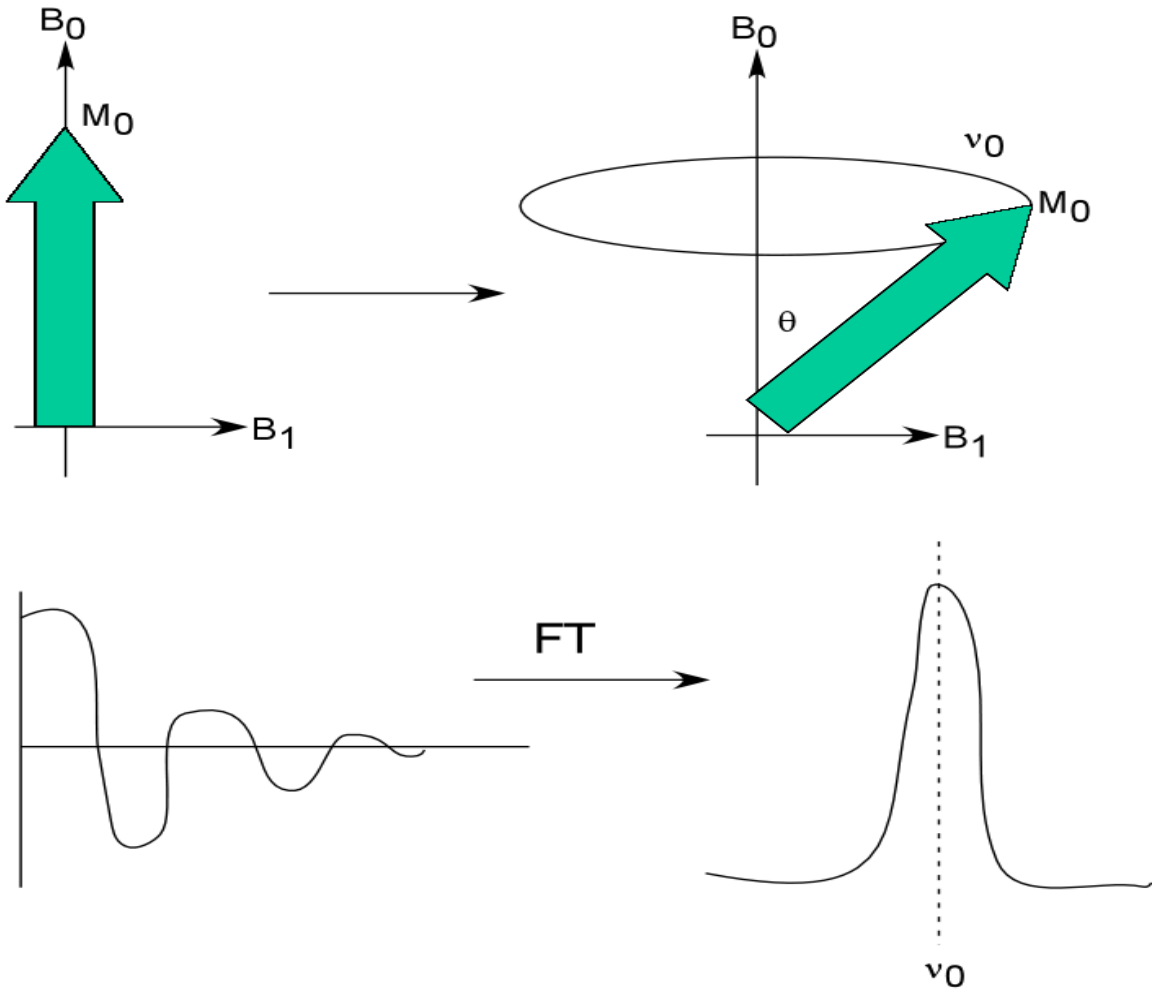

Figure 2. NMR Theory Diagrams (14) Top left green arrow indicates magnetic moment spinning around Bo field. When a pulse is applied along B1, the magnetic moment is precessing around Bo at an angle (top right). Bottom left shows free induction decay (FID) signal which is Fourier transformed (FT) into frequency domain signal (bottom right).

SSNMR Considerations

SSNMR spectroscopy is versatile technique with high selectivity, the only technique which can give information about structure, order **and** dynamics of solid state materials. A range of nuclei (with I = ½) can be observed, including ^{1}H, ^{13}C, ^{15}N, ^{31}P, ^{29}Si and ^{19}F. The relative sensitivity and natural abundance of these six nuclei are shown in Table 1.

Table 1. NMR Properties of Common Nuclei (14)

Nuclei	Natural abundance	Relative sensitivity
^{1}H	99.99%	1
^{13}C	1.13%	0.016
^{15}N	0.37%	0.001
^{19}F	100%	0.83
^{31}P	100%	0.0663
^{29}Si	4.90%	0.00784

^{19}F is particularly relevant to this discussion since AMG 517 has a CF_3 group. Fluorine, with 100% natural abundance and high (0.83) relative sensitivity, is a convenient and fast, nucleus to measure. The CF_3 group on the molecule is oriented differently between amorphous and crystalline forms and gives a strong signal, making it easy to detect differences between the two solid states.

High Speed Spinning and Magic Angle Spinning

Since SSNMR is dealing with solid samples rather than liquid samples, high speed spinning and magic angle spin (MAS) are used to mimic the molecular motion of a liquid sample and minimize effect of random orientation of molecules in a solid sample. Liquid molecules are in fast random motion already, giving high resolution of NMR peaks. In order to get high resolution for solids, a spin speed greater than the width of the CSA (chemical shift anisotropy) is needed.

In the SSNMR context, there are several types of interactions going on, indicated by the following equation:

$H = H_o + H_D + H_{CS} + H_Q,$ Equation 1

where H_o is due to the applied magnetic field B_o, H_{CS} is chemical shift interactions that we are interested in, H_D is a function of $3\cos^2\theta$-1 and angular momentum operators and H_Q only applies for $I > ½$. Magic angle spinning (MAS) was introduced to deal with the HD interactions. To eliminate the effect of molecular orientation in the magnetic field, set $3\cos^2\theta-1=0$ and solve for θ … $\theta = 54.4°$, the "magic angle". If the sample is set to spin at a physical orientation of 54.4°, the orientation dependence goes to zero. MAS is standard and SSNMR probes are commonly manufactured to run with samples spinning at the magic angle. (14)

Techniques to Evaluate Crystallinity of Stressed ASDs

^{19}F SSNMR - to Measure Percent (%) Crystallinity

SSNMR can be used to measure and quantify the percent crystallinity in ASDs. The amorphous and crystalline forms will give different SSNMR spectra. Comparing the integrated areas of crystalline and amorphous signals in a SSNMR spectrum of an ASD, the amount of crystallization for the sample can be determined. In a partially crystallized ASD sample, there will be signal from both amorphous and crystalline material in the sample. Integrating distinct peaks is a straight-forward way to quantify differences in form. However, when comparing an amorphous form with a crystal form of the same molecule, the amorphous signal will be broad, since it is an average of all the possible orientations of the molecule, including the orientation of the crystal form.

When the peaks are partially overlapping and quantitation is desired, de-convolution is needed to separate the signals from each form of the material. The percent crystalline can be simply calculated as Area Crystalline / Total Area * 100%. For molecules such as AMG 517 where the crystal form being studied has two molecules per unit cell, the SSNMR signal shows two distinct peaks for the crystal form. In this case the percent crystallinity is calculated by combining the areas of the two crystalline peaks and dividing by the total area of all three peaks.

Crystallization of ASDs

Traditional Solid State Stability

Traditionally, solid state stability studies on pharmaceutical formulations in development are performed by placing an aliquot of the formulation at elevated temp and/or RH conditions for accelerated stability studies. Typical conditions include 25 °C, 60%RH for controlled room temperature, 40°C, 75%RH for accelerated conditions. (15) Additional accelerated conditions

include 60 °C temperature at 30%RH and 75%RH. Using stability results from three or more temperatures, one can extrapolate to lower temperatures to predict the stability of the formulation in development.

A significant drawback to the traditional solid state stability method is the difficulty in predicting the endpoint for crystallization and the stability event can easily be missed. Traditional stability studies also tend to require gram-scale quantities of material to perform the experiment each condition, due to the need for having multiple time points. Typically the only information obtained from these studies is a general timeframe such as "> 6 months stability" at a given condition.

Isothermal Microcalorimetry to Evaluate Crystallization

The crystallization of amorphous ASDs of AMG 517 in HPMC-AS can be monitored by isothermal microcalorimetry. Isothermal microcalorimetry has proven to be a sensitive tool to monitor slow, low energy thermal events, such as chemical degradation and physical form change. Microcalorimetry is a complementary technique to DSC using a larger sample size and higher sensitivity to observe lower energy changes which are undetectable by DSC. (16) Isothermal microcalorimetry can be used to monitor crystallization reactions under controlled environmental conditions, allowing for control of the crystallization event. (17)

Temperature and relative humidity (%RH) are controlled using TAM isothermal microcalorimeter instrument. Miniature humidity chambers are created using hygrostats prepared in a small vials and placed inside the sample cup, to control the humidity of the sample.

Saturated aqueous salt solutions are available for temperatures from 0-100 °C with 5 - 98% humidity range. Temperature is accurately controlled and isothermal stability is provided by a 25L water bath (Figure 4) which controls temperature +/-0.0001 °C. An external water bath provides constant force against which the calorimeter heater must work. This gives the TAM extreme sensitivity to 0.1μW and it can detect 10^{-4} °C temperature difference. (18)

Isothermal heat conduction microcalorimetry measures heat flow dQ/dt, in μW units, from ongoing processes. The heat flow curve is integrated over a specific time interval to obtain heat Q, in Joules. (19) The peak area of the exotherm is proportional to the crystalline content since this relates directly to the heat of the crystallization event. The integrated heat flow of the crystallization event is detected by a heat conduction calorimeter. Heat is channeled from the sample cup through thermopiles, utilizing the Seebeck effect – with voltage generated due to temperature differences between metal junctions. The Twin Measuring Principle is used: The sum of the voltages from each pair of detectors ("Peltier Elements") is connected in series but in opposition, so that the resulting signal represents the difference in heat flow between the two measuring cups.

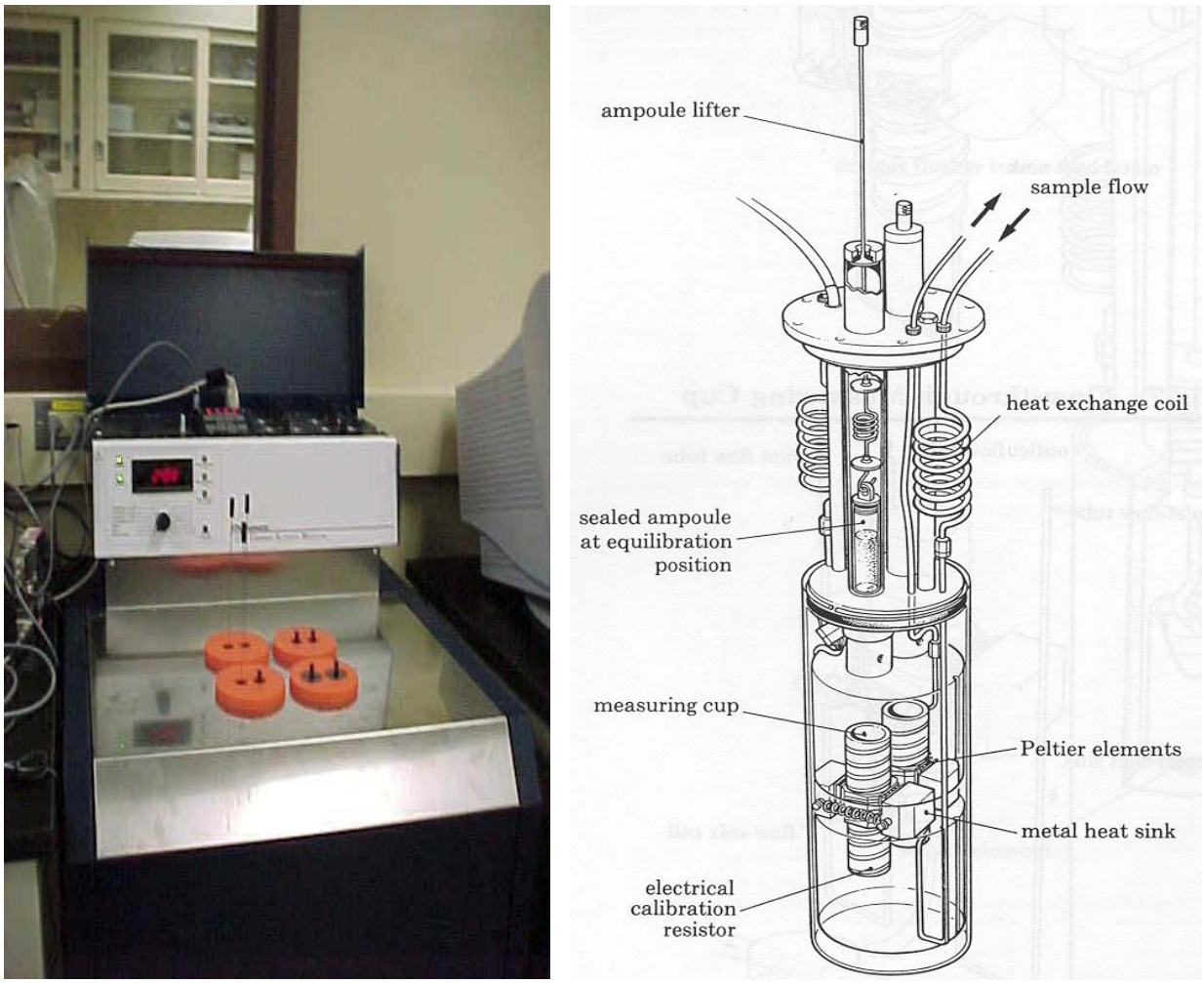

Figure 4. Left: The TAM consists of four microcalorimetry channels (orange caps shown) immersed in a 25L water bath. Right: A diagram of the inside of a typical microcalorimeter. The sample is placed into a sealed ampoule and lowered into the microcalorimeter using the ampoule lifter. During the experiment, any heat from the reaction is transferred from the ampoule into the heat sink and recorded. (20)

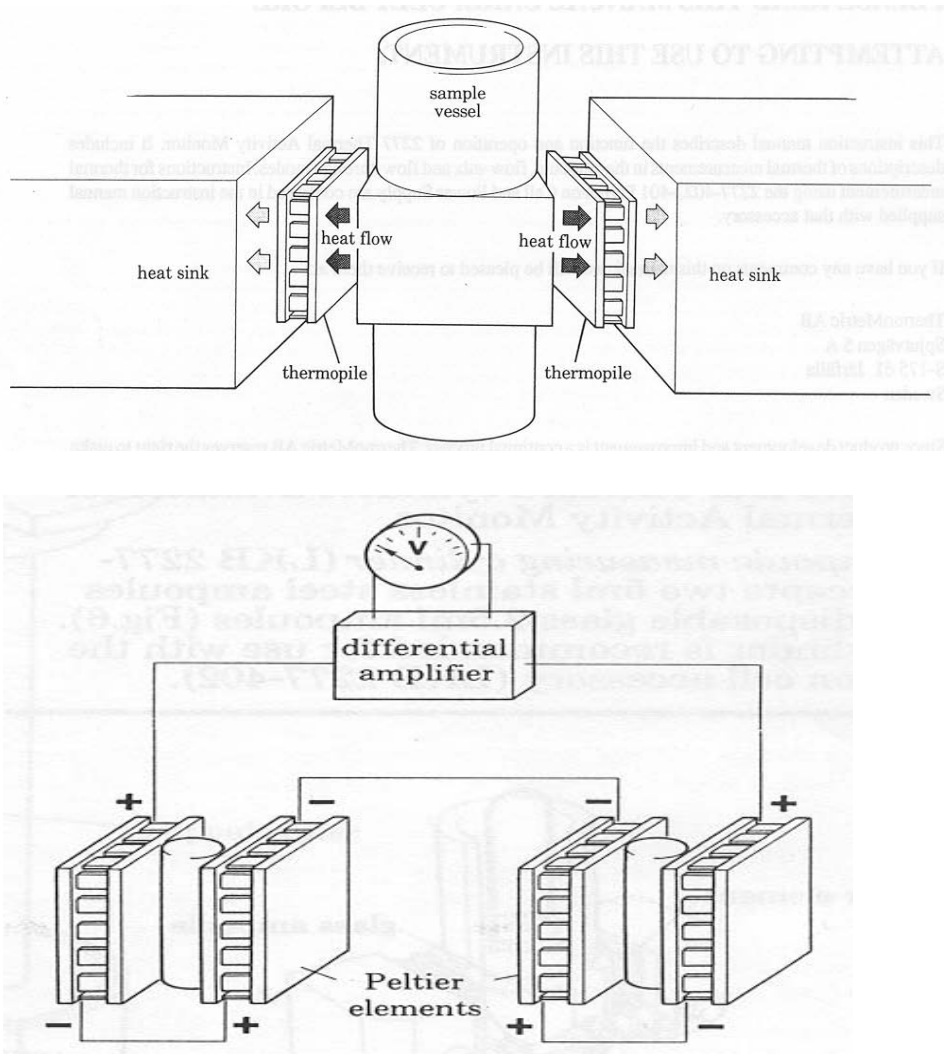

Figure 5. Top: Diagram of sample vessel where measuring cup is placed, surrounded by thermopiles which direct heat flow from the sample into the heat sink. Heat is channeled from the sample cup through thermopiles, utilizing the Seebeck effect – with voltage generated due to temperature differences between metal junctions. Bottom: Diagram of Peltier elements. The sum of the voltages from each pair of detectors ("Peltier Elements") is connected in series but in opposition, so that the resulting signal represents the difference in heat flow between the two measuring cups. (20)

The measured heat of a sample varies at higher temperatures due to changing humidity, so saturated salt solutions are used to control the humidity in the measuring cup during the experiment. Salt solutions for making hygrostats for this purpose can be referenced in CRC Handbook and others. (21, 22) The National Bureau of Standards (23) also has a great reference with tables of salt solutions at various temperature and humidity conditions. A table of relevant salt solutions is shown below.

Table 2. Salt Solutions

Salt	Temperature (°C)	Humidity (%RH)
MgCl2 / NaI	50	30.5/29.2
MgCl2 / NaI	65	28.5/24.6
MgCl2 / NaI	80	26.0/22.5
NaBr	50	50.9
NaBr	65	49.5
NaBr	80	51.4
NaCl	50	74.4
NaCl	65	74.7
NaCl	80	76.3
LiCl	65	10.9

Challenges in using isothermal calorimetry for crystallization of ASDs include 1) the possible overlap of crystallization and relaxation events (since isothermal microcalorimetry is not a specific technique and will detect all heat events associated with a process), 2) possible lack of induction period (nuclei formation not detected, if the crystallization conditions chosen for the crystallization experiment are too fast), 3) lower drug load samples being extremely

stable (such that crystallization is not observed in a relevant period of time) and 4) the potential degradation of excipients under high stress conditions, and the potential impact of residual solvent for incompletely dried samples. Previous studies have also discussed the effect of sample size (24) and plasticization when T_g drops below the measuring temp (25).

Sample amount used for the experiment can also have an effect, as increasing the amount of sample loaded into the sample cup was found to be a factor in retarding crystallization for (17) study. Another study with lactose also showed that recrystallization happens when the T_g drops below the measured temperature (plasticization) (26) so it is important to be aware of how the T_g changes with temperature and humidity.

For this project, isothermal microcalorimetry is used to study and predict the crystallization behavior of AMG 517 – HPMC-AS spray dried dispersions by establishing the relative stability of various systems under controlled conditions of temperature and %RH. The intention is to map the crystallization behavior as a function of polymer ratio, temperature and RH, and potentially predict shelf-life under various, specific environmental conditions.

Conclusion

Several techniques for understanding ASDs have been discussed, each technique giving slightly different information about the sample. HPLC, particle sizing and surface area are used to confirm the effectiveness of spray drying. The residual solvent drying process is measured using GC and TGA to determine the residual solvent content. The amorphous nature of the ASD

materials is verified with SEM and XRD. Miscibility and phase separation are evaluated with mDSC and SSNMR for glass transition and relaxation measurements, respectively. Isothermal microcalorimetry is used as an alternative to traditional accelerated stability conditions for monitoring the crystallization event in solid state stability studies. Finally, the % crystallinity is measured using 19F SSNMR. Using many different techniques to evaluate a system allows the scientist to obtain a thorough understanding of the materials being studied. Combining all of the methods discussed in this chapter should provide a detailed picture of the expected behavior of ASDs of AMG 517 and HPMC-AS.

References

1. Punitha S, Karthikeyan D, Devi P, Vedha Hari BN. Enhancement of solubility and dissolution of celecoxib by solid dispersion technique. :Journal of Pharmaceutical Science & Technology 2009;1(2):63-8.
2. Tran TT-D, Tran PH-L, Choi H-G, Han H-K, Lee B-J. The roles of acidifiers in solid dispersions and physical mixtures. International Journal of Pharmaceutics 2010;384(1-2):60-6.
3. Sympatec, editor. Sympatec Particle Measurement Documentation Particle Size, Shape and Sampling Seminar; 2010; Thousand Oaks, CA: Sympatec Inc.
4. Lin C-W, Cham T-M. Effect of particle size on the available surface area of nifedipine from nifedipine-polyethylene glycol 6000 solid dispersions. International Journal of Pharmaceutics 1996;127(2):261-72.
5. Zhang F, Aaltonen J, Tian F, Saville DJ, Rades T. Influence of particle size and preparation methods on the physical and chemical stability of amorphous simvastatin. European Journal of Pharmaceutics and Biopharmaceutics 2009;71(1):64-70.
6. O'Neil MJ, Ann Smith, Patricia E. Heckelman, John R. Obenchain Jr., Jo Ann R. Gallipeau, Mary Ann D'Arecca, Susan Budavari, editor. The Merck Index. 13th ed. Whitehouse Station, NJ: Merck Research Laboratories, Division of Merck & Co., Inc.; 2001.
7. Postek MT, Karen S. Howard, Arthur H. Johnson, Kathyln L. McMichael. Scanning Electron Microscopy: A Student's Handbook. Williston, Vermont: Ladd Research Industries; 1980.
8. Byrn SR, Ralph R. Pfeiffer, Joseph G. Stowell. Solid-State Chemistry of Drugs. 2nd Edition ed. West Lafayette, Indiana: SSCI, Inc.; 1999.
9. Gennaro AR, editor. Remington: The Science and Practice of Pharmacy. 20th ed. Baltimore, MD: Lippincott Williams & Wilkins; 2000.
10. Coleman NJ, Craig DQM. Modulated temperature differential scanning calorimetry: a novel approach to pharmaceutical thermal analysis. International Journal of Pharmaceutics 1996;135(1,2):13-29.
11. Rabel SR, Jona JA, Maurin MB. Applications of modulated differential scanning calorimetry in preformulation studies. J Pharm Biomed Anal 1999;21(2):339-45.
12. Edwards JC. Principles of NMR. Danbury, CT: Process NMR Associates LLC; 2003 [cited 2003]; www.process-nmr.com/nmr.htm].
13. Skoog/Leary. Principles of Instrumental Analysis.
14. Nagapudi K. Applications of Multinuclear Solid State NMR Spectroscopy in Characterizing Drug Substance and Drug Product. [Presentation]. In press 2010.
15. FDA. ICH Guidance for Industry: Q1A(R2) Stability Testing of New Drug Substances and Products. In: Administration FaD, editor. Rockville, MD: US Department of Health and Human Services 2003.
16. Giron D. Applications of Thermal Analysis and Coupled Techniques in Pharmaceutical Industry. Journal of Thermal Analysis and Calorimetry 2002;68(2):335-57.
17. Kawakami K, Tetsuya Numa, Yasuo Ida. Assessment of Amorphous Content by Microcalorimetry. Journal of Pharmaceutical Sciences. [Journal Article]. February 2002; 91(2):417-23.

18. Gilman L. What is Microcalorimetry? TAM Training. [PowerPoint presentation]. In press.
19. Sebhatu T, Angberg M, Ahlneck C. Assessment of the degree of disorder in crystalline solids by isothermal microcalorimetry. International Journal of Pharmaceutics 1994;104(2):135-44.
20. Thermometric. Instruction Manual for 2277 Thermal Activity Monitor. Thermometric AB: Jarfalla, Sweden, 2000.
21. Nyqvist H. Saturated salt solutions for maintaining specified relative humidities. Int J Pharm Technol Prod Manuf 1983;4(2):47-8.
22. Rumondor ACF, Stanford LA, Taylor LS. Effects of Polymer Type and Storage Relative Humidity on the Kinetics of Felodipine Crystallization from Amorphous Solid Dispersions. Pharmaceutical Research 2009;26(12):2599-606.
23. Greenspan L. Humidity Fixed Points of Binary Saturated Aqueous Solutions. Journal of Research of the national Bureau of Standards - A Physics and Chemistry1977 January-February;81A(1).
24. Darcy P, Buckton G. Quantitative assessments of powder crystallinity. Estimates of heat and mass transfer to interpret isothermal microcalorimetry data. Thermochimica Acta 1998;316(1):29-36.
25. Huang J, Wigent Rodney J, Schwartz Joseph B. Drug-polymer interaction and its significance on the physical stability of nifedipine amorphous dispersion in microparticles of an ammonio methacrylate copolymer and ethylcellulose binary blend. Journal of Pharmaceutical Sciences 2008;97(1):251-62.
26. Lehto V-P, Mikko Tenho, Kalle Vähä-Heikkilä, Päivi Harjunen,, Maarit Päällysaho JV, Pentti Niemelä, Kristiina Järvinen. The comparison of seven different methods to quantify the amorphous content of spray dried lactose. Powder Technology [Journal Article]. June 8, 2006;167 85-93.
27. Offerdahl TJ, Jonathon S. Salsbury, Zedong Dong, David J.W. Grant, Stephen A. Schroeder, Indra Prakash, Eric M. Gorman, Dewey H. Barich, Eric J. Munson. Quantitation of Crystalline and Amorphous Forms of Anhydrous Neotame using 13C CPMAS NMR Spectroscopy. Journal of Pharmaceutical Sciences December 2005;94:2594-605.
28. Bhugra C, Rama Shmeis, Steven L. Krill, and Michael J. Pikal. Predictions of Onset of Crystallization from Experimental Relaxation Times I-Correlation of Molecular Mobility from Temperatures Above the Glass Transition to Temperatures Below the Glass Transition. Pharmaceutical Research October 2006;23(10):2277-90.

Chapter 3. Characterization and Effect of Residual Solvent and Drug Concentration on Glass Transition Values of ASDs of AMG 517 and HPMC-AS

Introduction

Adding a polymer to drug to make amorphous solid dispersions (ASDs) can inhibit crystallization in both the solid and solution state for some drug-polymer systems. AMG 517 dispersed in HPMC-AS is investigated as a molecular dispersion of drug within a matrix material. The goal of making ASDs is for the drug to be completely miscible in the polymer, as this will produce the most stable situation for the amorphous drug. Drug and polymer phases are indistinguishable for an ASD, as the drug and polymer are miscible with each other in one phase.

The degree of phase separation varies based on preparation technique and drug load. Spray drying is a common manufacturing method for ASDs. A well controlled spray dry manufacturing process produces different lots of ASD material with similar particle size and other physical properties. ASDs for this study are manufactured using HPMC-AS polymer and ethyl acetate as solvent.

Residual solvent is known to have an effect on the glass transition temperature of the mixture. If the ASD is not sufficiently dried of residual solvent, the T_g of the mixture will appear lower than the true T_g. It is therefore important to dry the materials sufficiently prior to characterization and use. Using the Gordon-Taylor model to evaluate the ASD system over a range of drug loads can provide insight into the significance of interaction between the components of the ASD.

X-ray powder diffraction (XRPD) can be used to confirm amorphous nature of ASDs, but has a detection limit ~5-10%. Modulated differential scanning calorimetry (mDSC) is also able to provide information about the nature of the manufactured ASDs. The glass transition temperature (T_g) is the temperature at which an amorphous "glass" turns into a meta-stable, or super-cooled, liquid. The T_g of an ASD is a function of the molecular interactions between the molecules. One T_g for the solid dispersion indicates that the components are indistinguishable down to the 30μm scale. If more than one T_g is observed for a solid dispersion, this indicates phase separation of the components in the mixture and the two T_gs correspond to the individual components of the phase separated dispersion. (1) Phase separation usually happens before nucleation and crystal growth occur for the ASD.

This chapter describes the characterization of ASDs of AMG 517 in HPMC-AS manufactured by spray drying. The amorphous nature of the ASDs is confirmed by XRPD and modulated DSC. Residual solvent is evaluated by GC and TGA and the glass transition (T_g) is used to evaluate the drying process and to observe trends in several lots of AMG 517 in HPMC-AS with different drug loads.

Methods

Material Preparation - Spray Dry Manufacturing

Ten different ASDs of AMG 517 in HPMC-AS with 0 – 100% drug loads were spray dried using a modified B-290 Buchi Mini Spray Dry System. Additional ASDs of AMG 517 in PVP were spray dried with 30% and 80% drug load. Manufactured ASDs were stored at 2-8 °C with desiccant.

Table 1. Spray dry manufacturing conditions for ASDs

Parameter	Condition
Nozzle type	Ultrasonic
Inlet temperature	~75 °C
Outlet temperature	~ 50 °C
Drying Gas Flow	~ 0.34 kg/min
Atomizing Gas Pressure	~70 psi
Feed Flow Rate	2.0 ml/min

HPLC

ASDs were dissolved in DMSO at ~0.05 mg/ml concentration before being injected onto a C18(2) 150mm x 4.6mm x 5µm column on Agilent 1100 HPLC. Acetonitrile-water mobile phase with 0.1% TFA was used with a 15 minute gradient method.

Particle Size

A Sympatec Particle Size Analyzer with HELOS/RODOS/M disperser and 4mm ASPIROS injector was used. Measuring range used R3 lens (0.5/0.9µm – 175µm) and pressure conditions of 1bar, 30mm/sec.

Scanning Electron Microscopy

An XL-30 ESEM, manufactured by Philips, with Au-Pd sputter coater and 5.0 kV Beam was used to acquire images of spray dried ASD materials.

Residual Solvent and Drying

Drying Method

After spray drying, each ASD was transferred to a glass dish for drying, securely covered with a tissue (to protect from dust and to keep the powder in the dish during drying) and placed

into a vacuum oven at various temperatures ranging from 40 °C to 80 °C. After drying, material was placed in vials and stored in desiccated jars at 2-8 °C.

GC Method

Samples were prepared for GC analysis at ~20 µg/ml (~20mg in 1ml DMSO) and sonicated for 5 – 15 minutes in a sonic bath until the solid completely dissolved in DMSO solvent. The GC (Agilent 6890) system parameters are listed below.

Table 2. Conditions for GC analysis of ethyl acetate in ASDs

Parameter	Condition
Column	30m x 530µm x 3µm DB-624
Temperature Ramp	40 °C to 250 °C at 15 °C/min
Inlet Type	EPC Split-Splitless
Inlet Conditions	3.4 psi
Helium flow	30.2 ml/min
Split Ratio	5:1
Detector Type	FID
H_2 flow	40 ml/min
Air flow	350 ml/min
Makeup flow	20 ml/min

TGA Method

A TGA Q500 (TA Instruments) system was used with aluminum TGA pans. A 10 °C/min ramp was applied between ambient to 300 °C with dry nitrogen purge.

Amorphous Verification

XRPD

Amorphous content was analyzed using a Phillips X'Pert X-ray Powder Diffraction instrument with CuKa, fixed slit lens at room temperature.

Table 3. Conditions for XRPD analysis of ASDs

Parameter	Conditions
Power Settings	45kV, 40mA
Range of detection angle	3.000 deg to 35.000 degrees 2-theta
Steps	0.00837 degree steps at 35.56 sec/degree
	3823 steps
Stage revolution time	2.000 seconds/ revolution

Modulated DSC (mDSC)

A DSC Q1000 (TA Instruments) system was used with crimped aluminum DSC pans and dry nitrogen purge. A heating ramp of 5 °C/min was applied from 25 °C to 250 °C with modulation amplitude of +/- 0.5 °C every 30 seconds.

Hotstage Microscopy

ASD particles were immersed in Resolve Microscope Immersion Oil and observed using a Nikon Eclipse E600 POL microscope with cross-polarizing lens at 50X magnification. The temperature was controlled with Linkam LNP TMS94 hotstage programmed with a 2°C/min ramp.

Results

Material Preparation - Spray drying

Spray dry manufacturing results are shown in Table 4 and Table 5. An exceptionally high yield was obtained due to a modification of the spray dryer system with customized glassware. Sufficient material was generated for use in characterization and crystallization experiments for ASDs of AMG 517 in HPMC-AS and AMG 517 in PVP.

Table 4. Spray dry manufacturing results for HPMC-AS ASDs.

Sample Name	% AMG 517	% HPMC-AS	Amount Sprayed, mg	Yield, (mg)	Yield, %
ASD1	0	100	3000	2100	70
ASD9	15	85	1875	953	51
ASD10	30	70	1875	1113	59
ASD2	50	50	4000	2715	68
ASD3	62	38	4000	2860	72
ASD4	70	30	4000	2660	66
ASD5	75	25	5500	3770	69
ASD6	82	18	6000	4150	69
ASD8	95	5	6250	3915	63
ASD7	100	0	4750	2925	62

Table 5. Spray dry manufacturing results for PVP ASDs.

SampleName	% AMG 517	% PVP	Amount Sprayed, mg	Yield, (mg)	Yield, %
ASD11	50	50	5000	2550	51
ASD12	80	20	5000	3220	64

HPLC Concentration Analysis

Concentration analysis for ASDs shows assay recovery for all ASDs. Most of the ASDs show good recovery, with only a couple exceptions. ASD8 targeted 95% drug load in HPMC-AS with only 86.5% drug load recovered. ASD11 targeted 50% AMG 517 in PVP and shows low recovery of 33%. It is possible that there may be significant heterogeneity in these lots, or that some loss of drug occurred during the spray dry manufacturing process.

Table 6. HPLC Analysis for ASDs prepared by spray drying with HPMC-AS and PVP

Sample Name	Target Drug load (%)	Assay Recovery % AMG 517
ASD1 (100% HPMC-AS)	0	0
ASD2 (50% AMG 517 in HPMC-AS)	50	54.0
ASD3 (62% AMG 517 in HPMC-AS)	62	62.3
ASD4 (70% AMG 517 in HPMC-AS)	70	69.4
ASD5 (75% AMG 517 in HPMC-AS)	75	75.1
ASD6 (82% AMG 517 in HPMC-AS)	82	81.7
ASD7 (100% AMG 517)	100	99.6
ASD8 (95% AMG 517 in HPMC-AS)	95	86.5
ASD9 (15% AMG 517 in HPMC-AS)	15	15
ASD10 (30% AMG 517 in HPMC-AS)	30	25
ASD11 (50% AMG 517 in PVP)	50	33
ASD12 (80% AMG 517 in PVP)	80	80

Particle Size Distribution

A clear relationship between drug load and particle size exists. Particle size trends smaller with higher drug load in the ASDs. In addition, all spray dried ASDs of AMG 517 and HPMC-AS have a d90 particle size between 15 and 40 µm with a small distribution, indicating the spray dry conditions used control the process reasonably well.

Figure 1. Particle size Overlay for selected ASDs of AMG 517 in HPMC-AS.

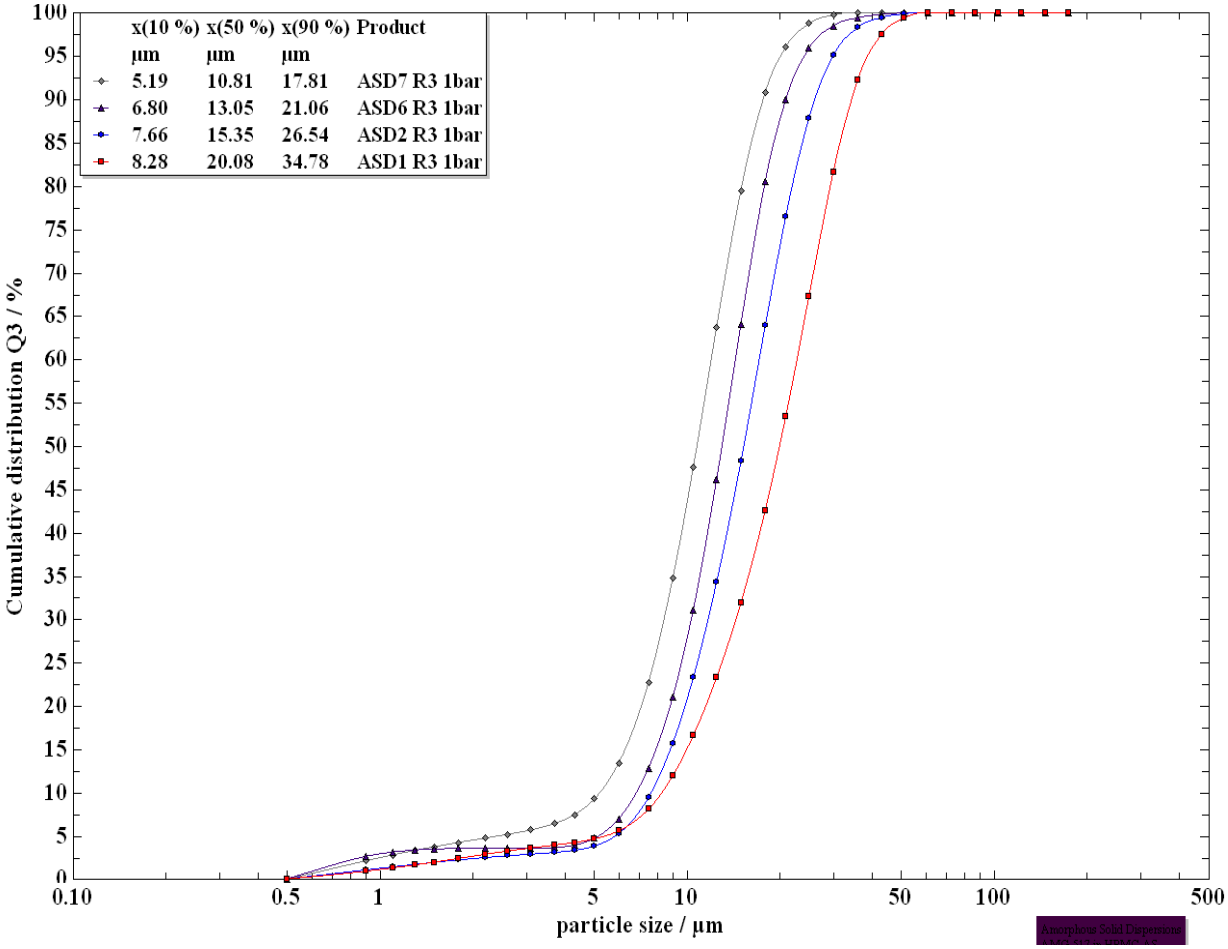

SEM Results

In Figure 2 are shown images of ASDs. Lower drug load ASD particles such as ASD2 (50% AMG 517 in HPMC-AS) appear wrinkled (like deflated soccer balls), while higher drug load ASD particles such as ASD5 (75% AMG 517 in HPMC-AS) are closer to being spherical. It could be that the amorphous drug is stabilized by filling in the space between polymer strands. Crystalline AMG 517 is shown bottom left, with partially crystallized ASD shown bottom right. The partially crystallized ASD appears to have crystalline particles coming out of the spherical ASD particles and from the surface of the particles.

ASD2 (50% AMG 517 in HPMC-AS)

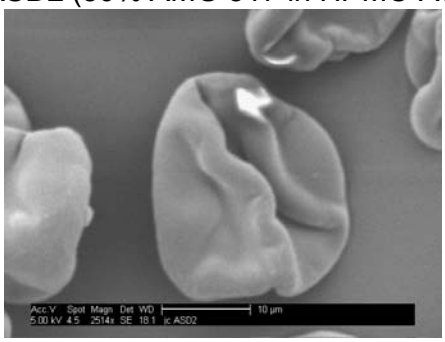

ASD5 (75% AMG 517 in HPMC-AS)

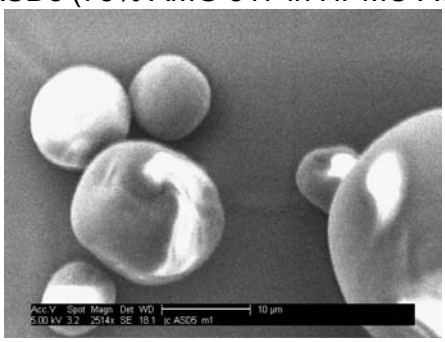

Crystalline AMG 517

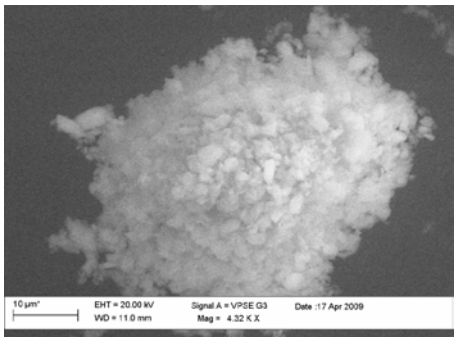

ASD6 (82% AMG 517 in HPMC-AS) after 60°C, 75% RH for 14 days

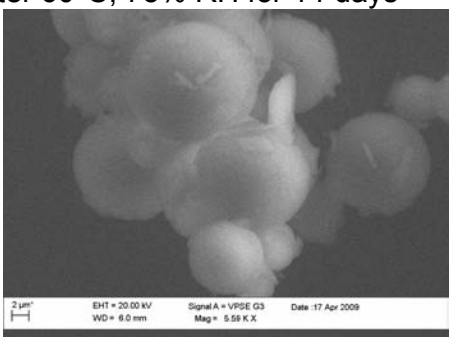

Figure 2. SEM images of ASDs. Top left: ASD2 (50% AMG 517 in HPMC-AS). Top right: ASD5 (75% AMG 517 in HPMC-AS). Bottom left: Crystalline AMG 517. Bottom right: partially crystallized ASD6 (82% AMG 517 in HPMC-AS) after stability 60°C/75% RH.

Residual solvent and Drying

TGA Results

TGA results for ASDs after drying are shown in Table II. The detection limit is ~ 0.05% weight loss. The boiling point of ethyl acetate is 77 °C, but TGA thermograms show weight loss above 100 °C. This suggests that solvent is incorporated into the ASD material lattice, not surface bound. Higher drug load ASDs appear to hold the solvent in the material longer, and it is probable that the drug is interacting with the residual ethyl acetate solvent. Surface bound water is also expected to come off ~ 100 °C, and TGA cannot distinguish between solvent weight loss and water weight loss. A method specific to ethyl acetate is needed to confirm that the weight loss at ~ 100 °C is from residual solvent and not water.

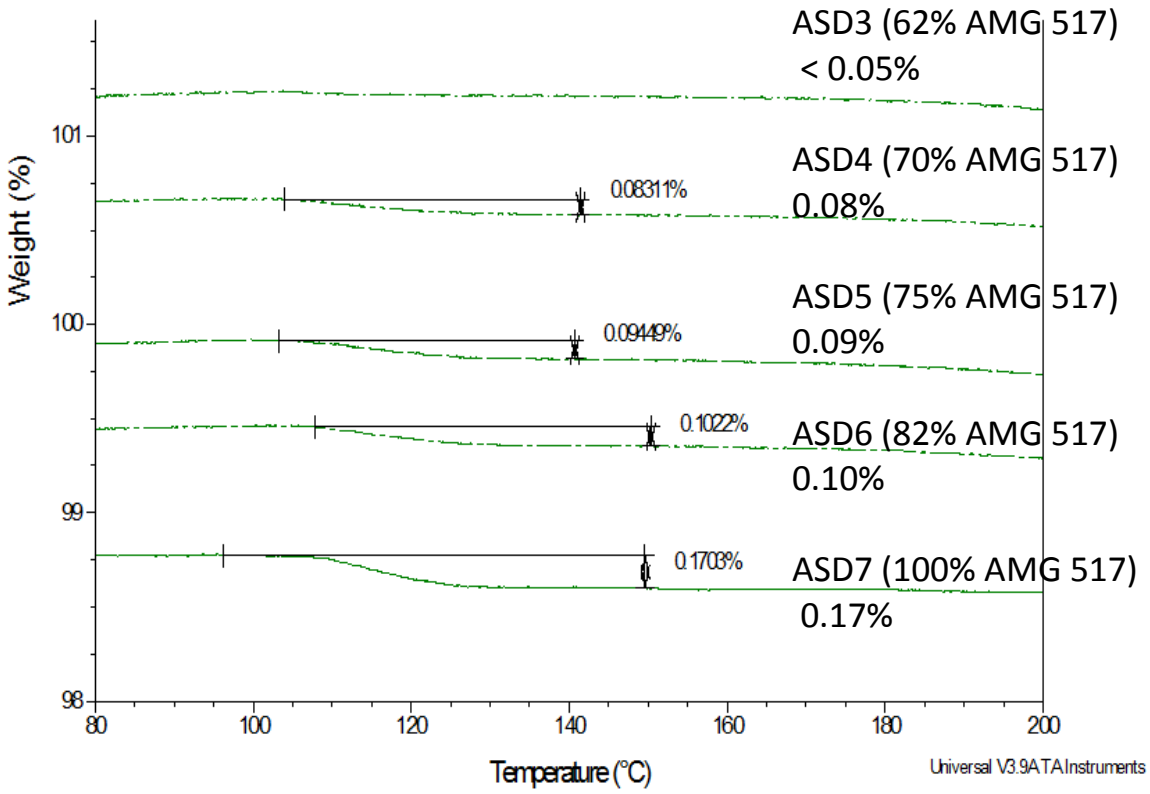

Figure 3. Residual ethyl acetate aolvent weight loss by TGA for various ASDs.

Gas Chromatography (GC)

The GC method used here is specific to ethyl acetate. GC results are compared with TGA and found to compare relatively well for results above 0.05%, as shown in the Table 7. Either method could be used to measure residual ethyl acetate solvent in ASDs of AMG 517 in HPMC-AS. From the GC analysis, it is clear that the solvent loss observed by TGA is ethyl acetate, not water or any other solvent. The GC method is also more sensitive than TGA below 0.05% ethyl acetate and should be used to quantify lower levels of ethyl acetate for ASDs of AMG 517 in HPMC-AS.

Table 7. GC and TGA Results for Residual Solvent

Sample Name	Composition	% EtOAc by GC	% wt loss by TGA
ASD1	HPMC-AS only (no drug)	0.02	< 0.05
ASD9	15% AMG 517 in HPMC-AS	--	< 0.05
ASD10	30% AMG 517 in HPMC-AS	--	< 0.05
ASD2	50% AMG 517 in HPMC-AS	0.01	< 0.05
ASD3	62% AMG 517 in HPMC-AS	0.03	< 0.05
ASD4	70% AMG 517 in HPMC-AS	0.08	0.08
ASD5	75% AMG 517 in HPMC-AS	0.10	0.09
ASD6	82% AMG 517 in HPMC-AS	0.11	0.10
ASD8	95% AMG 517 in HPMC-AS	--	0.07
ASD7	100% AMG 517 (no polymer)	0.17	0.17
ASD11	50% AMG 517 in PVP	--	0.74
ASD12	80% AMG 517in PVP	--	0.22

ASD11 and ASD12 are PVP ASDs. For these, some spray dried material was set aside to compare with dried material of the same lots. PVP ASDs were manufactured in methanol-methyl acetate solvent and not analyzed by GC. The drying time to remove residual solvent for PVP ASDs is longer than for HPMC-AS ASDs. It required > 21 days to dry ASD11 to 0.74% residual solvent and ASD12 to 0.2% residual solvent.

Drying method

Drying curves for the residual solvent drying process is illustrated in the Figure 4 below. Higher drug load ASDs are shown to hold onto residual solvent longer during drying. ASD7 (100% AMG 517) requires longer than 78 hours to dry to 0.17% ethyl acetate, while ASD1 (0% drug) dries to ~ 0.02% in about 30 hours.

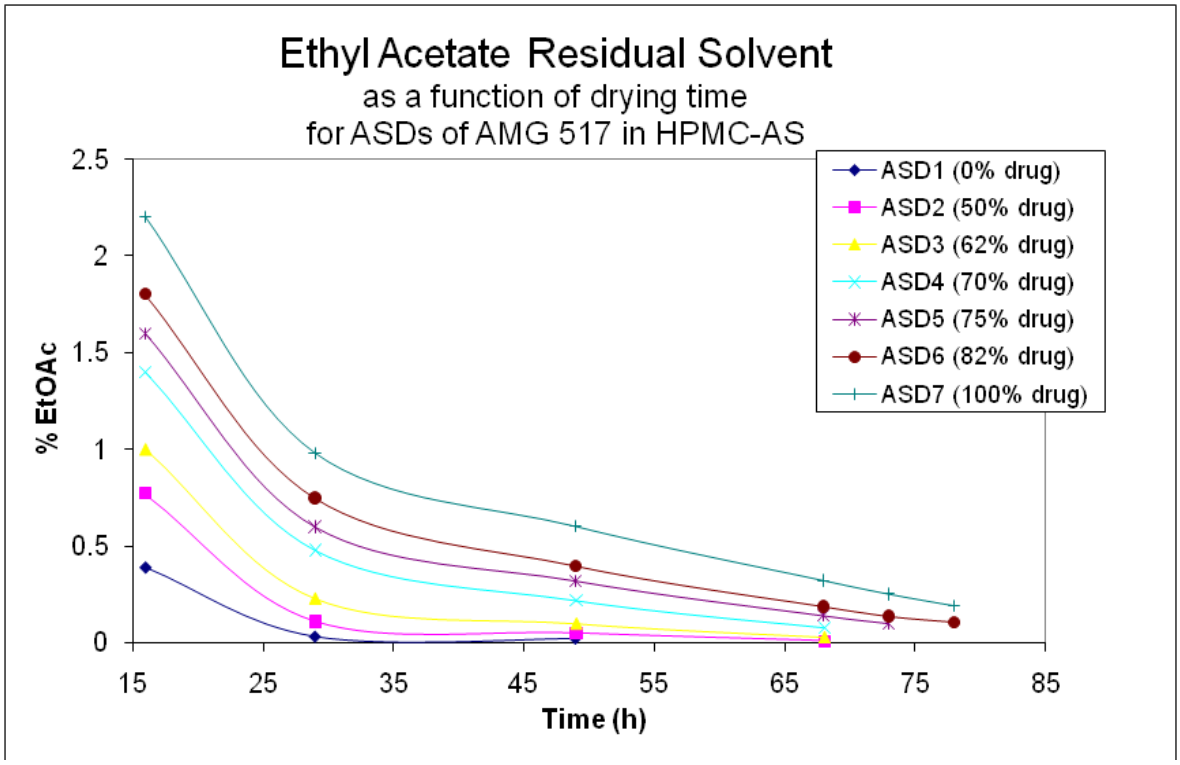

Figure 4. Ethyl acetate residual solvent as a function of drying time for ASDs of AMG 517 in HPMC-AS

Effect of Residual Solvent on ASDs

The T_g of an ASD is affected by residual solvent. As the ASD dries, the T_g of the material generally increases, as illustrated in Figure below for ASD8 (95% AMG 517 in HPMC-AS). There is minimal change in T_g below 0.2 % residual solvent and residual solvent appears increasingly difficult to remove below 0.1%. Drying below 0.2% ethyl acetate is sufficient to stabilize the T_g of AMG 517 in HPMC-AS ASDs for crystallization studies.

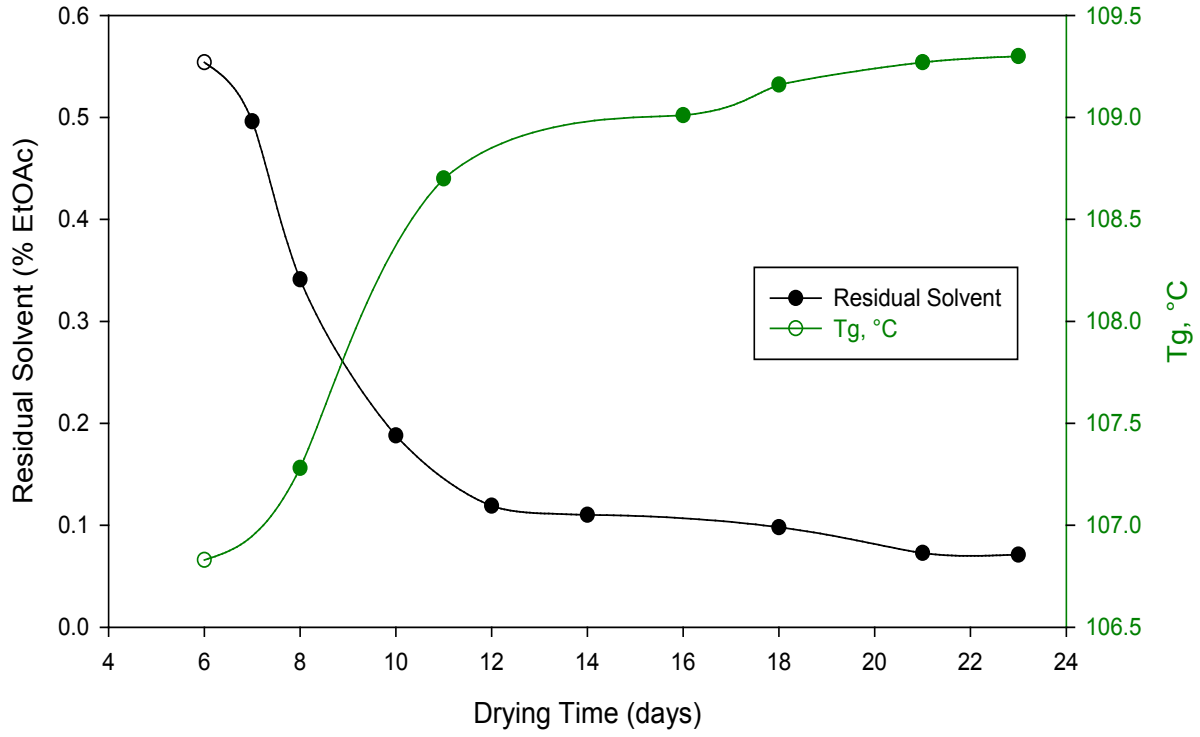

Figure 5. Drying curves for ASD8 (95% AMG 517 in HPMC-AS). Comparison of Residual Solvent (% Ethyl acetate) and T_g as a function of drying time.

Amorphous Verification

XRPD

No crystallinity is observed in the XRPD spectra for the spray dried ASDs, only broad halos indicating a lack of long-range order. The detection limit for crystalline AMG 517 in HPMC-AS is approximately 3%. All manufactured ASDs are initially X-ray amorphous after drying to < 0.2% residual solvent, as discussed in the drying section above.

Comparing the XRPD patterns for ASDs of different drug load, it appeared that the halos for higher drug load ASDs are higher than the halos for ASDs with lower drug load. However, ASD8 (95% AMG 517 in HPMC-AS) has high drug load and discounts the idea that drug load alone is responsible for height of the amorphous halos. It has been recently suggested in the literature that water sorption of the polymer affects the high and low angle halo. (2) Recalling from Table 5, ASD8 has residual ethyl acetate level of 0.07%. Now it is seen that for this ASD system, the XRPD halo height trends with ethyl acetate, rather than drug load.

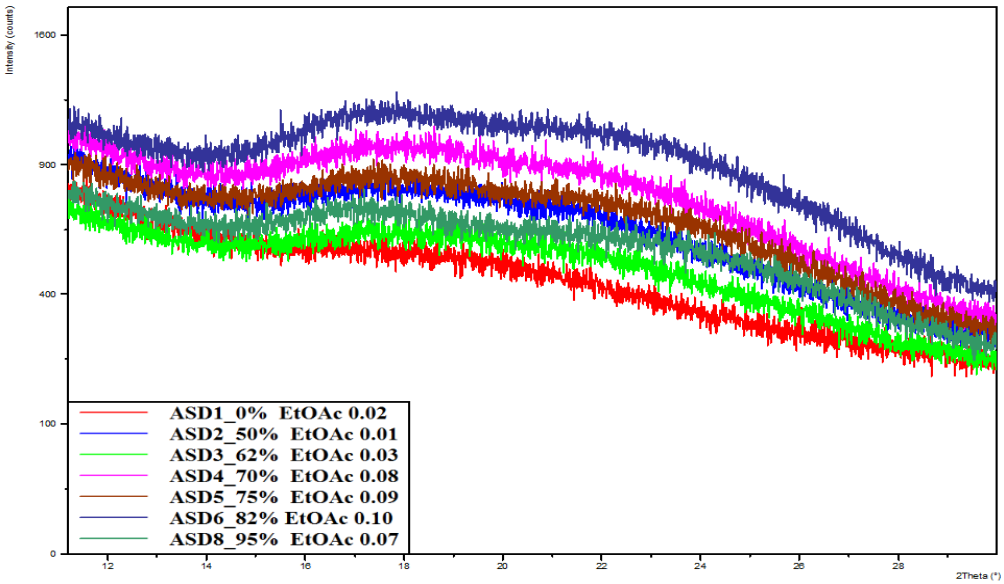

Figure 1. XRPD analysis for spray dried ASDs of AMG 517 in HPMC-AS. All ASDs are initially X-ray amorphous.

Modulated DSC (mDSC) and Hotstage

The total heat flow mDSC thermogram of ASD2 (50% drug load) is shown below. As indicated, the sample is amorphous solid below T_g, then the sample undergoes a slight physical change as a meta-stable liquid before re-crystallization and then melts to become a liquid. The total heat flow curve combined with hotstage pictures gives a helpful visual illustration of the crystallization of an amorphous solid dispersion of AMG 517 in HPMC-AS.

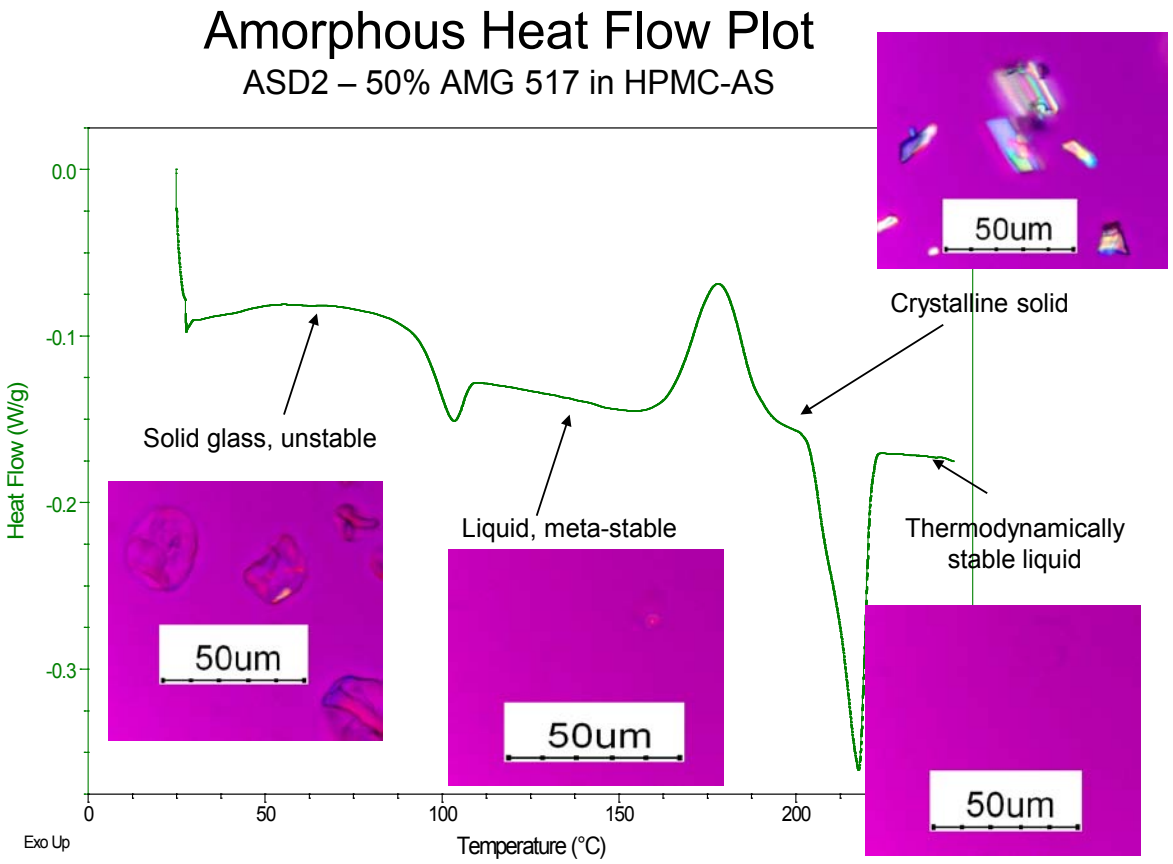

Figure 7. Heat flow plot for ASD2 (50% AMG 517 in HPMC-AS) with images showing particles at different stages.

Glass Transition

The Figure below shows an overlay of mDSC data for selected ASDs and physical mixtures of AMG 517 and HPMC-AS. The polymer HPMC-AS has a T_g around 124.8 °C, while the drug, AMG 517, has a T_g around 110.6 °C. A physical mixture of HPMC-AS and AMG 517 is observed to have two T_g, at 109.5 °C and 124.8 °C, indicating no interaction between the two components of the mixture. Spray dried ASDs of various drug loads, however, are observed have only one single T_g, while the physical mixture has a separate T_g for each component. All the ASDs manufactured for this study are observed to have a single T_g by mDSC analyses.

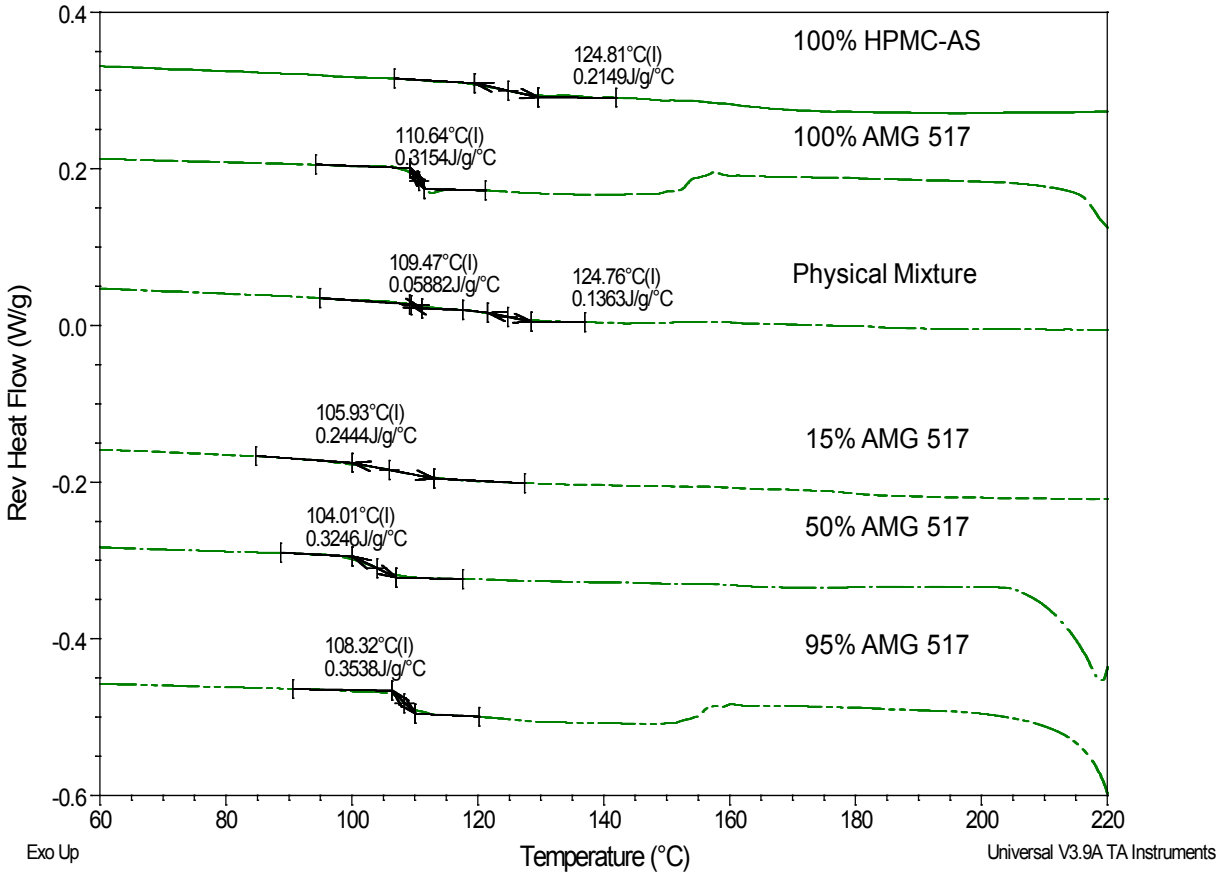

Figure 8. Glass transition of Selected ASDs, as seen in the reversing heat flow curve.

Summary of mDSC Results

Figure 5 shows modulated DSC thermal data for ASDs of varying drug load of AMG 517 in HPMC-AS. Each ASD was analyzed in triplicate and error bars are shown. The melting point of HPMC-AS is measured ~ 290°C and ASDs with drug load below 50% have melting point ~ 290°C, while ASDs with drug load above 50% have T_m ranging from 217°C to 229°C. Similar to a eutectic for crystalline materials, this low T_m for midrange drug load for the ASD system suggests that below 50% drug load, AMG 517 is soluble in HPMC-AS.

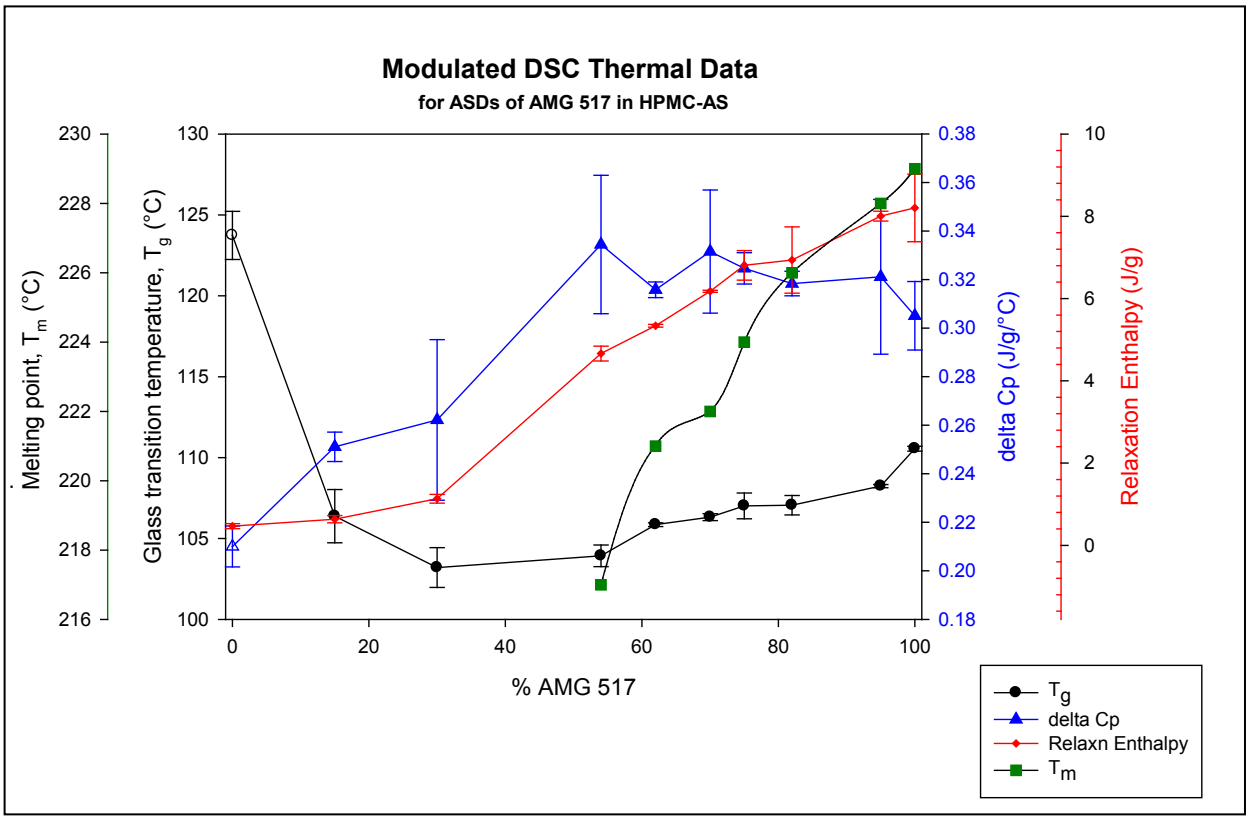

Figure 9. Summary of Modulated DSC Thermal Data for triplicate runs of ASDs of AMG 517 in HPMC-AS. Glass transition temperature, T_g, delta C_p (heat capacity), Enthalpy of Relaxation and Melting point trends are plotted in the graph.

Gordon-Taylor Predictions

Significant T_g depression is observed for ASDs compared to the T_g values predicted by the Gordon-Taylor equation. An extended version of the Gordon-Taylor equation for a ternary system containing solvent, drug and polymer to account for the presence of additional components such as ethyl acetate was also described in Chapter 1. None of the prediction equations account for T_g depression interactions between the ASD components.

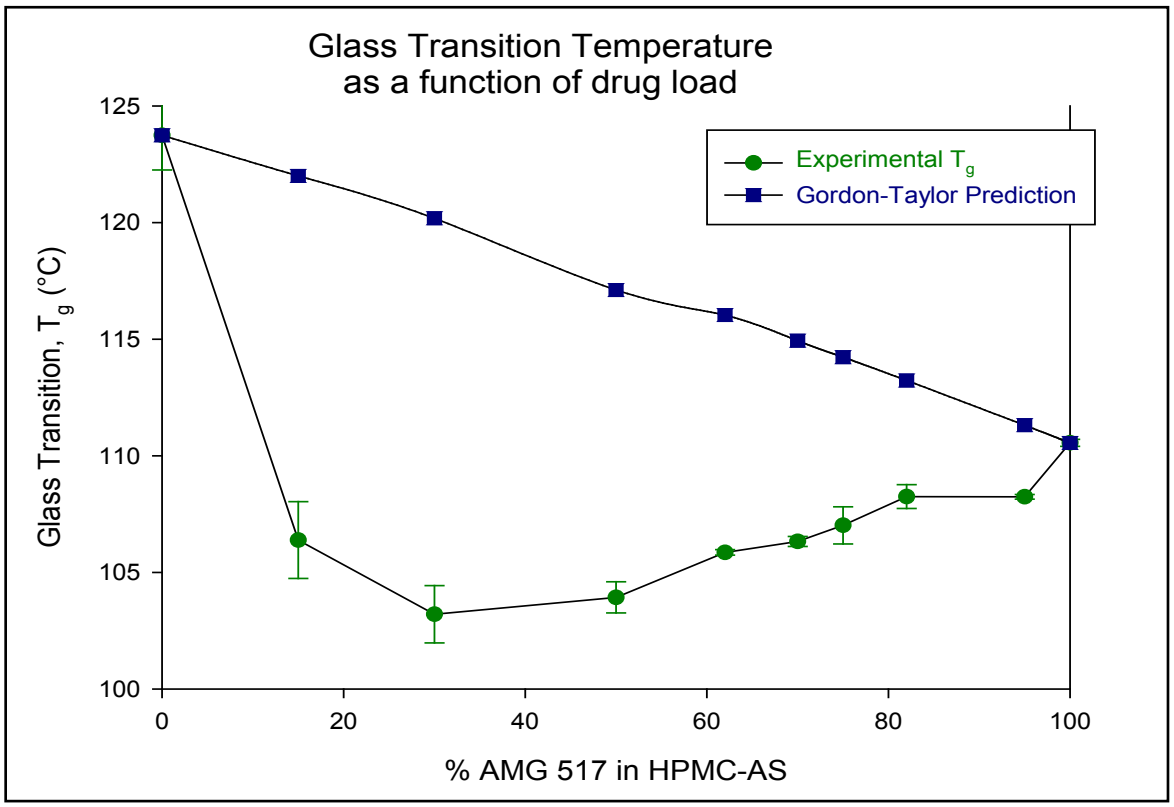

Figure 10. Gordon-Taylor predictions of glass transition compared with experimental T_g values.

The T_g depression observed here indicates that the attractive forces between the drug (AMG 517) and the polymer (HPMC-AS) are less than the drug-drug or polymer-polymer interactions. (3) The molecules of the two components are forced together into one phase by the spray drying and the HPMC-AS provides a barrier to mobility of AMG 517, causing kinetic stabilization.

Conclusions

Amorphous ASDs were manufactured by a spray drying process and residual solvent was dried off. For future characterization with these ASDs, residual ethyl acetate solvent levels below 0.1% are considered dry. Although solvent contributes to the depression of T_g values of manufactured ASDs in general, significant T_g depression is seen which is not accounted for by residual solvent effects. T_g depression observed here indicates drug-polymer interactions with lower attractive strength than drug-drug or polymer-polymer interactions. Further studies with spectroscopic methods could be performed to determine miscibility of AMG 517 in HPMC-AS amorphous solid dispersions.

References – Chapter 3

1. Hancock BC, George Zografi. Characteristics and Significance of the Amorphous State in Pharmaceutical Systems. Journal of Pharmaceutical Sciences1997 August 1, 1996;86(1):1-12.
2. Teng J, Bates S, Engers DA, Leach K, Schields P, Yang Y. Effect of water vapor sorption on local structure of poly(vinylpyrrolidone). Journal of Pharmaceutical Sciences2010;99(9):3815-25.
3. Six K, Berghmans H, Leuner C, Dressman J, Van Werde K, Mullens J, et al. Characterization of Solid Dispersions of Itraconazole and Hydroxypropyl methyl cellulose Prepared by Melt Extrusion, Part II. Pharmaceutical Research2003;20(7):1047-54.

Chapter 4. Crystallization and Stability of ASDs of AMG 517 and HPMC-AS

Introduction

Solid state stability studies are traditionally performed by placing solid samples at controlled temperature and humidity conditions and analyzing the samples at multiple time points. One drawback to this method is the labor-intensive requirements of analyzing multiple times. Another is the uncertainty of not knowing when the actual stability-indicating event happens. Stability prediction can be elusive in these situations, with results often reported in general terms such as "> 6 months stability". Isothermal microcalorimetry offers an alternative way to monitor the stability of solid state samples, offering continuous real-time heat flow data for a single sample at controlled user-specified temperature and humidity conditions. Isothermal microcalorimetry is becoming a more popular technique for studying crystallization of pure amorphous materials. It is proposed to explore the limits of isothermal microcalorimetry in an effort to better understand the behavior of ASDs.

One challenge for analyzing the stability of ASDs is quantifying the crystallinity in ASDs, especially partially crystallized ASD. The presence of polymer in significant amounts can interfere with the sensitivity of techniques such as XRPD. However, SSNMR is a sensitive and specific technique which can distinguish between amorphous and crystalline forms of many drugs. AMG 517 has a CF_3 functional group which experiences different environments in the amorphous and crystalline states, making ^{19}F SSNMR an ideal technique to use for crystallinity analysis of ASDs of AMG 517 in HPMC-AS.

In this chapter, the crystallization of ASDs of AMG 517 in HPMC-AS is evaluated by traditional solid state stability method and by isothermal microcalorimetry. The crystallinity of the stability samples is determined by ^{19}F SSNMR. Rate constants are calculated using Avrami kinetics and statistical predictions are made using JMP design software. In addition, ASDs of AMG 517 in PVP are also evaluated by isothermal microcalorimetry to evaluate the effect of polymer on crystallization rate.

Methods

TAM Crystallization

A 2277 Thermal Analysis Monitor (TAM) isothermal microcalorimeter was used to monitor the crystallization of ASDs of AMG 517 and HPMC-AS at various accelerated stability conditions of temperature and relative humidity. Temperature was controlled using the TAM water bath. Salt solution hygrostats were used to control the relative humidity in each sample cell. After stabilizing the TAM water bath at the desired experimental temperature, each channel was calibrated prior to beginning the crystallization experiments. Between 30 – 150mg of ASD sample was placed into a stainless steel ampoule and hygrostat vials containing appropriate saturated salt solutions were used to control relative humidity inside the ampoule. Reference ampoules either contained reference material and a hygrostat or were left empty. The sample ampoule and reference ampoule for each experiment were simultaneously lowered into the "equilibration position" and held in that position for ~30 minutes to equilibrate before being moved to the sample position to monitor the crystallization reaction. Experiments were

continued until the crystallization event was completed, or 42 days, whichever was shorter. Digitam software was used to record heat flow during the experiment.

Crystallization Conditions

Conditions used for TAM crystallization were chosen to cover a range of possible crystallization rates, using 3 variables: polymer (or drug load), temperature and relative humidity (RH), as illustrated in Box 1. The drug load range is 50 – 100%, temperature range is 50 – 80°C, and RH ranges between 10% – 75%. The temperature and RH range was chosen based on conditions required to sustain the ASDs at or below the predicted T_g value during the experiments. TAM crystallization conditions used are indicated in Figure 1, and also listed in Table 1 and Table 2.

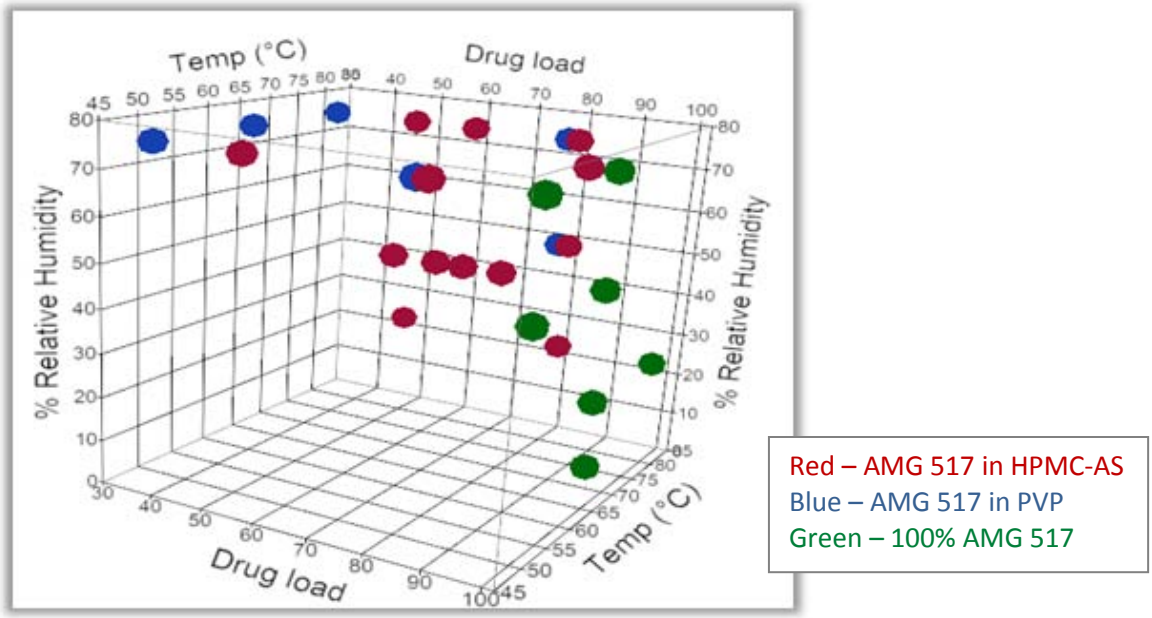

Figure 1 – Box representation of Conditions for TAM Crystallization Experiments. Red circles represent AMG 517 in HPMC-AS, blue circles represent AMG 517 in PVP and green circles represent 100% AMG 517.

Table 1. TAM Crystallization Experimental Information for HPMC-AS ASDs

Sample Information		TAM Condition Information		
ASD name	Drug load (% AMG 517)	Temperature (°C)	Relative Humidity (%)	Salt Solution
ASD2 5075	50	50	75	NaCl
ASD2 8025	50	80	25	$MgCl_2$
ASD2 8075	50	80	75	NaCl
ASD3 6550	62	65	50	NaBr
ASD3 8075	62	80	75	NaCl
ASD4 6550	70	65	50	NaBr
ASD5 6550	75	65	50	NaBr
ASD6 5025	82	50	25	$MgCl_2$
ASD6 5075	82	50	75	NaCl
ASD6 6550	82	65	50	NaBr
ASD6 8025	82	80	25	$MgCl_2$
ASD6 8050	82	80	50	NaBr
ASD6 8075	82	80	75	NaCl
ASD8 6575	86	65	75	NaCl
ASD7 5050	100	50	50	NaBr
ASD7 5075	100	50	75	NaCl
ASD7 6510	100	65	10	LiCl
ASD7 6525	100	65	25	$MgCl_2$
ASD7 6550	100	65	50	NaBr
ASD7 6575	100	65	75	NaCl
ASD7 8025	100	80	25	$MgCl_2$

Table 2. TAM Crystallization Experiment Information for PVP ASDs

Sample Information			TAM Condition Information		
Sample name	Drug load (% AMG 517)	% EtOAc	Temp (°C)	% RH	Salt Solution
ASD11 5075	33	Not Dry	50	75	NaCl
ASD11 5075	33	Dry	50	75	NaCl
ASD11 6575	33		65	75	NaCl
ASD11 8075	33	Not Dry	80	75	NaCl
ASD11 8075	33	Dry	80	75	NaCl
ASD12 5075	80		50	75	NaCl
ASD12 8050	80		80	50	NaBr
ASD12 8075	80	Not Dry	80	75	NaCl
ASD12 8075	80	Dry	80	75	NaCl

Vapor sorption (DVS)

Vapor sorption experiments are used to predict the T_g of each ASD at the experimental conditions. The amount of water taken up at a given RH is determined from water uptake isotherms for ASDs at 25°C, 40°C, 50°C and 60°C. Using water uptake isotherms for an ASD at several temperatures, the "Water Uptake vs. Temperature" curve can be generated for a given RH. Using the water uptake value at a specific set of temperature and RH conditions and applying the Gordon-Taylor equation, the T_g of the sample at those conditions can be predicted. Water vapor sorption experiments were run at conditions listed in Table 3 below.

Table 3. Vapor sorption Conditions

Vapor Sorption Instrument	DVS Advantage 1 (Surface Measurement Systems)
Temperature	25°C, 40°C, 50°C, 60°C
Cycle details	0 - 90 - 0% RH, 10% RH steps, one full cycle
	0.003% dmdt (change in mass per minute), 3 hr max per step
Sample size	5 - 10mg

Traditional Solid State Stability

To compare with TAM crystallization studies, a series of "traditional" solid state stability experiments were set up, using ASD samples of drug load between 50 and 100% AMG 517 in HPMC-AS were placed on stability at four different conditions (25°C/60% RH, 40°C/75% RH, 60°C/30% RH and 60°C/75% RH). Sealed jars containing saturated salt solutions were used for 60°C/30% RH and 60°C/75% RH conditions, while electronically controlled humidity chambers were used for 25°C/60% RH and 40°C/75% RH conditions. Crystallinity was evaluated by XRPD and/or mDSC at appropriate time points ranging from 0 to 19 months, using the same XRD and mDSC methods described in Chapter 3. Samples were removed from the stability

condition when >10% crystallization was observed by XRD and stored at 4°C under desiccation. SSNMR was used to measure crystallinity after the final time point. Figure 2 shows a box representation of the conditions used for the traditional solid state stability experiments.

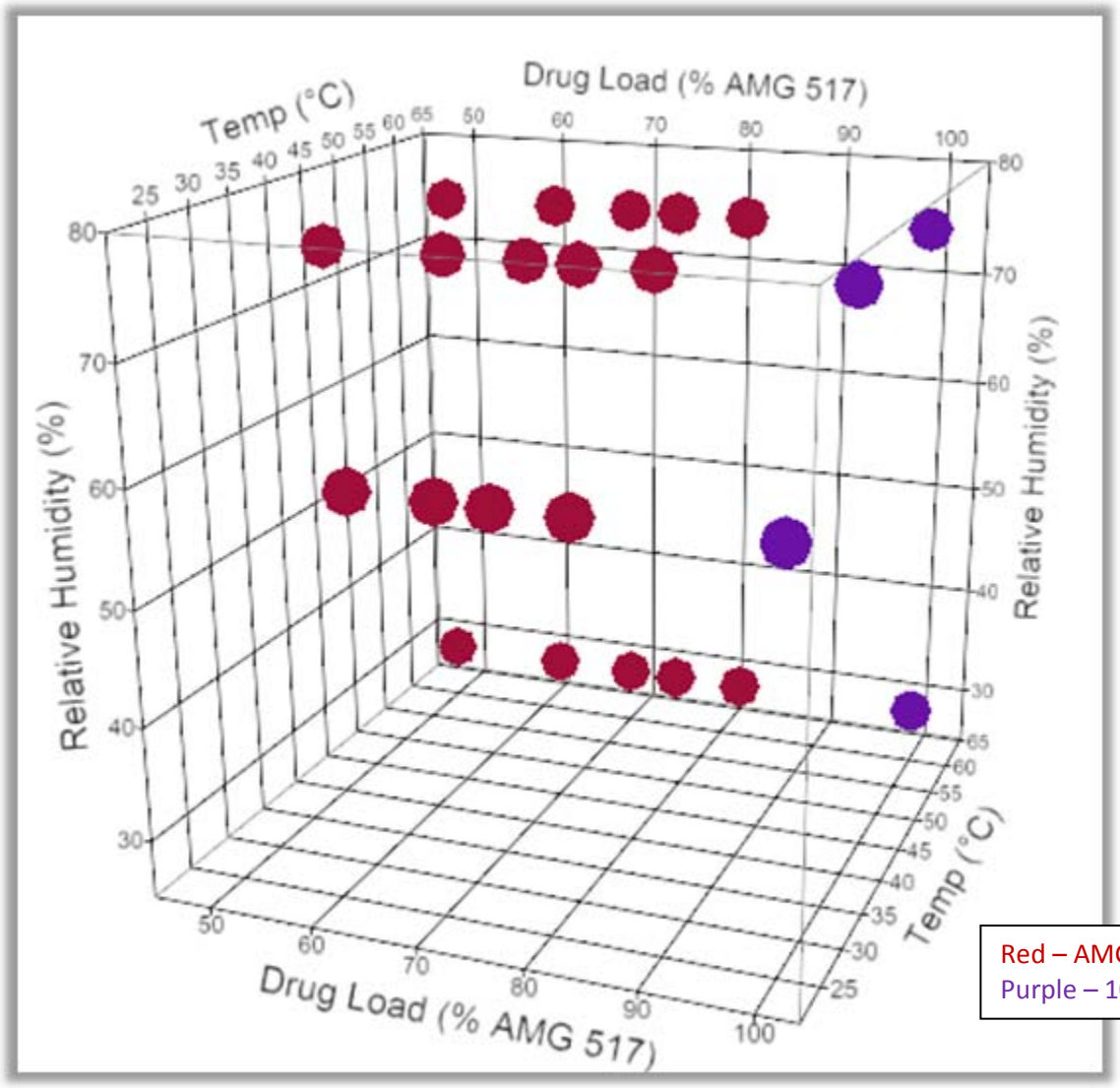

Figure 2 – Box representation of Solid State Conditions. Red circles represent conditions used for ASDs of AMG 517 in HPMC-AS and purple circles indicate 100% AMG 517 conditions.

Crystallinity by SSNMR

All SSNMR measurements were conducted using a Bruker DSX spectrometer operating at a 1H resonance frequency of 600MHz. A Bruker 2.5-mm double resonance magic angle spinning (MAS) probe head was used to record all NMR data. ^{19}F SSNMR spectra were recorded using routine one pulse sequence with sample spinning at 30 kHz. 8 scans were collected for each sample for signal to noise averaging. A recycle delay of 20 seconds was used for all samples. Natural abundance teflon with the fluorine peak at 146.89ppm was used as the chemical shift reference.

^{19}F SSNMR is used to quantify the % crystallinity for samples crystallized by TAM or traditional solid state stability. Pure amorphous and pure crystalline AMG 517 samples are used as reference materials. The % crystalline AMG 517 in each ASD crystallization sample is determined using de-convolution software from Mestrenova.

Crystallization Kinetics

Avrami rate constants are calculated for each TAM crystallization sample, using rate data from the TAM where possible. For experiments where complete crystallization rate data from TAM was not possible, rate constants were estimated using a single end point by estimating n=2, with crystallization times from the end of the TAM experiment and % crystallinity from ^{19}F SSNMR measurements associated with the endpoint of the TAM experiment. Based on the rate constant values, trends were observed for relative humidity and temperature. In addition, it was shown that a log plot of rate constants against drug load could be used to aid selection of drug load for development lots.

Results / Discussion

Crystallization Conditions

The results from water vapor sorption experiments used to predict T_g at crystallization conditions are shown in the Tables below for ASD6 (82% AMG 517 in HPMC-AS). Table 4 shows the % water uptake data for ASD6 (82% drug load) at various temperatures and RH conditions.

Table 4. Vapor Sorption Data for ASD6 (82% drug load), showing % water uptake at various temperature and RH conditions.

DVS Temp	25% RH		50% RH		67% RH		75% RH	
°C	% Water Uptake	T_g °C	% Water Uptake	T_g °C	% Water Uptake	T_g °C	% Water Uptake	T_g °C
25	0.417	104.1	0.699	101.5	0.874	99.9	0.949	99.3
40	0.46	103.7	0.717	101.3	0.913	99.5	1.002	99.0
50	0.487	103.4	0.797	100.6	0.989	98.9	1.08	98.5
60	0.662	101.8	1.016	98.6	1.271	96.4	1.401	95.9
80	1.203*	97.0	--	--	--	--	2.43*	86.4

*These water uptake values are taken from the extrapolated lines for the fitted RH curves.

The data are plotted in Figure 1 to show % Water uptake vs. Temperature. Extrapolating from the lines, according to the fitted equations, it can be roughly predicted what the water uptake would be at higher temperatures. For example, at 80°C/75%RH, the predicted water uptake is approximately 2.4%. The Gordon-Taylor equation (1) predicts ASD6 (82% AMG 517 in HPMC-AS) with 2.4% water to have T_g of approximately 86°C, as indicated in Table 4.

This result suggests that a condition of 80°C/75%RH borders the T_g for ASD6 (82% AMG 517 in HPMC-AS). It is expected that crystallization would occur rapidly above this condition and be significantly slower below this condition. All the other conditions tested for TAM

crystallization have water uptake that predicts T_g well above the experimental conditions. An important question for ASDs is whether crystallization progresses at conditions below T_g as has been suggested previously. (2) Analysis of ASDs by TAM crystallization experiments below T_g can help answer this question for the ASD system of AMG 517 in HPMC-AS.

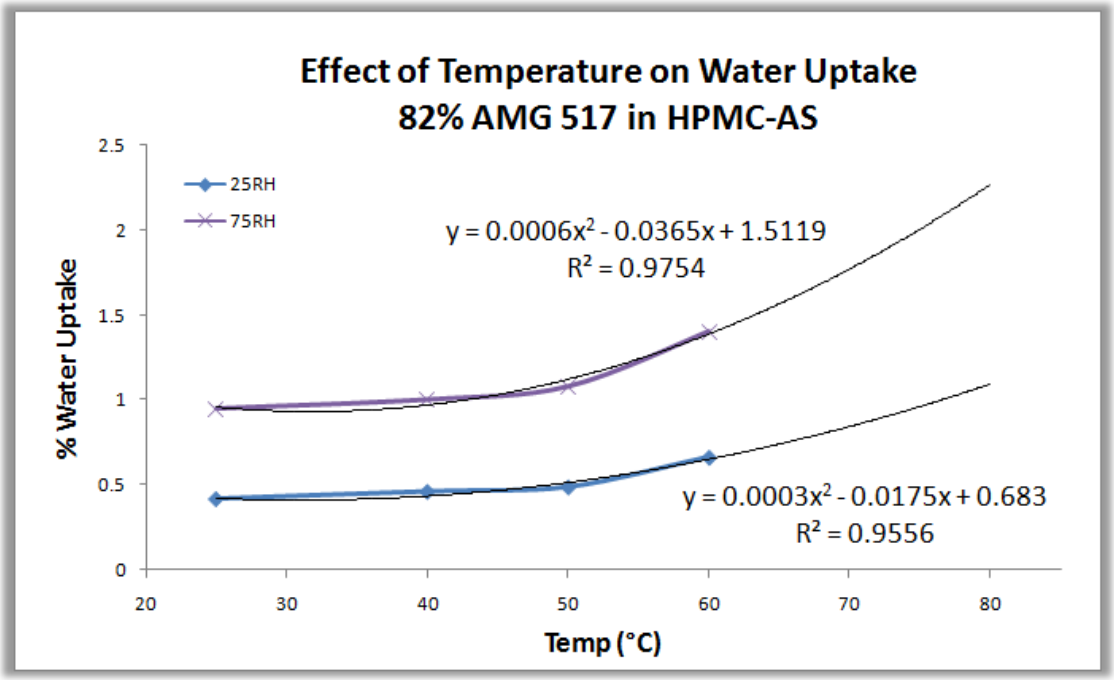

Figure 3. Effect of Temperature on Water Uptake for 82% AMG 517 in HPMC-AS.

The equations shown here are fitted to the data using Excel software. It is unknown what the parameters of the fitted equations correspond to, but the fitting is still useful in determining an approximation of water uptake for T_g predictions which are used to choose relevant crystallization conditions for ASDs.

TAM Crystallization

A TAM plot for ASD7 (100% AMG 517) at 65°C, 25%RH is shown in Figure 2. The heat flow-time curve is shown. At the beginning of the experiment, a short equilibrium is observed, as the temperature of the sample/ampoule is stabilizing with respect to the temperature of the TAM bath. This equilibrium process can take up to several hours, depending on how much pre-equilibration is done prior to the start of the experiment.

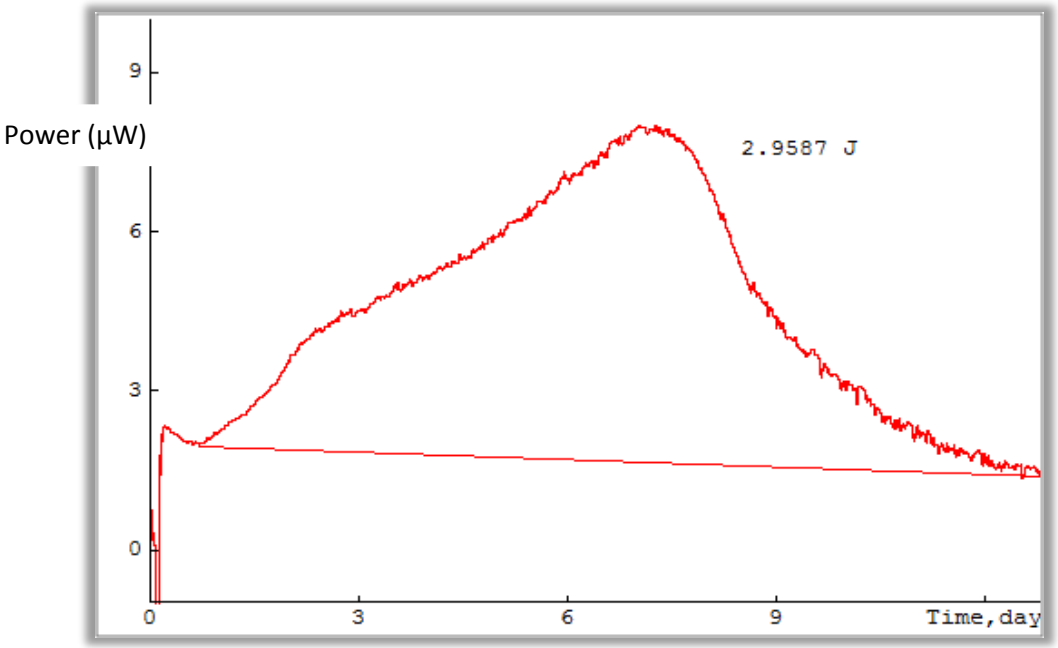

Figure 4. Illustration of the integration for ASD2 (50% AMG 517) at 80°C/75%RH.
The area under the curve is integrated (2.9587 J) and divided by the sample weight (150 mg).
Heat of crystallization for this sample is ΔH_c = 39.6 J/g, after adjustment for drug load.

The TAM plot in Figure 4 shows the heat flow- time curve. A positive heat flow indicates that energy is released during the thermal event. The start of the peak indicates the induction time, while the end of the peak is "t", the time to crystallization. The area under the curve is integrated to give heat in Joules, a measure of the energy involved in the thermal event.

Heat of crystallization, ΔH_c, is calculated for the crystallization peaks by integrating the area under the curve and dividing by the sample weight, as illustrated in Figure 2.

If crystallization is the only heat event happening during the experiment, then analysis is straightforward. However, the TAM is sensitive to very small temperature changes and will pick up thermal events such as crystallization, evaporation and condensation as deviations from zero baselines. The TAM does not differentiate between different types of thermal events and thermal events may overlap if they happen simultaneously, so results can be difficult to interpret if multiple events are happening in the experimental environment.

Due to the sensitivity of the microcalorimeter, an equilibration event is observed at the beginning of the experiment for all of the TAM plots. This is primarily because the temperature of the ampoules is not completely equilibrated with the temperature of the microcalorimeter bath. In some instances, the hygrostat also takes time to equilibrate with the sample inside the ampoule at the experimental temperature and this evaporation/condensation process can extend the apparent equilibration time beyond the first couple hours of the experiment. This was observed in several of the experiments at 25%RH, rendering much of the 25%RH ASD data unusable for observing crystallization. The samples are typically placed in the "equilibration position" to hasten temperature equilibration before being lowered into the sample position. Extended equilibration of the sample prior to the start of the experiment can risk missing part of the crystallization event. In some cases, the crystallization event may begin before the system has completely equilibrated.

TAM Noise and Detection Limits

The TAM noise specifications are +/- 20 nW for an empty 4mL channel. The detection limit is typically considered to be 3 – 5 times the signal-to-noise ratio for an analytical method. Based on this criteria, the detection limit for this method is < 100nW (or 0.1 μW).

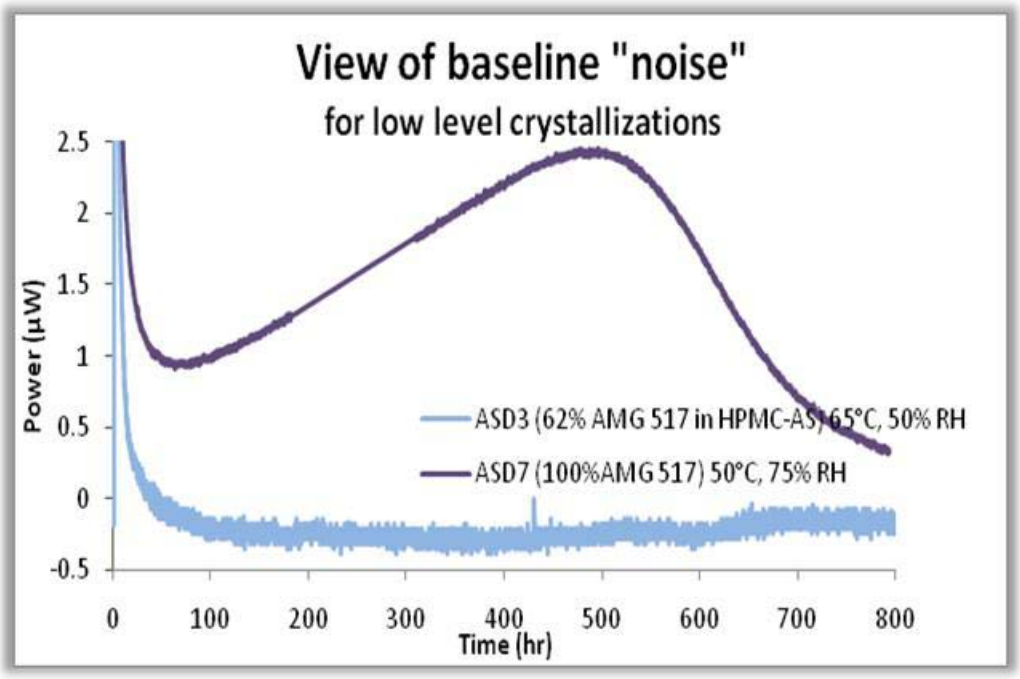

Figure 5. ASD7 (100% AMG 517) at 50°C/75% RH compared with ASD3 (62% AMG 517 in HPMC-AS) at 65°C/50%RH.

A comparison of the baselines for ASD7 at 50°C/75%RH and ASD3 at 65°C/50%RH is shown in Figure 5. A clear crystallization event is observed for ASD7 (100% AMG 517) at 50°C/75%RH, with low power over several weeks. The crystallization for ASD3 (62% AMG 517 in HPMC-AS) is so slow that little change is detected over several weeks. The response is slightly higher than the detection limit for the instrument, indicating there may be some real heat signal buried in the noise.

Crystallizations with 100% ASD (No Polymer)

Crystallization of amorphous spray dried drug (100% drug load) was evaluated. Clear crystallization events were observed for spray dried 100% AMG 517 at several of the crystallization conditions chosen in the experimental design. Crystallinity analysis with ^{19}F SSNMR after the TAM experiments confirms that each of the 100% AMG 517 samples crystallized completely during the TAM experiments.

Effect of Relative Humidity

An overlay of ASD7 (100% DL) at 65°C/10%RH, 65°C/25%RH and 65°C/75%RH is shown in Figure 6. As expected, crystallization proceeds faster with higher humidity conditions for samples run at the same temperature. The peaks generated from fast crystallizations are higher and sharper, and the peaks for slower crystallizations are lower and broader. The crystallization at 65°C/10%RH proceeds so slowly that it requires 42 days to complete and when plotted on the same scale as the faster crystallizations, the "peak" is barely apparent.

For the slow crystallization at 65°C/10% RH in Figure 4, there is a significant rise and fall in the baseline of ~ 2 μW over several weeks, resulting in a defined crystallization peak.

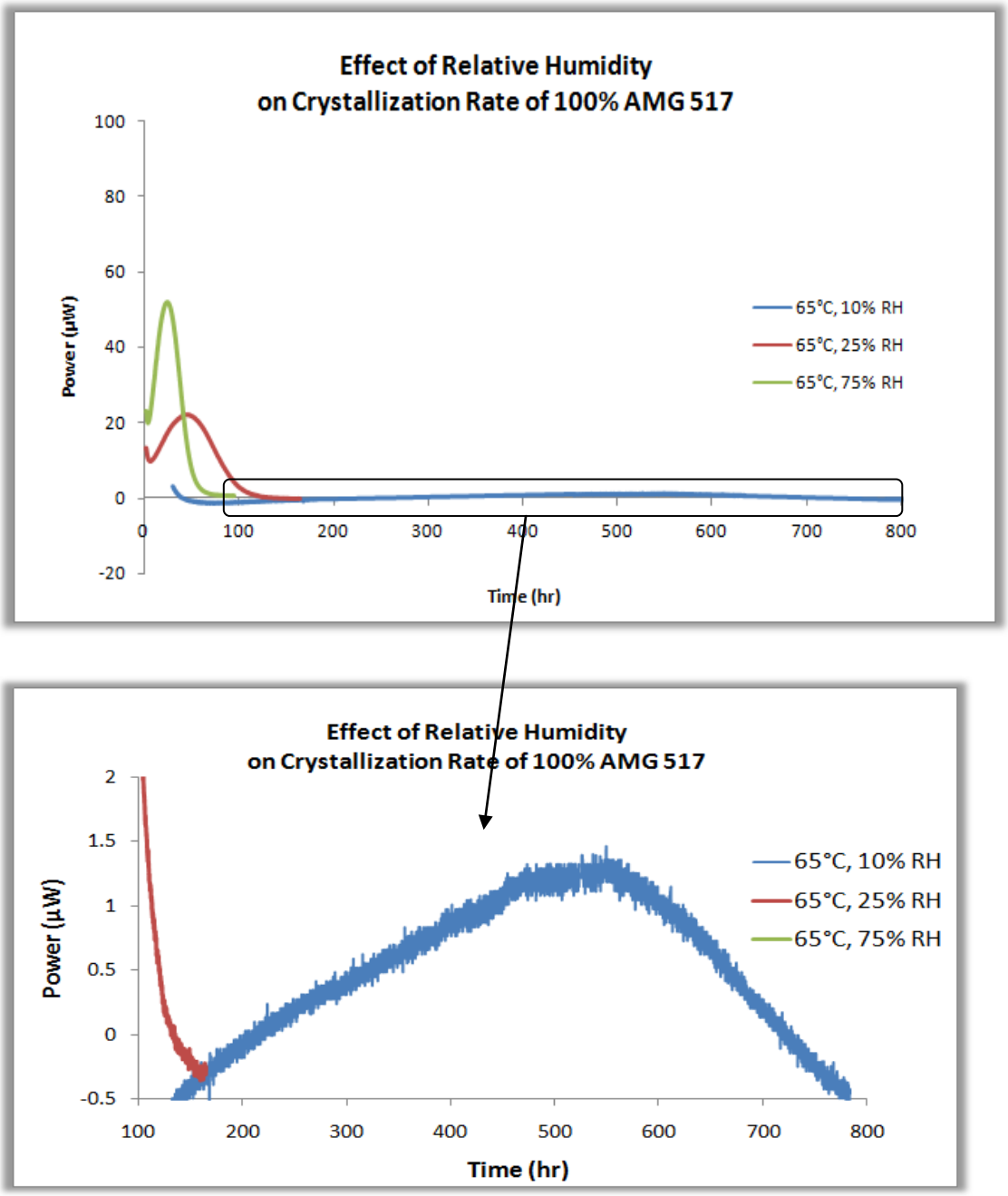

Figure 6. Effect of relative humidity (RH) on crystallization rate for ASD7 (100% DL). Higher RH increases crystallization rate for samples at the same temperature. At conditions of 65°C/10%RH (blue), slow crystallization occurs over 42 days and the peak is barely detected in this experiment. Crystallinity was confirmed at the end of the experiment for each sample. Enthalpy of crystallization, ΔH_c, values are 26.3, 39.4 and 41.3 J/g, for 10%RH, 25%RH and 75%RH, respectively.

Effect of Temperature

Temperature also has a significant effect on the crystallization rate of spray-dried AMG 517, as shown by the TAM experiments at 25%RH. An overlay of ASD7 (100% DL) 80°C/25%RH (red) with 65°C/25%RH (green) is shown in Figure 7. Higher temperature increases crystallization rate, with the 80°C experiment completing crystallization in less than 2 days and the same sample at 65°C takes about 5 days to complete the crystallization.

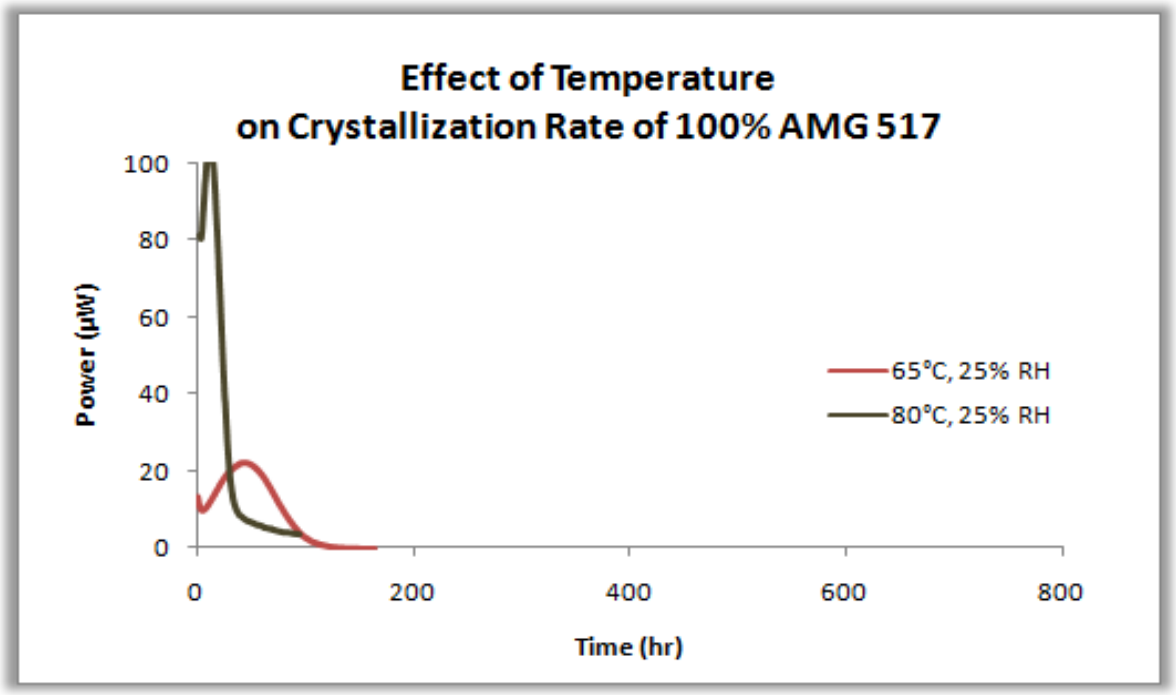

Figure 7. Effect of temperature on crystallization rate of 100% AMG 517 at 25%RH. Higher temperature increases crystallization rate. Crystallinity was confirmed at the end of the experiment for each sample. Integrated areas under the peaks for each sample yield enthalpy of crystallization, ΔH_c, values of 43.3 and 39.4, for 80°C/25%RH and 65°/25%RH, respectively.

At 75%RH the same temperature trend is observed, with higher temperature causing much faster crystallization, as shown in Figure 5. At 50°C/75%RH, a slow crystallization is observed by TAM, with a slow crystallization event completing in about 33 days.

It is interesting to note that the heat of crystallization, ΔH_c, for 100% AMG 517 is found to be ~ 40 J/g for most conditions. The total heat of crystallization is expected to remain the same for the same material. However, less stressful experimental conditions appear to not only slow down the rate of crystallization, but also reduce the crystallization energy. This may suggest an issue with using the TAM to detect low levels of heat flow over long experimental times, but could also indicate a real change in crystallization mechanism at milder conditions.

Overall, the experiments with 100% AMG 517 show that crystallization events can be detected by TAM at elevated temperature and RH, if the crystallization rate is fast enough to complete within six weeks. In general, the expected trend of increased crystallization rate with increased temperature and relative humidity is confirmed. As the crystallization rate decreases, the observed crystallization peaks broaden and shorten. At lower temperature and relative humidity conditions, very slow crystallization is observed to occur over a period of days to weeks.

Crystallizations with HPMC-AS ASDs

ASDs have been reported to inhibit crystallization of certain drugs, including AMG 517. (3) The TAM crystallization experiments clearly show this to be the case for ASDs of AMG 517 in HPMC-AS. The trends and insights gained from observing the crystallization of ASDs of AMG

517 in HPMC-AS with TAM at different conditions are discussed. ^{19}F SSNMR crystallization analysis confirms the partial crystallization of ASD samples at most conditions (data shown in Table 7).

The highlighted region for Figure 8 displays the low level signals for the very slow reactions of ASDs at 65°C/50%RH, where the pure drug crystallized completely in less than 7 days. At a glance, the TAM experiment does not appear to be able to detect such slow crystallizations, but it is more instructive to consider detection limits. The detection limit of the instrument is < 0.1 μW. For these experiments, the signal noise is ~ 150 - 200 nW which is higher than the detection limit and supports the proposal that some real heat signal is being observed. It is possible that some of the apparent "noise" in these TAM plots has buried in it low levels of heat change associated with crystallization for these samples. However, the process is so slow that, for practical purposes, no clear crystallization can be defined for these ASD samples at these conditions.

For each ASD at 65°C/50%RH, no crystallization peaks are defined by the TAM. However, each of the ASD samples in Figure 8 has between 5 – 10% crystalline as measured by ^{19}F SSNMR. This means that there is a very slow crystallization taking place which only begins to crystallize within the 6 week experimental timeframe and is not energetic enough to be detected by the TAM instrument.

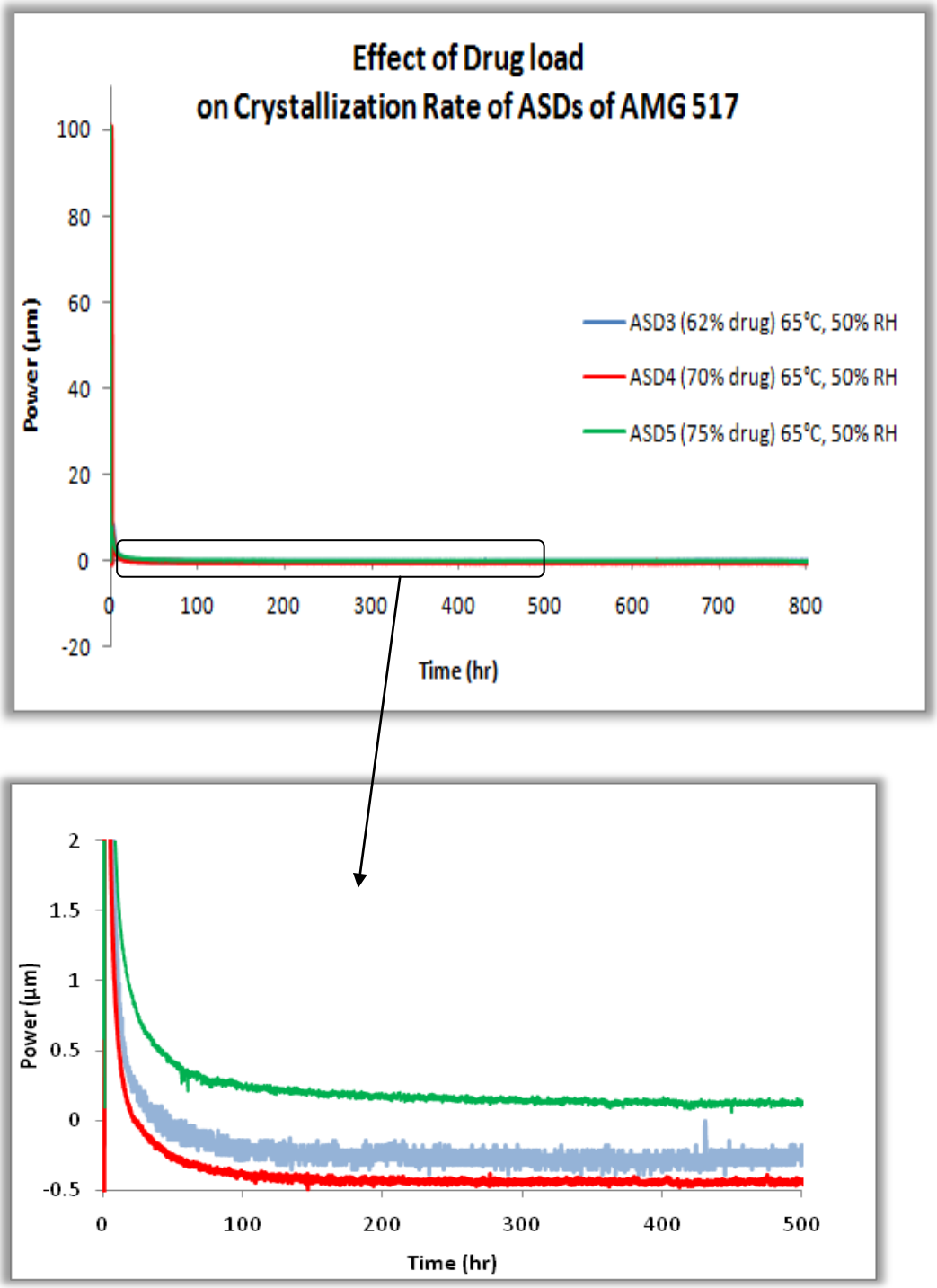

Figure 8. Effect of Drug load on Crystallization Rate of AMG 517 in HPMC-AS at 65°C/75%RH. No clear crystallization events are observed in these plots over a period of 4-6 weeks.

Effect of Temperature, Humidity and Drug load on ASD Crystallization

Due to the slow crystallization of ASDs compared to drug-only samples, good crystallization data was rare for ASDs. The presence of polymer makes a big difference in slowing the crystallization rate. As long as some polymer is present, the crystallization is significantly slower; the amount of polymer in the ASD is less important than the effect of temperature and relative humidity. HPMC-AS inhibits crystallization, but if the experimental conditions are stressful enough, the ASDs will crystallize.

An overlay of showing the effect of relative humidity on ASD crystallization rate is shown in Figure 9. An overlay of ASD6 (82% AMG 517 in HPMC-AS) at 50°C/75%RH, 65°C/75%RH and 80°C/75%RH is shown in Figure 10. Similar to the trends seen for the pure drug, crystallization proceeds faster with higher humidity and higher temperature conditions for samples run at the same temperature. The energy associated with the crystallization is much slower for ASDs, although the general trends are similar. The only conditions that show a clear crystallization event for 82% AMG 517 in HPMC-AS is at 80°C/75%RH. For the lower conditions, crystallization of the ASDs proceeds so slowly that it requires >>42 days to complete and the crystallization plot from the TAM does not provide useful rate data.

The effect of drug load on crystallization rate is shown in Figure 11 for conditions of 80°C/75% RH with drug load of 50%, 62% and 82% AMG 517 in HPMC-AS. All three ASDs have crystallization events around 12-15 days.

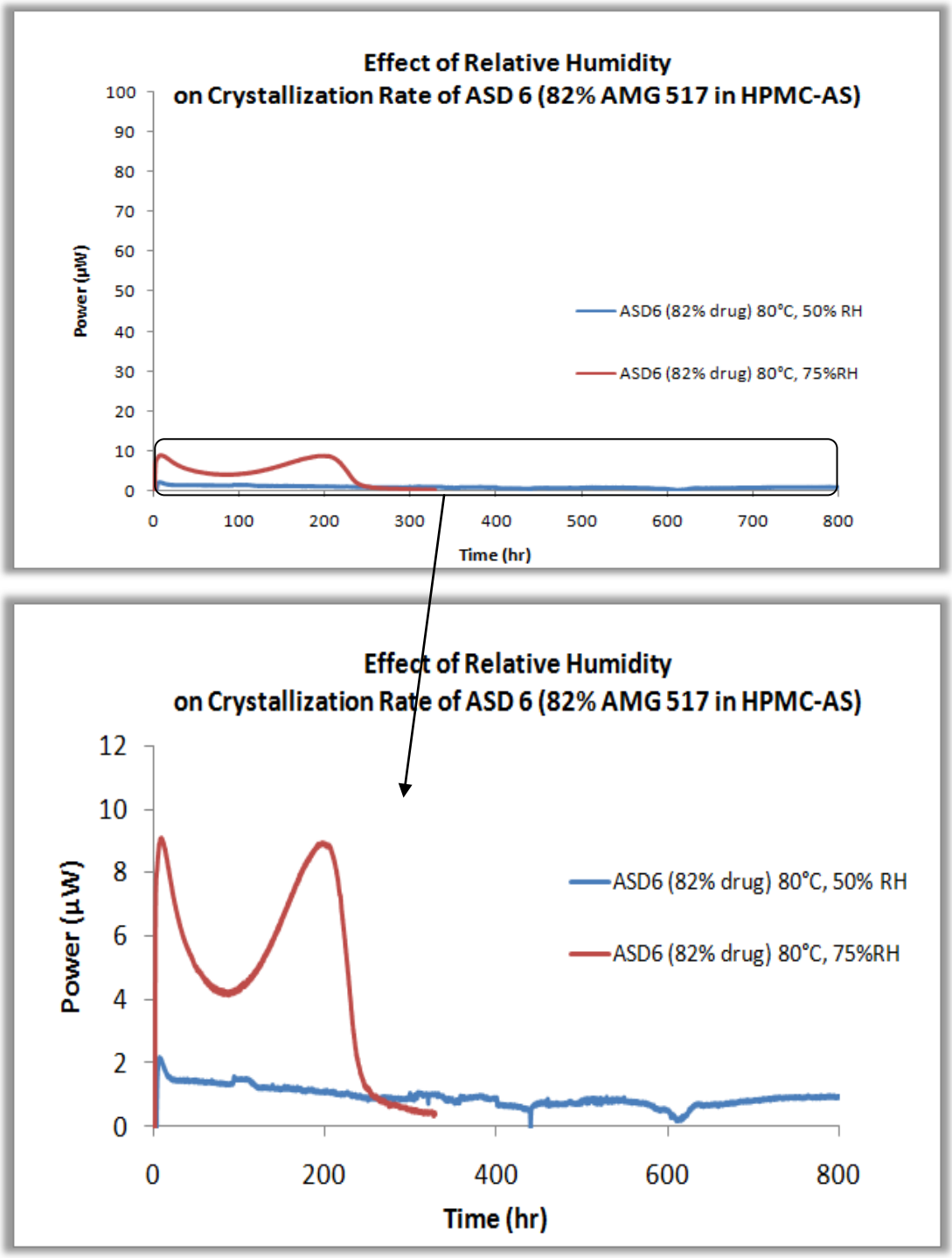

Figure 9. Effect of Relative Humidity on the Crystallization Rate of ASD6 (82% AMG 517 in HPMC-AS). At 80°C/75%RH causes crystallization, but 50%RH does not provide clear crystallization data for the sample.

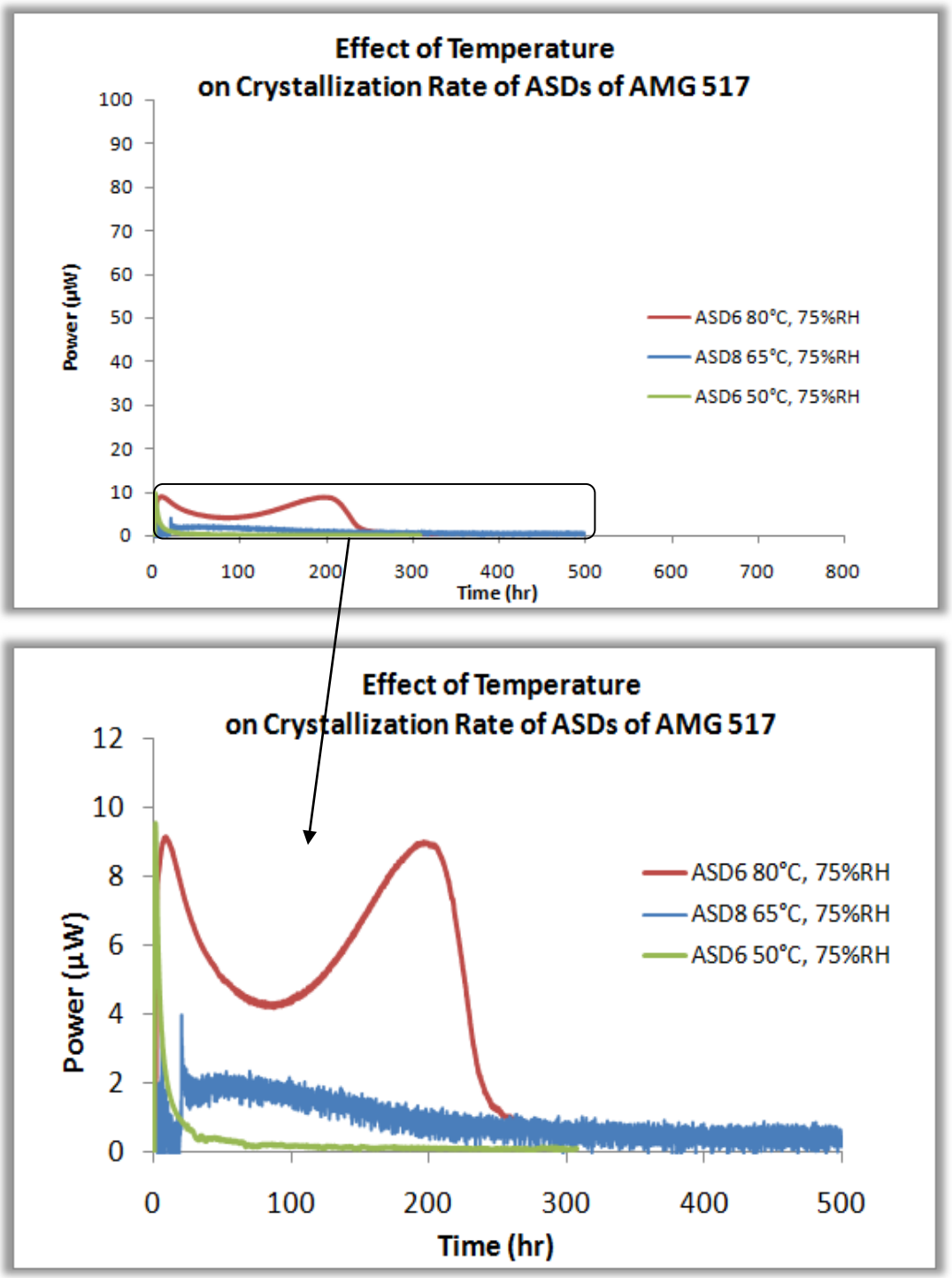

Figure 10. Effect of Temperature on the Crystallization Rate of ASD6 (82% AMG 517 in HPMC-AS). At 75%RH, 80°C causes crystallization, but 65°C and 50°C does not appear to induce crystallization of the ASD.

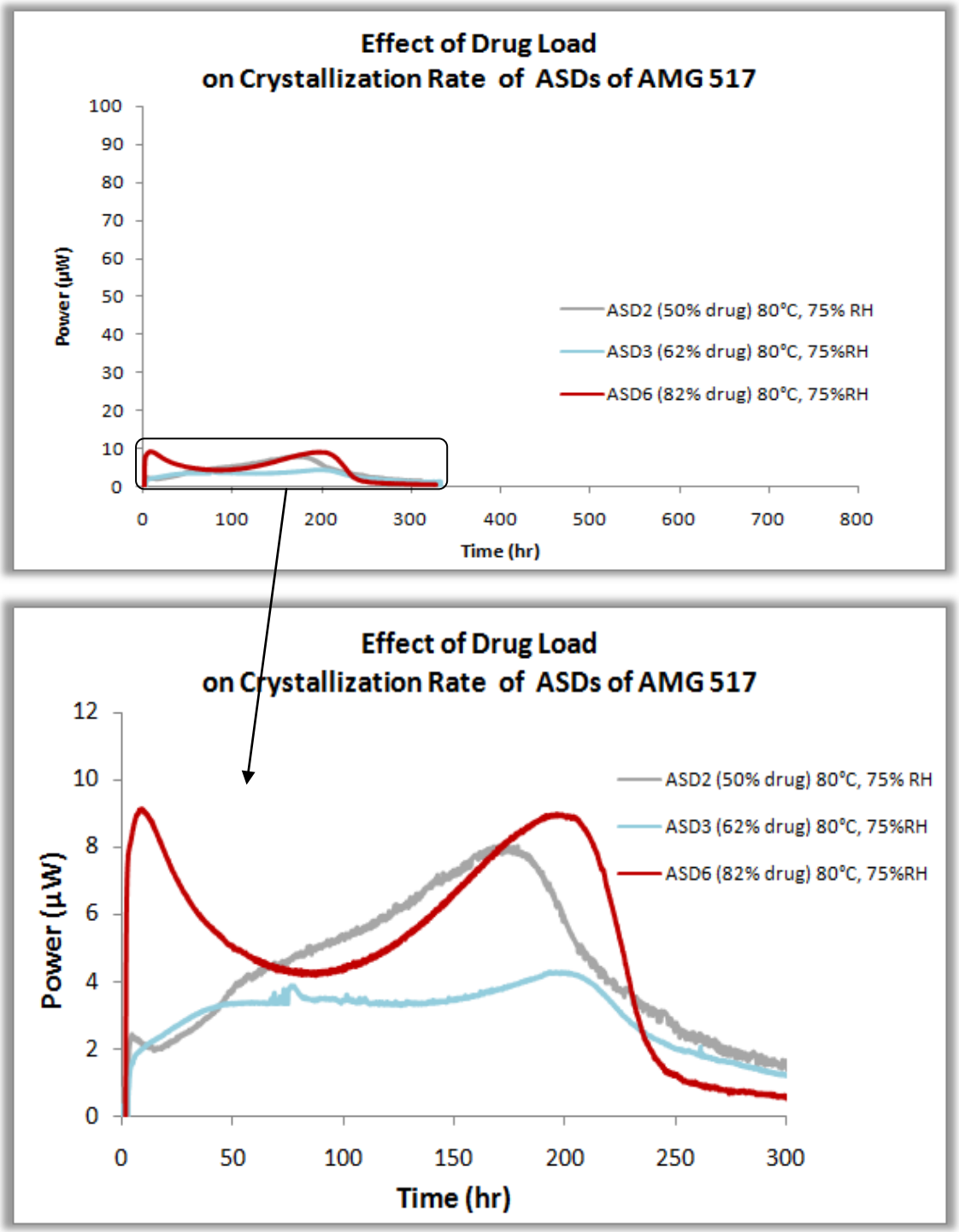

Figure 11. Effect of drug load on crystallization for ASDs of AMG 517 in HPMC-AS at 80°C/75% RH. At first glance, drug load does not appear to significantly affect the crystallization rate of ASDs of AMG 517 in HPMC-AS.

Looking more closely at the TAM profile at 80°C/75%RH from Figure 11, there appears to be two distinct crystallization events happening for the 82% drug load sample. As drug load decreases to 62% AMG 517 in HPMC-AS, the two events run together and at 50% AMG 517 in HPMC-AS, the early event appears to be absent and only the main crystallization event is apparent. This drug load dependent behavior suggests a phase separation that was not observable by mDSC. If the super-saturation level of the ASD system is around 50%, the first crystallization event corresponds to a drug-rich domain, with the second event corresponding to a more intimately mixed domain.

After the TAM experiments, each sample was analyzed for crystallinity by ^{19}F SSNMR. One surprising result from ^{19}F SSNMR data is that ASDs do not appear to crystallize completely – there is a mixture of amorphous and crystalline drug in the "crystallized" ASD. Not all the drug in the ASD crystallizes during the crystallization event. This suggests that a third domain may exist. It could be imagined that very small drug domains exist and are bound up in the polymer such that they cannot nucleate to initiate crystallization. From the ^{19}F SSNMR, it is measured that ~60-80% of the drug in each ASD is crystallizing at 80°C/75%RH leaving ~ 20 – 40% of the drug in the ASD in a phase mixed state, even after the crystallization event has occurred.

Summary of Crystallization Data for ASDs of AMG 517 in HPMC-AS

A summary of all the crystallization data is available in Table 5. Although the TAM plots for ASD samples are not as clean as the 100% drug data, ASDs display the same general temperature and humidity trends as drug-only samples and some important insights can be gained from the ASD crystallization data. First, in terms of predicting the crystallization time, the amount of ASD in the sample appears to matter less than the conditions used. That is, a small amount of polymer added to the pure drug has a dramatic effect. The presence of HPMC-AS with AMG 517 causes slower crystallization compared with pure drug.

Second, the crystallization rates of ASDs are slower than drug alone, but the temperature and relative humidity trends are shown to be the same. Like the 100% AMG 517 (pure drug) samples, ASDs with polymer also crystallize faster with higher temperature and humidity conditions. This is basically a T_g effect – the closer the conditions are to the T_g, the faster the crystallization progresses. The ASD conditions which show clear crystallization of the drug in polymer have predicted T_g values right at the experimental conditions.

Third, the polymer system does a good job of stabilizing the drug against rapid crystallization, but the crystallization still happens. The crystallization event for ASDs may take days, weeks or longer to complete and may not be observable even with sensitive isothermal microcalorimetry methods, but other methods such as SSNMR show the crystallization is still occurring. Even at less stressful conditions, slow crystallization is still observed. This finding is consistent with the T_g depression observed. Sometimes the slow crystallization is virtually undetectable by TAM experiments and there may be several different factors influencing the rate

and extent of crystallization. For such slow crystallizations, orthogonal methods of assessing crystallization (such as SSNMR) can be useful in determining crystallization rates.

Fourth, the TAM profiles indicate a drug load-dependent phase separation for ASDs, causing distinct crystallization events which may be the result of drug-rich domains existing above the miscibility of the AMG 517 in HPMC-AS. The drug-rich domains could account for the relatively fast first crystallization event for higher drug load ASDs. In addition, the *incomplete* crystallization of ASDs suggests a third phase which is stuck in the polymer and doesn't crystallize at all.

Finally, the crystallization enthalpy, ΔH_c, is approximately 40 J/g for pure spray dried AMG 517, and approximately 20 J/g for ASDs of HPMC-AS. The measured crystallization enthalpy for ASDs is approximately half that of pure drug samples.

TAM Crystallizations with PVP ASDs

Polymer type and residual solvent content also affect the crystallization of ASDs. Two additional ASDs at 80% AMG 517 and 33% AMG 517 were prepared using PVP as the polymer matrix instead of HPMC-AS.

Effect of Polymer on Crystallization of AMG 517

Figure 12 shows a comparison of ASD12 (80% AMG 517 in PVP) with ASD6 (82% AMG 517 in HPMC-AS) with the PVP ASD having faster crystallization than the HPMC-AS ASD, suggesting that HPMC-AS may stabilize the drug more than PVP. A possible cause for this is that PVP sorbs much more water than HPMC-AS, and the T_g of PVP ASDs due to water uptake is predicted to be lower than HPMC-AS ASDs at the same conditions.

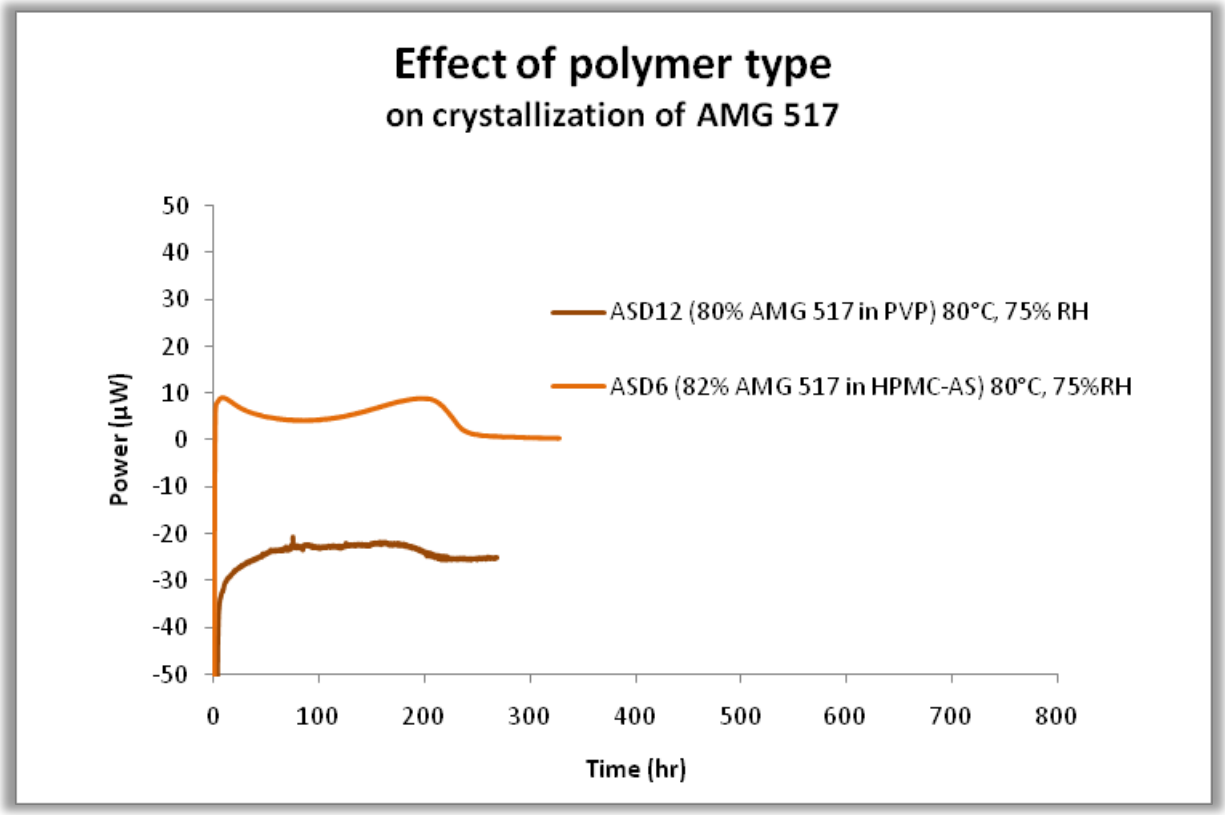

Figure 12. Effect of polymer type on crystallization of AMG 517 at 80% drug load. An overlay of 80% AMG 517 in PVP with 82% AMG 517 in HPMC-AS at 80°C/75%RH indicates that PVP crystallizes slightly faster than HPMC-AS.

Effect of Residual Solvent on Crystallization Rate

Figure 13 shows an overlay of ASD11 (33% AMG 517 in PVP) with dried and non-dried samples at conditions of 80°C/75%RH. Comparison of dried and non-dried PVP ASDs shows a faster crystallization rate for the non-dried sample. ^{19}F SSNMR data indicates the dried PVP ASD (gray line) crystallizes more of the drug than the non-dried PVP ASD (pink line). The crystallization enthalpy, $\Delta H_{c,}$ values are 19.0 J/g for non-dried ASD11 (33% AMG 517 in PVP) and 19.7 J/g for dried ASD11 (33% AMG 517 in PVP).

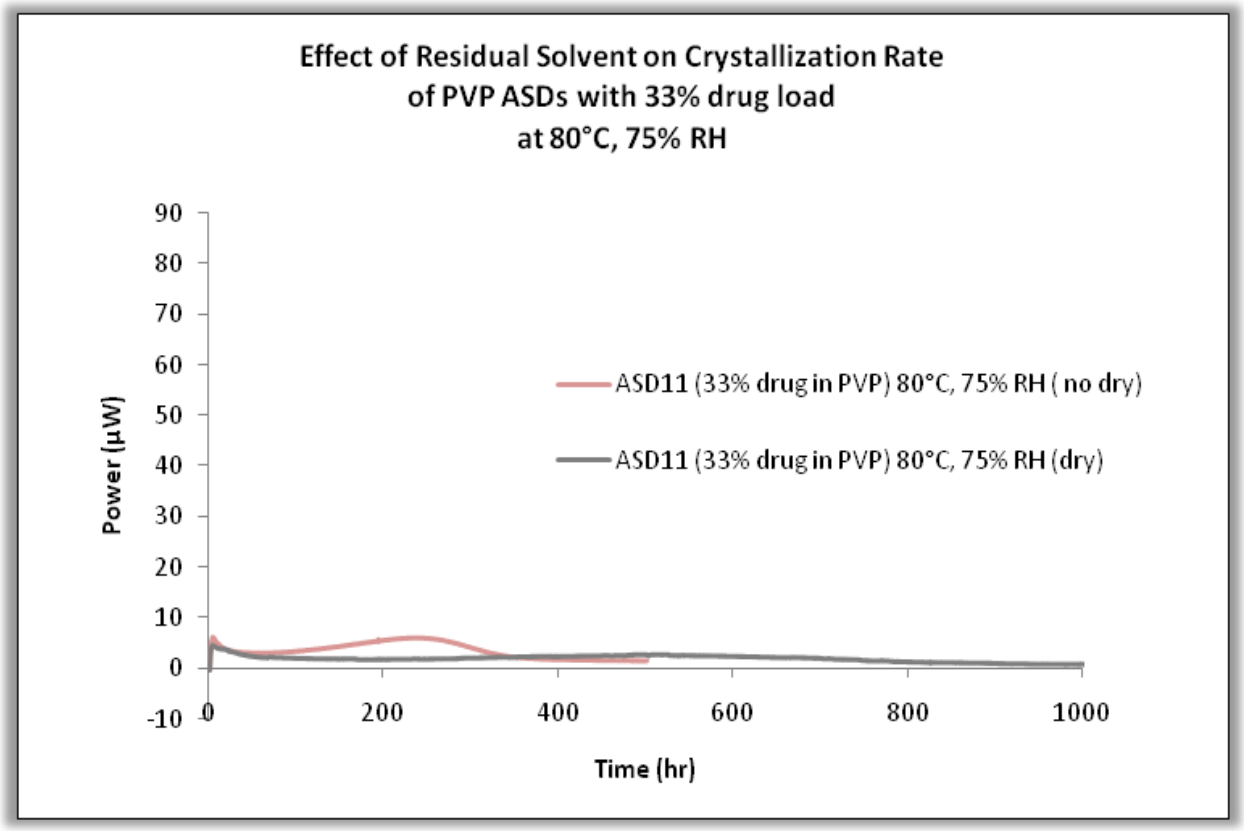

Figure 13. Effect of residual solvent on crystallization rate of PVP ASDs at 80°C, 75%RH

Summary of Effects of Polymer on Crystallization

Overall, the PVP ASDs behave similarly to HPMC-AS ASDs, with PVP ASDs having faster crystallization times at 80°C/75%RH condition possibly due to less complete drying of residual solvent. The crystallization of AMG 517 appears to be affected by polymer choice in other ways. The starting material form is consistently recovered for HPMC-AS ASDs. However, the form of AMG 517 crystallizing out of the ASD is not the same form as what is recovered from HPMC-AS ASDs. As indicated in Table 7, for ASD11 (33% AMG 517 in PVP) and ASD12 (80% AMG 517 in PVP), a different form was recovered after the TAM crystallizations. The higher T_g suggests this could be a more stable form, possibly an EtOAc solvate.

Residual solvent level differences are more pronounced for ASD11 (33% AMG 517 in PVP) and ASD12 (80% AMG 517 in PVP) and TAM experiments comparing dried and non-dried samples are listed in Table 7. For ASD11 (33% AMG 517 in PVP) at 80°C/75%RH experiments comparing 0.71% ethyl acetate and 3.81% ethyl acetate, there is a clear difference between dried and non-dried materials. Crystallization begins sooner and proceeds faster with a higher level of ethyl acetate. However, a lower ΔH_c and lower % crystallinity for non-dried samples indicates that the residual solvent may inhibit completion of the crystallization process.

Figure 14 shows the relative crystallization time for each TAM experimental condition, with longer times indicated by larger circles. Unexpectedly, most of the ASDs at conditions below 80°C/75%RH required crystallization times longer than 42 days to complete crystallization, so the samples were taken down and evaluated as partially crystallized materials after 42 days. The

slow crystallization of AMG 517 in ASDs shows that polymer does kinetically stabilize the amorphous drug against crystallization, with both HPMC-AS and PVP.

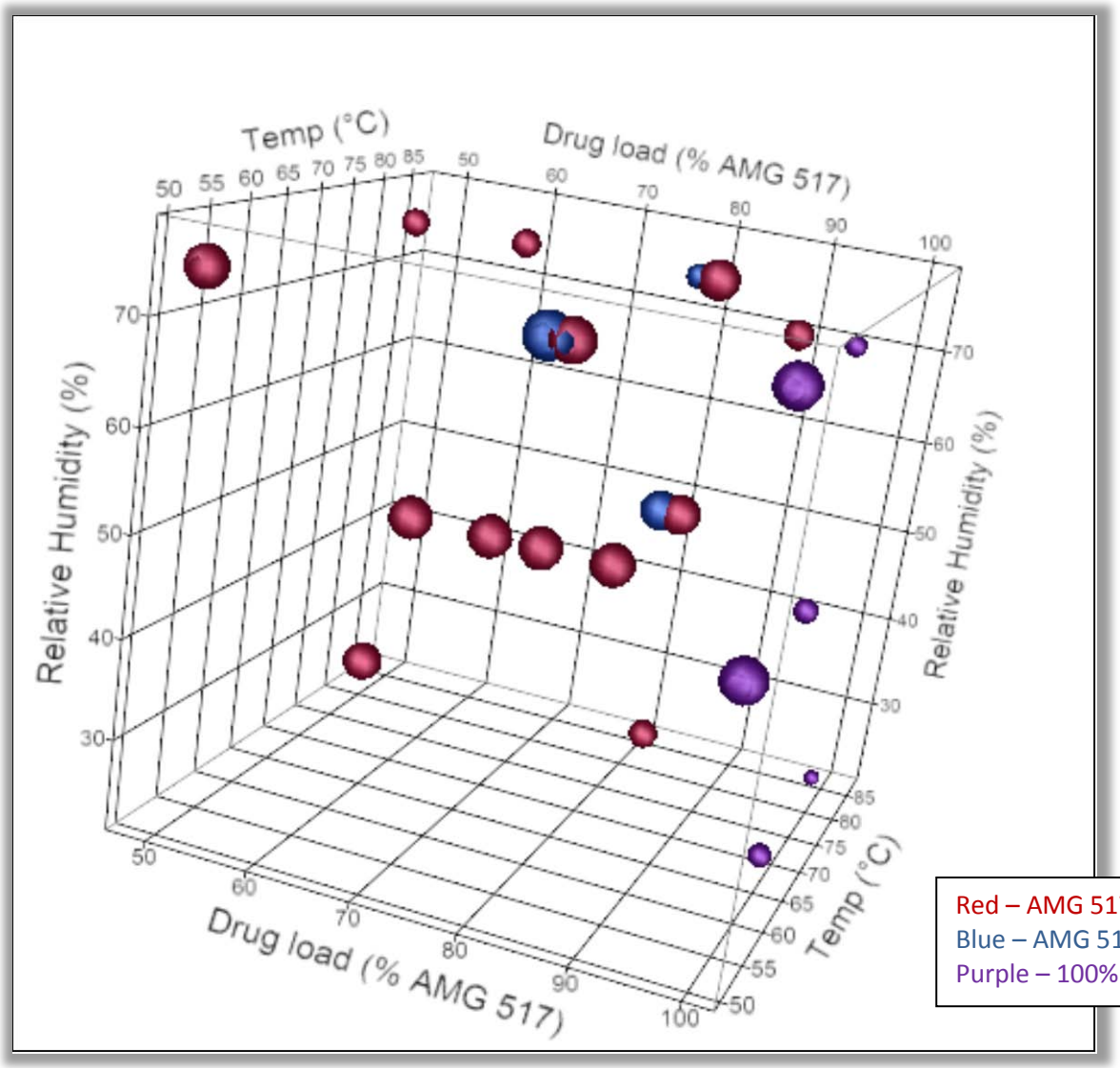

Figure 14 – Box representation of Crystallization Time. Crystallization time is indicated for each crystallization condition used for TAM experiments. Circle size indicates length of time (i.e. larger circles required longer time to crystallization). Maximum time for TAM experiments is 42 days.

Table 5. Summary of TAM crystallization data. Basic solid state characterization was performed on all TAM crystallization samples when the TAM experiments were finished. XRD and mDSC were inspected to verify the form of crystallized AMG 517 material.

Sample Information					TAM Crystallization Data				mDSC
ASD Name	Drug load %	Temp °C	RH %	EtOAc %	t0 (day)	Time (day)	ΔH_c (J/g)	XRD % Xln	T_g, C
ASD2 5075	54	50	75	0.01	5.0	33.2	0	<3	104.3
ASD2 8025	54	80	25	0.01	2.2	42	0	3-10	103.5
ASD2 8075	54	80	75	0.01	0.729	12.9	39.4	>>17	99.5
ASD3 6550	62	65	50	0.03	4	42	0.54	<3	105.3
ASD3 8075	62	80	75	0.03	0.25	13.8	31.9	>>17	105.2
ASD4 6550-1	70	65	50	0.08	2	34	0	<3	106.7
ASD4 6550-2	70	65	50	0.08	6.5	42	0	<3	108.2
ASD5 6550-1	75	65	50	0.10	5	22.8	0	<3	106.7
ASD5 6550-2	75	65	50	0.10	15	42	0	<3	108.8
ASD6 5075	82	50	75	0.11	25	33.1	0	<3	107.5
ASD6 6550	82	65	50	0.11	2.8	42		3-10	108.7
ASD6 8025	82	80	25	0.11	8.6	42	0	17	105.4
ASD6 8050	82	80	50	0.11	4	40.7	12.6	>17	102.7
ASD6 8075	82	80	75	0.11	3.5	11	37.9	100	na
ASD8 6575	95	65	75	0.08	0.62	15.5	11.7	100	109.3
ASD7 5050	100	50	50	0.19	22.8	37.8	0	>17	108.8
ASD7 5075	100	50	75	0.19	2.7	33.2	23.0	100	na
ASD7 6510	100	65	10	0.19	3.5	40.9	26.3	100	Tm 229C
ASD7 6525	100	65	25	0.19	0.25	6.5	39.4	100	Tm 229.3
ASD7 6550	100	65	50	0.19	0.69	6.75	42.9	100	Tm 229C
ASD7 6575	100	65	75	0.19	0.15	3.75	41.3	100	Tm 229.2
ASD7 8025	100	80	25	0.19	0.17	2.3	43.3	100	107.4
ASD11 5075d	33	50	75	0.74	12	42	0	<3	116.3
ASD11 5075nd	33	50	75	3.81	18	42	0	<3	141.5
ASD11 6575nd	33	65	75	3.81	2.0	19.7	182	New	165
ASD11 8075d	33	80	75	0.71	7	42	108	New	Unclear
ASD11 8075nd	33	80	75	3.81	2.5	20.9	95	New	Unclear
ASD12 5075nd	80	50	75	2.11	10	42	0	New	140.6
ASD12 8050nd	80	80	50	2.11	10	42	0	<3	117.6
ASD12 8075d	80	80	75	0.22	1.8	9.3	26.0	100	180
ASD12 8075nd	80	80	75	2.11	1.0	9.0	19.9	100	na

Note: d – dried sample, nd – non-dried sample.

Solid State Stability Results

Results of traditional solid state stability experiments show similar (and expected) trends compared to those discussed from TAM experiments. Crystallization is faster with higher temperature and higher humidity. XRPD is used to determine when the sample reaches >10% crystalline and removed from stability condition at that time. For some of the ASDs, 19 months on condition still shows < 3% crystallinity by XRPD and stability is reported as > 19 months.

At 60°C/30%RH condition, the samples were found to be damp the 12 week time point and XRPD showed >>17% crystallinity. The samples crystallized sometime between 9 weeks and 12 weeks and the 10% crystallization point was missed, most likely due to condensed water from hygrostats in the controlled humidity jars causing crystallization.

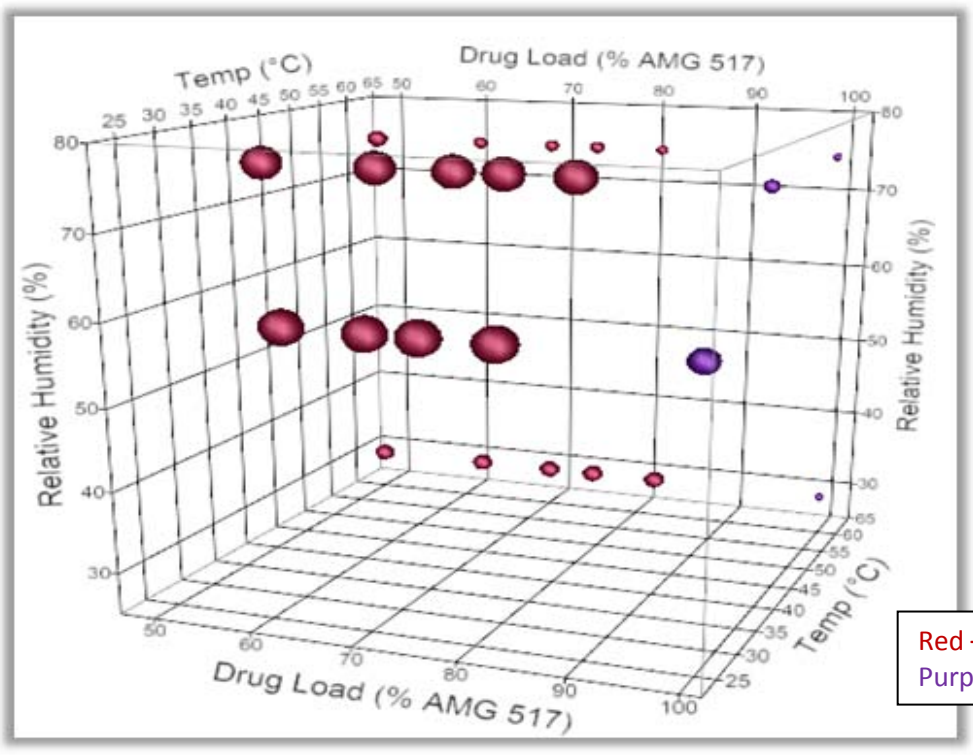

Figure 15 – Box representation of experiment end times for traditional solid state stability. Circle size indicates length of time (i.e. larger circles required longer time to crystallization).

XRPD for ASDs after storage at various conditions shows crystalline AMG 517 forming from the ASDs. Physical mixtures containing 3%, 10% and 17% crystalline AMG 517 are used as references to compare with stability samples.

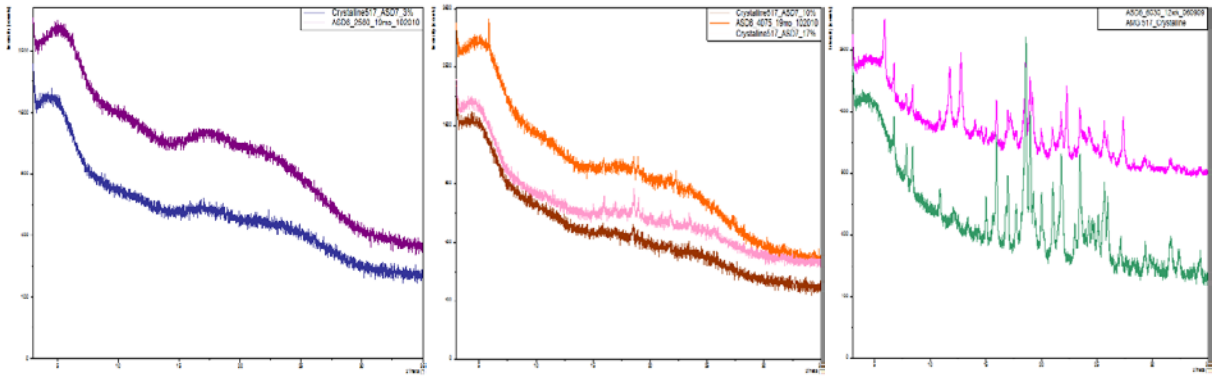

Figure 16. Crystallinity analysis of ASD6 (82% AMG 517 in HPMC-AS) by XRPD after storage at 25°C/60%RH for 19 months, 40°C/75%RH for 19months and 60°C/30%RH for 12 weeks.

XRPD for PVP ASDs indicate that a different form of AMG 517 crystallizes out of PVP ASDs at elevated temperature and humidity conditions.

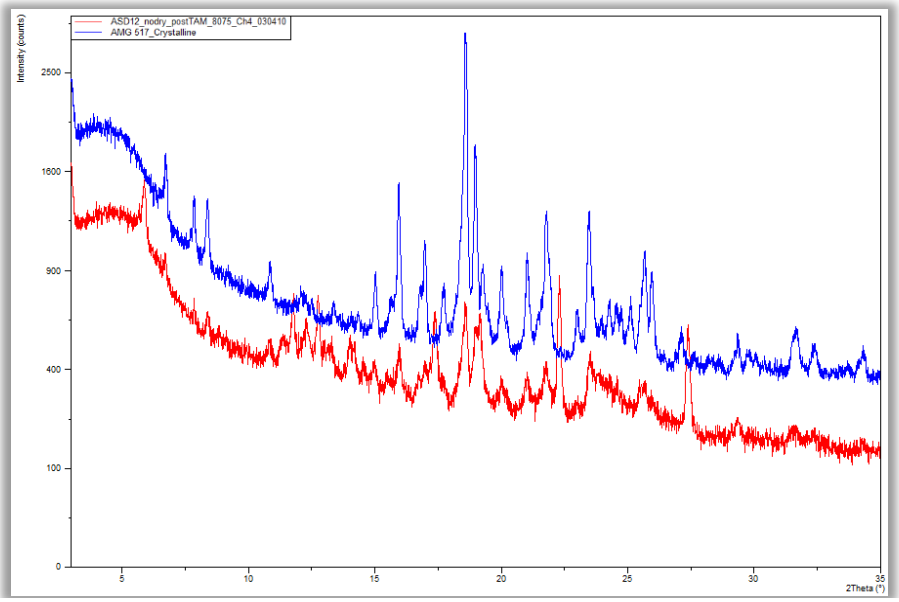

Figure 17. XRPD spectrum for crystallized ASD12(80% AMG 517 in PVP) overlaid with crystalline AMG 517. The form of the crystallized AMG 517 is different from the starting form.

Figure 18 shows an example of the mDSC data obtained for ASDs after stability at various conditions. ASD6 (82% AMG 517 in HPMC-AS) does not indicate a phase separation after storage at 25°C, 60%RH for 19 months. However, the ^{19}F SSNMR indicates 6.1% crystallinity after storage at these conditions. Even as the AMG 517 begins to crystallize out of the ASD, a single T_g is observed by mDSC. Another technique would most likely be needed to determine phase separation for the partially crystallized samples.

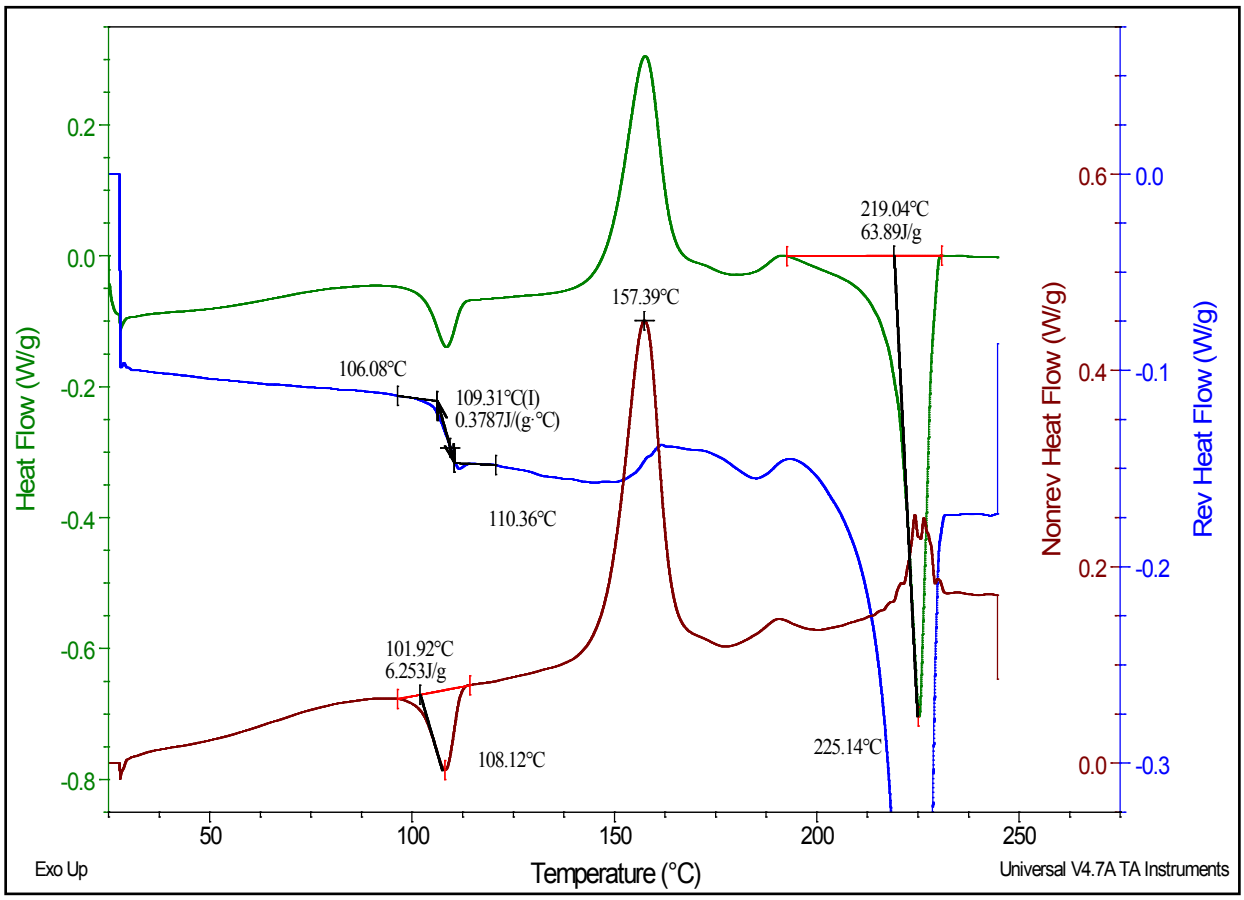

Figure 18. Modulated DSC heat flow curves for ASD6 (82% AMG 517 in HPMC-AS) with less than 10% crystallinity after storage at 25°C/60%RH for 19 months. A single T_g is observed in the reversing curve, with large enthalpic relaxation in the non-reversing curve.

Table 6 shows the solid state data for all the stability samples. XRPD indicates whether the crystallinity is < 3%, 3-10%, 10-17% or >17% crystalline AMG 517. Modulated DSC T_g values are listed. The % crystalline AMG 517 in each ASD sample is determined from ^{19}F SSNMR measurements at the end of the study. Avrami rate constants, calculated as described in the next section, are listed. The time required to reach a detectable level of crystallinity in the ASD sample by XRPD is indicated in the "Time to >10% X" column.

Table 6. Solid State Data for Traditional Stability Studies of ASDs of AMG 517 in HPMC-AS

Sample Information					^{19}F SSNMR		
ASD	% Drug Load	Condition	XRD	T_g	% Crystalline	Time to >10% X	Rate constant
ASD2	54	25°C/60%RH	<3	104.2	0	19mo	0
		40°C/75%RH	<3	104	6.3	19mo	2.00283e-7
		60°C/30%RH	>>17	103	80.9	12wk	0.00023462
		60°C/75%RH	~10	102.8	13.0	12wk	1.97367e-5
ASD3	62	25°C/60%RH	<3	104.6	0	19mo	0
		40°C/75%RH	<3	104.2	4.1	19mo	1.28853e-7
		60°C/30%RH	>>17	114.8	74.4	12wk	0.00019311
		60°C/75%RH	10-17	105.4	8.1	28d	0.00010774
ASD4	70	25°C/60%RH	<3	106.8	2.5	19mo	7.79249e-8
		40°C/75%RH	<3	104.6	5.2	19mo	1.64361e-7
		60°C/30%RH	>>17	116	60.9	12wk	0.00013309
		60°C/75%RH	>17	105.4	10.7	28d	0.00014435
ASD5	75	25°C/60%RH	<3	107.1	0	19mo	0
		40°C/75%RH	<3	106.9	4.1	19mo	1.28853e-7
		60°C/30%RH	>>17	101.4	59.8	12wk	0.00012915
		60°C/75%RH	10-17	107	11.0	28d	0.00014864
ASD6	82	25°C/60%RH	<3	109.3	6.1	19mo	1.93721e-7
		40°C/75%RH	10-17	109	9.5	19mo	3.07234e-7
		60°C/30%RH	100	102.8	40.2	12wk	0.00007287
		60°C/75%RH	~10-17	107.1	10.7	14d	0.00057739
ASD7	100	25°C/60%RH	10-17	110.9	5.8	6mo	1.84414e-6
		40°C/75%RH	3-10	111.3	10.6	4wk	0.00014292
		60°C/30%RH	100	111.6	68.6	7d	0.02364005
		60°C/75%RH	100	NA	100	7d	0.09398307

Figure 19 shows a box representation of the crystallization conditions again, this time with circle size indicating larger values for Avrami rate constants for each condition, meaning faster crystallization of AMG 517 from ASD for conditions with larger circles.

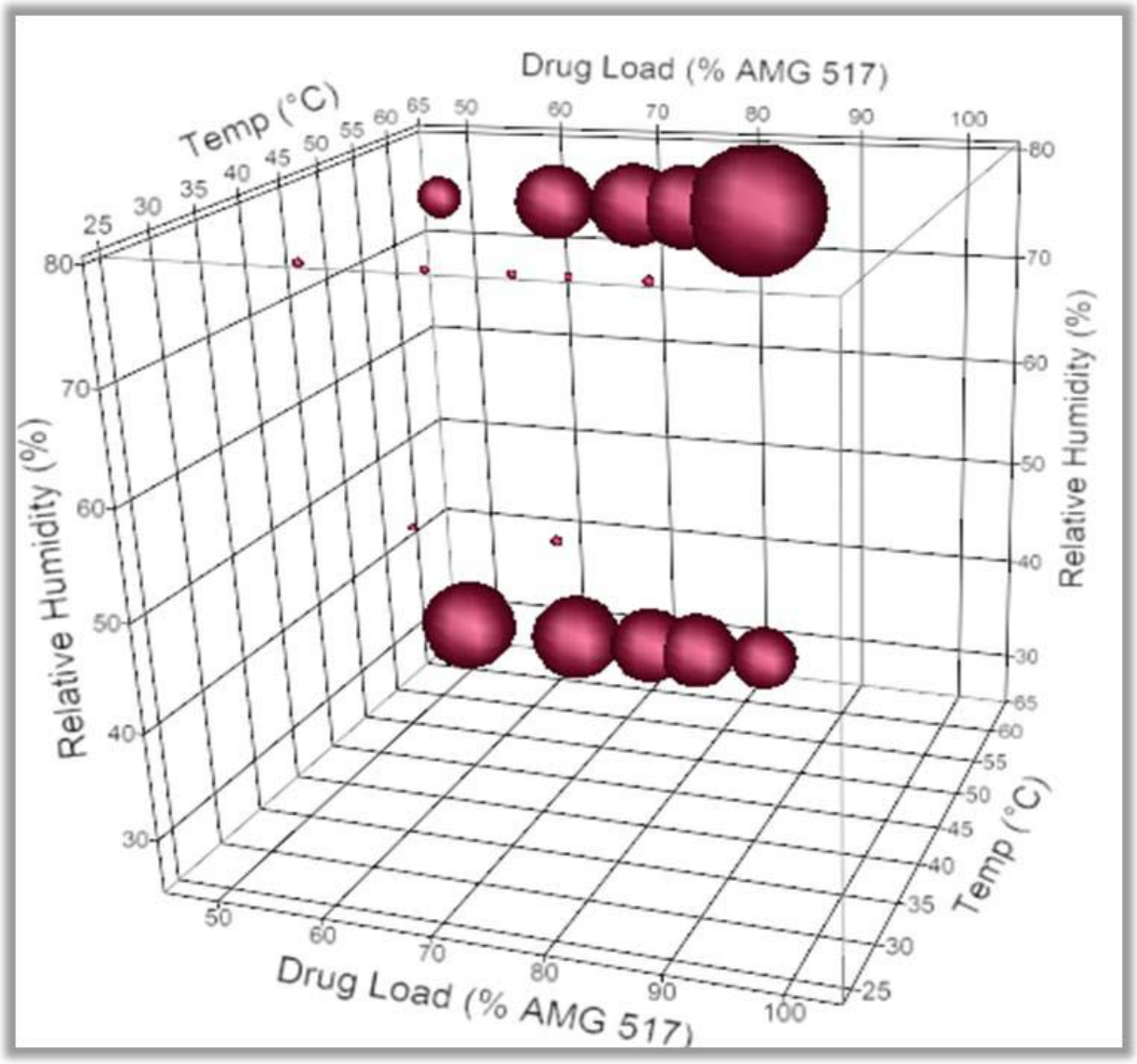

Figure 19 – Box representation of rate constants for traditional solid state stability experiments. Circle size indicates larger crystallization rate constant.

Crystallinity by SSNMR

^{19}F SSNMR is used to determine the amount of crystalline versus amorphous for each ASD sample. SSNMR is an accurate assessment of the crystallinity of these samples, but only practical to analyze at the end, after the sample has been taken down from the accelerated stability condition. A spectrum of pure crystalline AMG 517 is shown in blue in Figure 20 overlaid with a spectrum of pure amorphous ASD7 (100% AMG 517) shown in red. The observed crystalline form of AMG 517 has two molecules per unit cell, and two peaks are seen in the crystalline spectrum. The amorphous peak and the second crystalline peak have overlapping chemical shifts, enabling distinction between the amorphous and crystalline forms. The detection limit of ~3% crystalline AMG 517 in amorphous or ASD material is achieved.

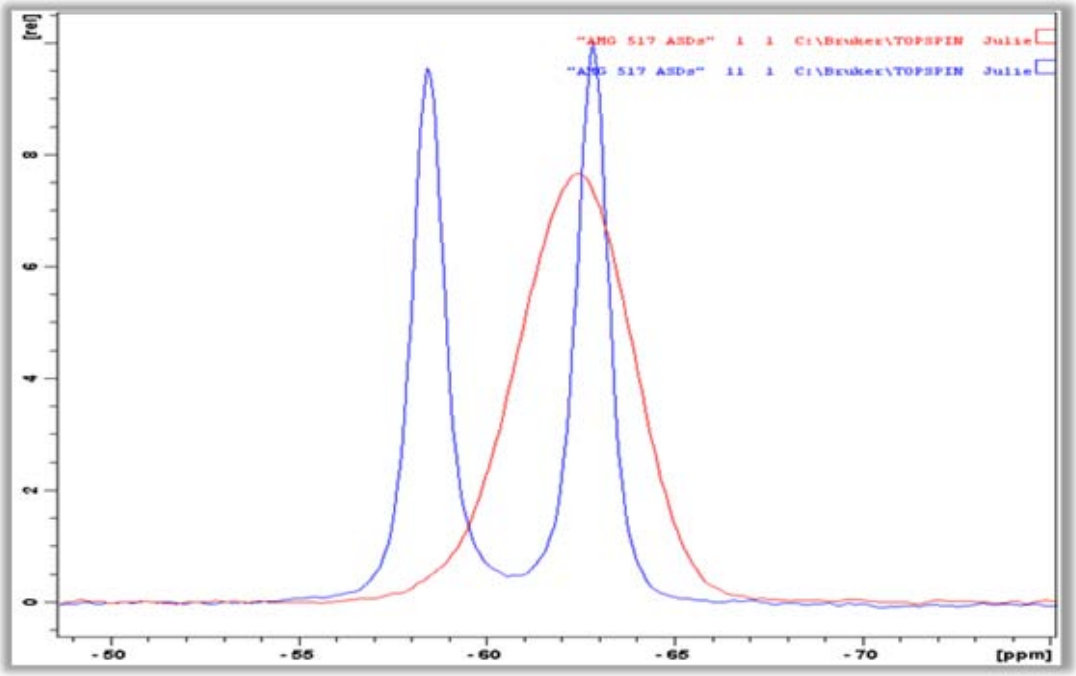

Figure 20. ^{19}F SSNMR spectra for amorphous AMG 517 (red) and crystalline AMG 517 (blue). There is some overlap in the spectra for the different forms, but also a clear distinction, which allows for quantification of the crystalline content in a mixture.

An example of ^{19}F SSNMR spectra for a partially crystallized ASD is shown in Figure 21 below. In this example for ASD6 (82% AMG 517 in HPMC-AS) at 80°C/75%RH, the amorphous peak is overlapping with the second crystalline peak. The signals for the amorphous and crystalline forms in the material can be de-convoluted using Mestrenova software and the percent crystallinity is calculated based on the de-convoluted areas of the peaks. The integrated areas for the three peaks (two crystalline and one amorphous) are indicated in the box.

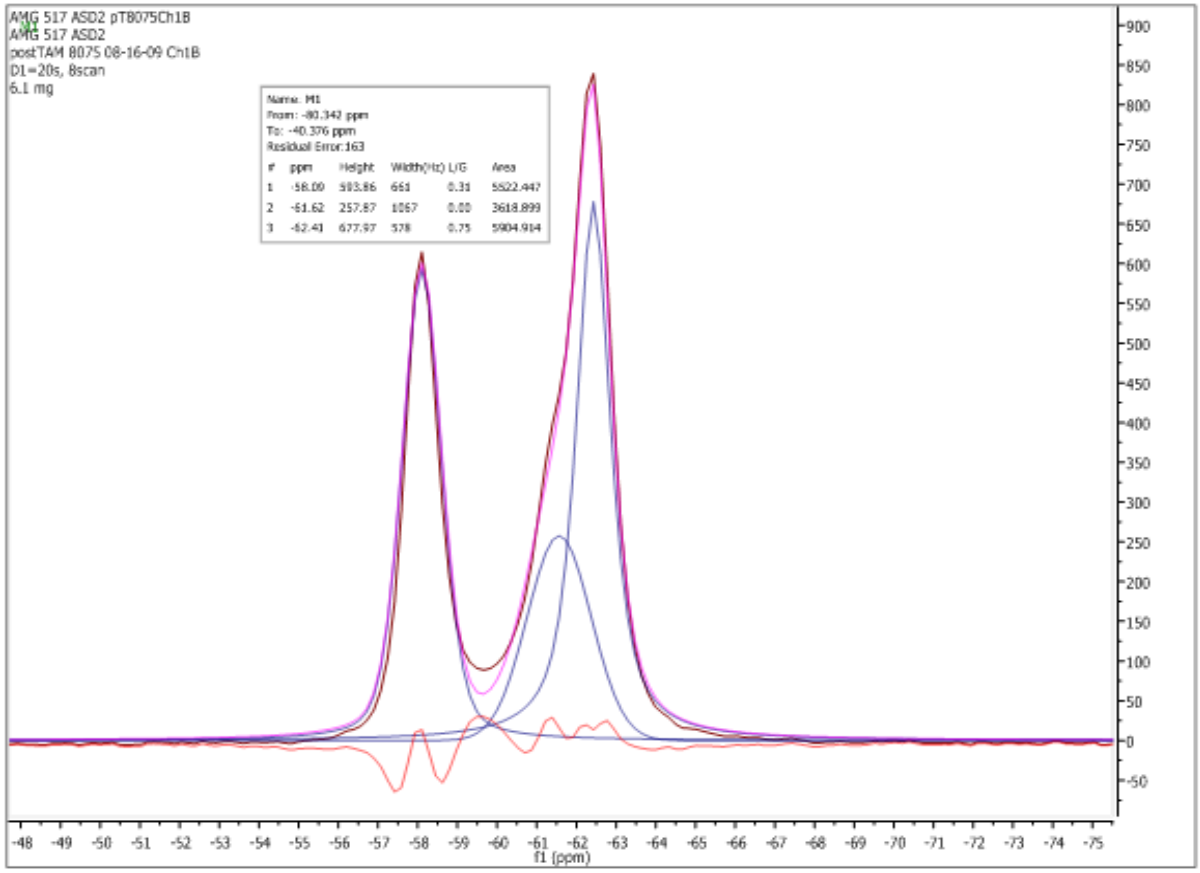

Figure 21. Deconvolution using MNOVA software for ^{19}F SSNMR spectra of ASD6 (82% AMG 517 in HPMC-AS) after 12 days in the TAM at 80°C/75%RH. For the deconvolution, the blue lines represent the theoretical signals from the individual amorphous and crystalline signals, the dark pink line is the addition of those peaks and the lighter trace is the actual data. The residual signal (difference between actual data and additive signal from theoretical peaks) is shown in red. Comparing the fitted areas for the theoretical amorphous and crystalline peaks, % crystallinity for the sample is calculated.

After de-convolution, the sample shown in Figure 21 is determined to have 59.7% crystallinity; that is, 59.7% of the AMG 517 in the sample is in the crystalline form. The de-convolution has a calculated error of ~1% for this sample, which is typical of all de-convolutions in this study. The ASD samples contain various levels of crystalline AMG 517 and the de-convolution results are listed as "% crystalline" in Table 6 and Table 7 for all of the traditional solid state stability experiments and TAM crystallization experiments, respectively. The amount of crystallinity determined by ^{19}F SSNMR appears to correlate well with XRPD and mDSC analyses. The % crystallinity results from ^{19}F SSNMR also align well with crystallization conditions, with less strenuous conditions of temperature and relative humidity having lower levels of crystallinity after storage.

Crystallization Kinetics

Rate constants are calculated for each TAM crystallization sample using the Avrami equation, where t is the end of crystallization peak or the end of the experiment time, whichever is sooner and X is the percent crystallized, based on ^{19}F SSNMR deconvolution data.

Since many of the ASD crystallizations with AMG 517 were slow, the TAM experiments were run for a maximum of 42 days, so the maximum time used in the Avrami calculations is 42 days. Single point calculations were used to estimate Avrami rate constants and n values where full rate data was not available from the TAM. In many cases, the crystallization was too slow to observe a clear crystallization event by TAM, although partial crystallization can be measured by ^{19}F SSNMR. A lower limit of k is calculated as $6.0 \times 10^{-5}/day^2$ for TAM experiments using t=42 days, assuming n=2 for rod shaped particles and X=0.1 with 10% crystallization as a "stability

failure" criteria. Rate constants for solid state stability experiments and for TAM crystallization experiments are included in Table 6 and Table 7, respectively.

Table 7. Estimated rate constant calculations for a single point end point) using ^{19}F SSNMR crystallinity & TAM experiment times and n = 2 for calculating Avrami rate constants

Sample Name	Drug Load	Temperature °C	Relative Humidity	19F SSNMR % Crystalline	Time (days)	Rate constant, k, (single point)
ASD2 5075	54	50	75	0 <10	33.2	0.000096
ASD2 8025	54	80	25	7.8 < 10	42	0.000060
ASD2 8075	54	80	75	75.9	12.9	0.008551
ASD3 6550	62	65	50	10.1	42	0.000060
ASD3 8075	62	80	75	74.8	13.8	0.007238
ASD4 6550-1	70	65	50	6.3 <10	34	0.000060
ASD4 6550-2	70	65	50	5.4 <10	42	0.000060
ASD5 6550-1	75	65	50	5.0 <10	27.8	0.000060
ASD5 6550-2	75	65	50	4.3 <10	42	0.000060
ASD6 5075	82	50	75	9.4 <10	33.1	0.000097
ASD6 6550	82	65	50	11.3	42	0.000068
ASD6 8025	82	80	25	10.1	42	0.000060
ASD6 8050	82	80	50	28.7	40.7	0.000204
ASD6 8075	82	80	75	61.8	11	0.007953
ASD8 6575	95	65	75	53.5	15.5	0.003187
ASD7 5050	100	50	50	28.0	37.8	0.000230
ASD7 5075	100	50	75	96.6	33.2	0.003068
ASD7 6510	100	65	10	100	40.9	0.004129
ASD7 6525	100	65	25	100	6.5	0.163497
ASD7 6550	100	65	50	100	6.75	0.151611
ASD7 6575	100	65	75	98.3	3.75	0.289745
ASD7 8025	100	80	25	100	2.3	1.305814
ASD11 5075d	33	50	75	12.8	42	0.000078
ASD11 5075nd	33	50	75	11.7	42	0.000071
ASD11 6575nd	33	65	75	23.7	19.7	0.000697
ASD11 8075d	33	80	75	55.7	42	0.000462
ASD11 8075nd	33	80	75	17.6	20.9	0.000443
ASD12 5075nd	80	50	75	6.7 <10	42	0.000060
ASD12 8050nd	80	80	50	4.5 <10	42	0.000060
ASD12 8075d	80	80	75	52.3	9.3	0.008559
ASD12 8075nd	80	80	75	36.0	9.0	0.005510

Note: d – dried sample, nd – non-dried sample.

Avrami rate constants are also shown graphically in Figure 22, with larger circle size indicating a higher rate constant and faster crystallization of AMG 517 at elevated conditions of relative humidity and temperature.

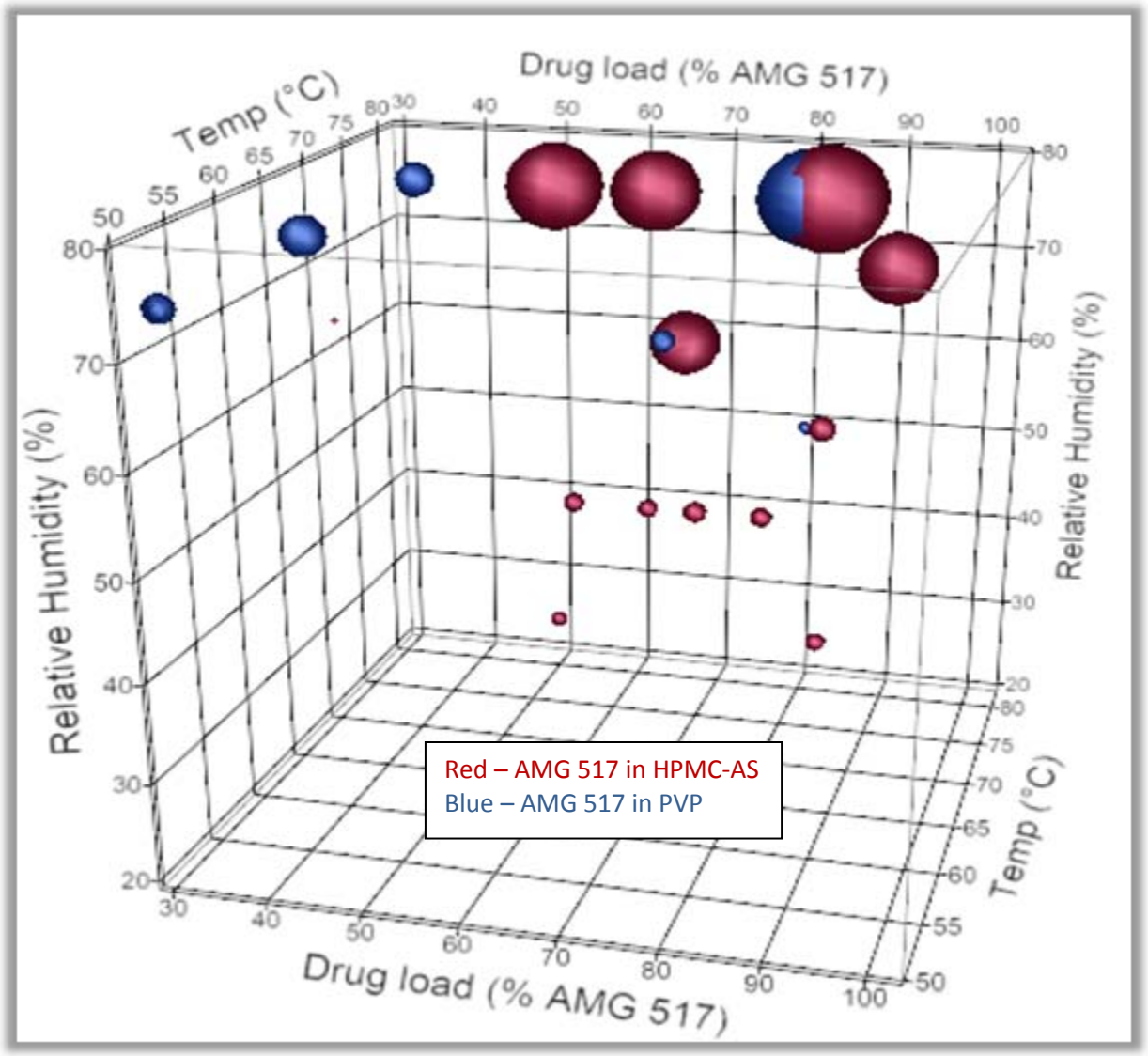

Figure 22 – Box representation of rate constants for ASDs based on TAM crystallization experiments.

Analysis of Rate Data from TAM Crystallization Experiments

For experiments which had significant crystallization over the experimental time frame, rate data from the TAM was integrated as in Figure 23 and Figure 26, and plotted as in Figure 24 and Figure 27, for ASD2 (50% AMG 517 in HPMC-AS) at 80°C/75%RH and ASD6 (82% AMG 517 in HPMC-AS) at 80°C/75%RH, respectively. Rearrangement of the Avrami equation allows for fitting of the crystallization rate data to obtain the Avrami constants n (geometric factor) and k (rate constant), as shown in Figure 25 and Figure 28. For the crystallization of ASD6 (82% AMG 517 in HPMC-AS) at 80°C/75%RH, Figure 22 - 28, the two events are treated separately to obtain separate rate constants for each event. Where two events are apparent, as in Figure 26, it is assumed that the heat of crystallization is proportional to the % crystallinity for the entire sample, and the two events are treated as if the heat of crystallization is the same.

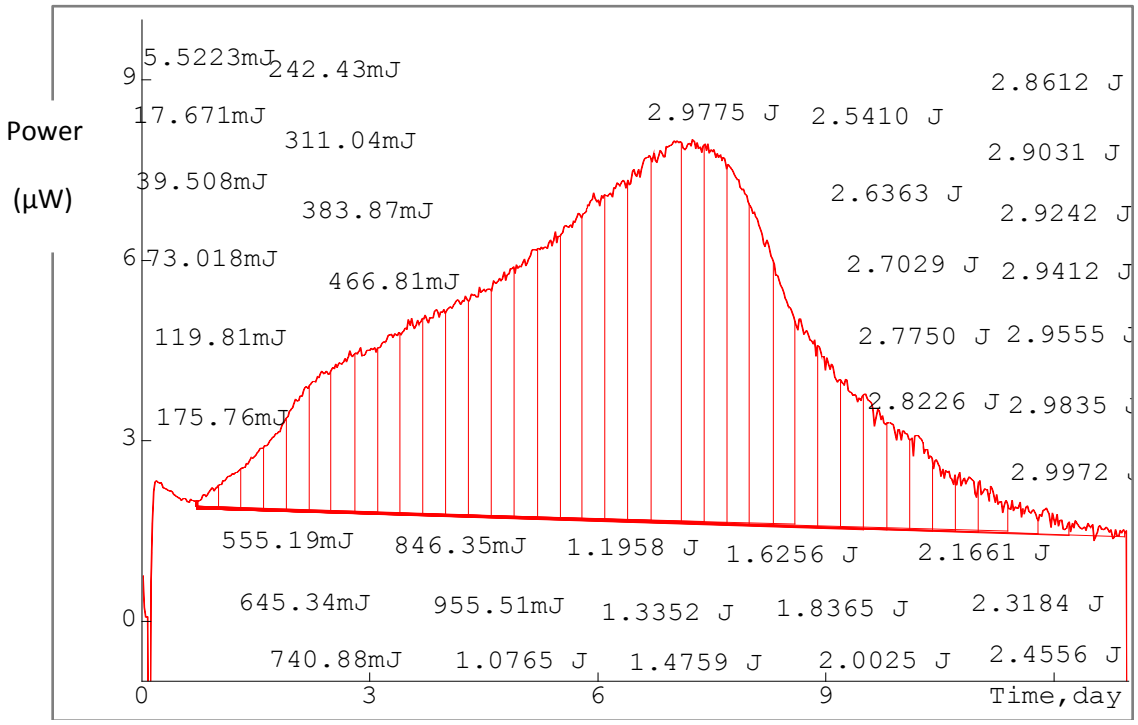

Figure 23. Raw data showing TAM profile for ASD2 (50% AMG 517 in HPMC-AS) at 80°C/75%RH integrated at 5-10 hour intervals.

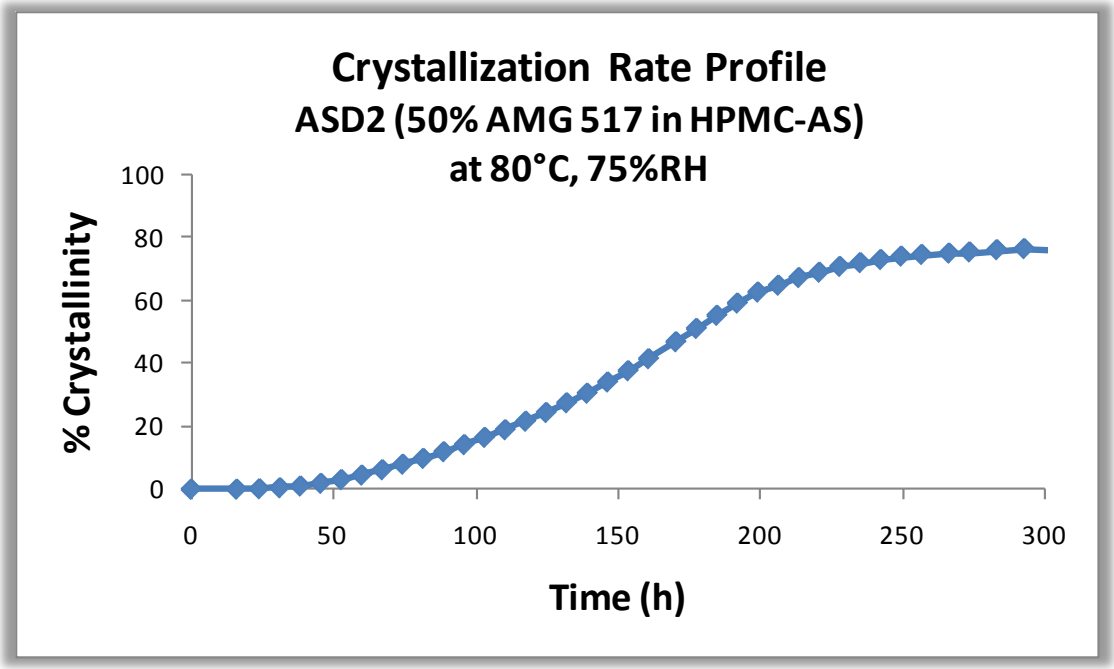

Figure 24. Crystallization Rate profile for ASD2 (50% AMG 517 in HPMC-AS) at 80°C/75%RH.

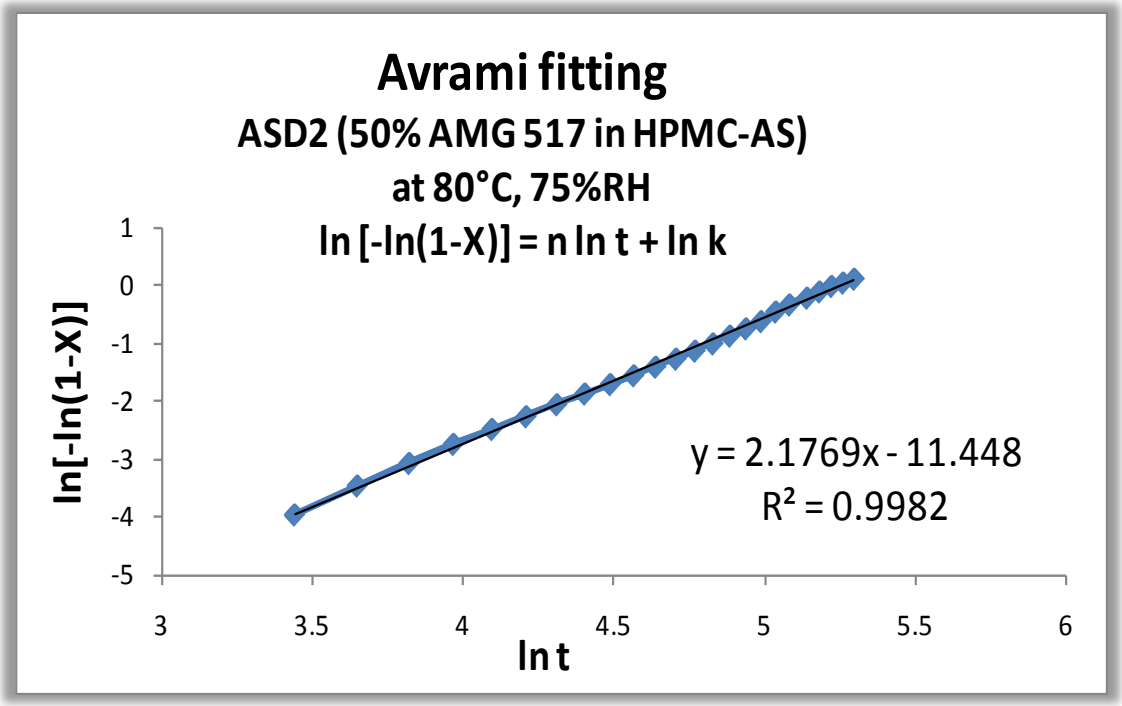

Figure 25. Fitting of Avrami constants for crystallization rate data for ASD2 (50% AMG 517 in HPMC-AS) at 80°C/75%RH.

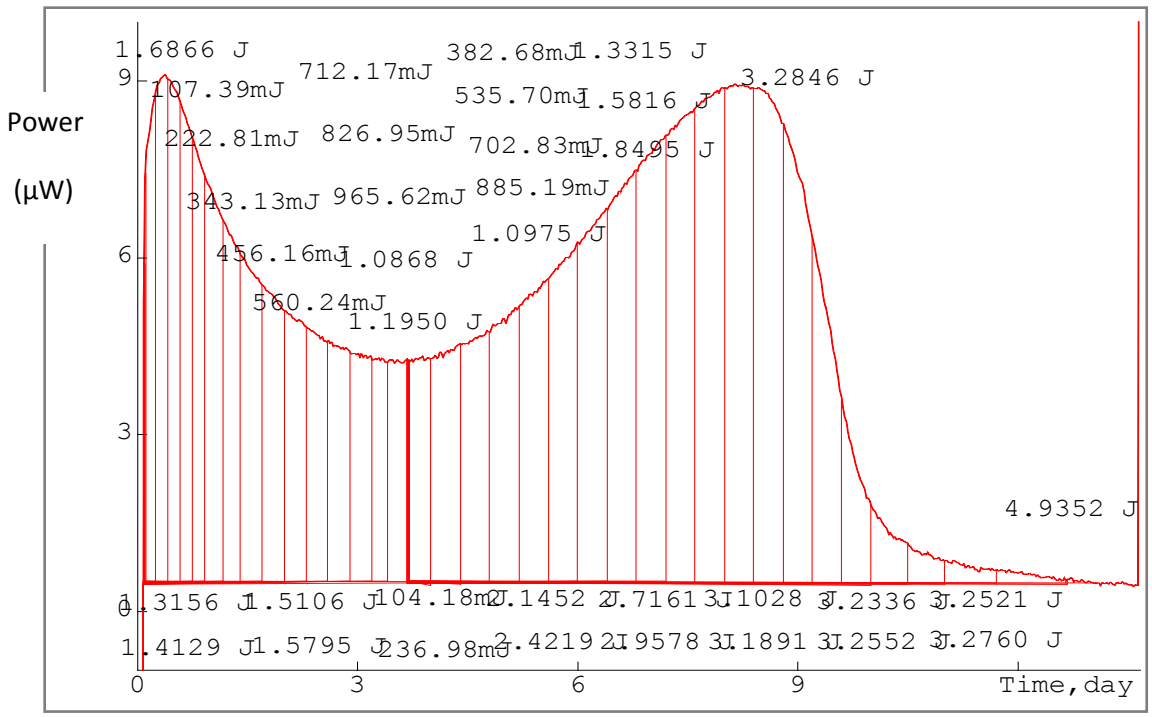

Figure 26. Raw data showing TAM profile for ASD6 (82% AMG 517 in HPMC-AS) at 80°C/75%RH integrated at 5-10 hour intervals.

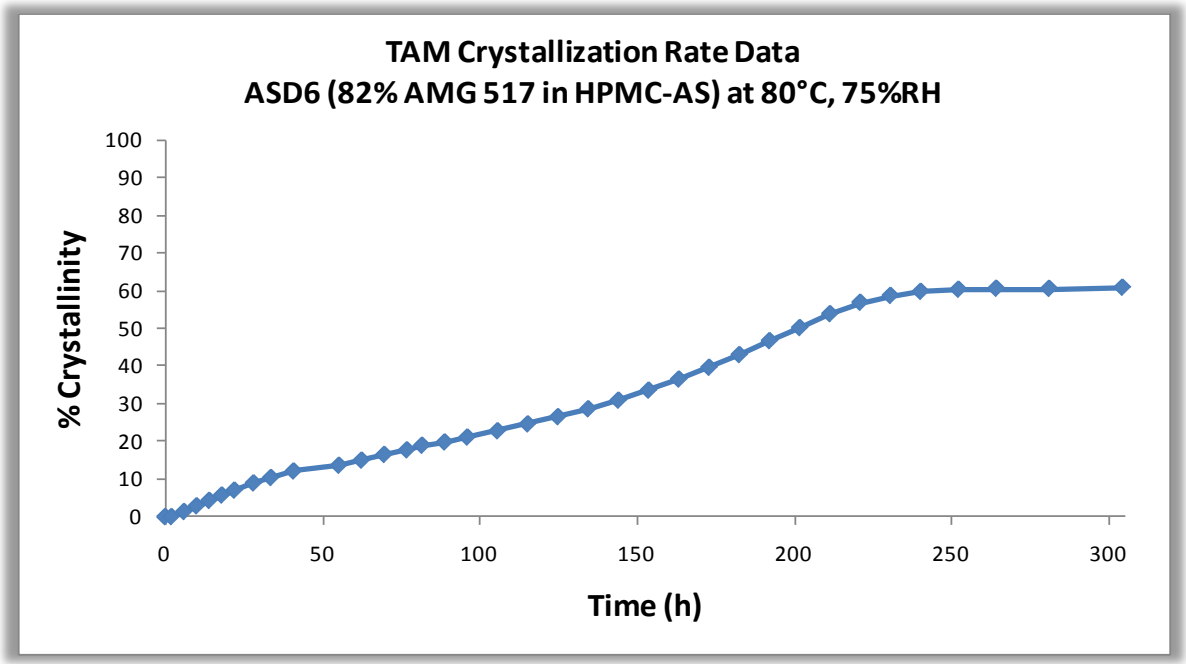

Figure 27. Crystallization rate profile from integrated TAM data. Crystallization of ASD6 (82% AMG 517 in HPMC-AS) shows two kinetic events, over 300 hours (13 days).

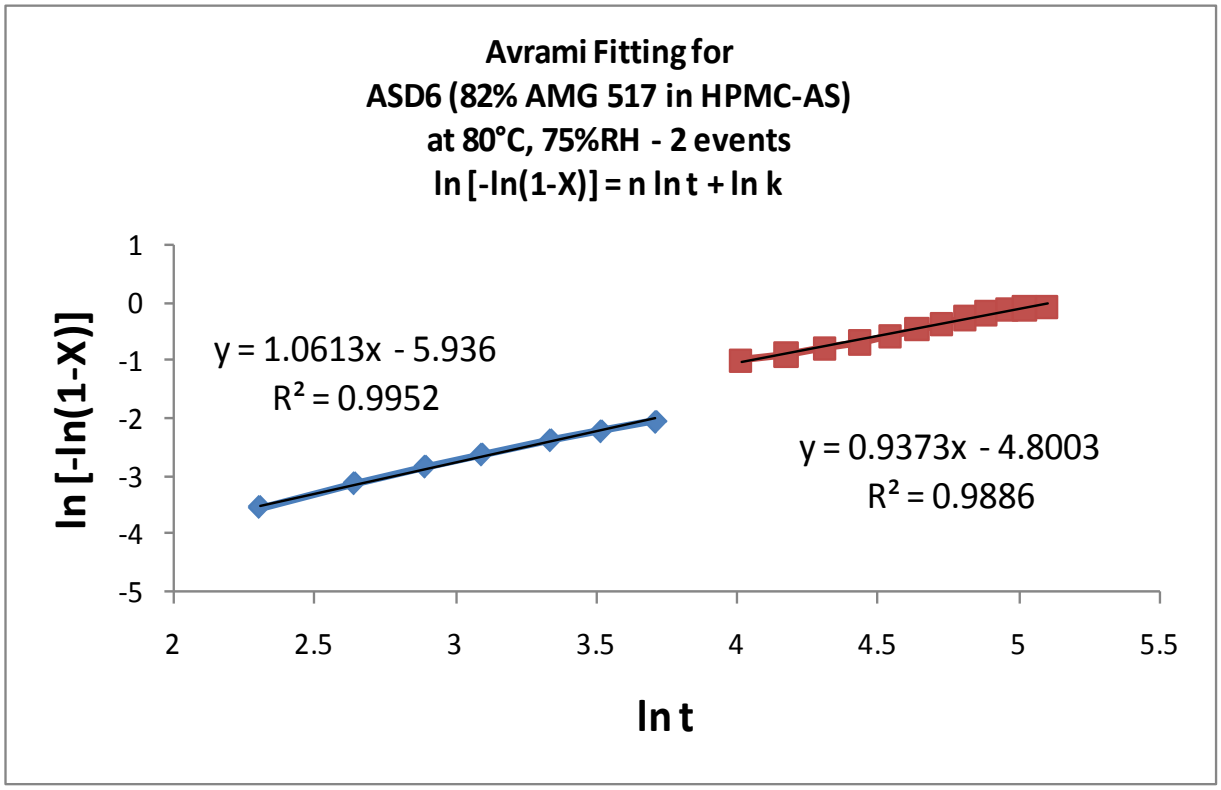

Figure 28. Avrami fitting of TAM crystallization rate data to obtain Avrami rate constants n and k for the two crystallization events observed during the experiment. Rate constants for the first and second kinetic events are fitted separately.

The Avrami fittings using double ln have some built-in error due to the nature of log-type plots, but it is still useful to obtain estimates and to observe crystallization trends relating to drug load in the ASDs. Table 8 shows the rate constants and n constants for the 80°C/75%RH crystallization experiments with the TAM.

Table 8. Avrami constants after fitting the rate data

		Avrami rate constant		Geometric constant	
Sample Name	% Drug Load	First event k1	Second event k2	First event n1	Second event n2
ASD2 8075	50	1.07×10^{-5}	'--	2.18	'--
ASD3 8075	62	2.4×10^{-5}	7.3×10^{-5}	1.92	1.65
ASD6 8075	82	2.6×10^{-3}	8.2×10^{-3}	1.06	0.94
ASD8 8075	95	1.2×10^{-2}	1.0×10^{-5}	0.33	2.29

A plot of log k1 vs ASD drug load, in Figure 29, shows that drug load has an impact on crystallization rate constant for ASDs of AMG 517 in HPMC-AS. The rate constant for the first event, k1, is used for the evaluation of drug load, since the first crystallization event is more relevant for determining stability of the material. Considering that the phase separation causing the more rapid rate constants above 50% drug load, it may be that miscibility of AMG 517 in HPMC-AS is slightly lower than 50% and crystallizations below this level will have similar rate constants. From the graph, it is apparent that the amount of polymer used in the ASD affects the stability. However, ~ 40% polymer (or 60% drug load) appears to be sufficient for obtaining maximum stability for the ASD system. Additional polymer is expected to have a less significant effect, as indicated by the leveling off of the curve.

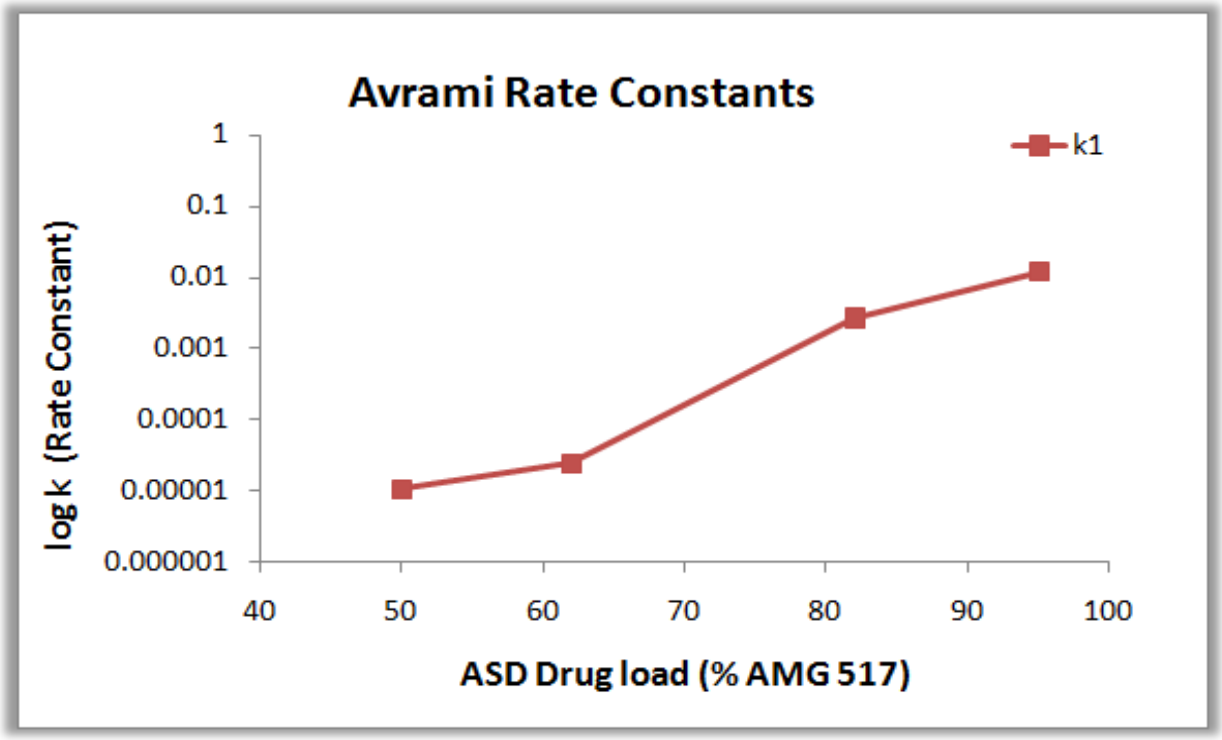

Figure 29. Avrami rate constant, k1, as a function of drug load of AMG 517 in HPMC-AS amorphous solid dispersions.

Arrhenius Prediction

Rate predictions based on the Avrami model are only valid within the experimental range. To predict outside this range, extrapolation from the experimental data must be used. Arrhenius plots are commonly used for this purpose in chemical degradation studies; here we apply the Arrhenius equation to extrapolate from TAM experimental conditions to ambient conditions. An Arrhenius plot is shown in Figure 30 for rate data from the TAM crystallization experiments for 75% RH at temperatures of 80°, 65°C, 50°C from TAM.

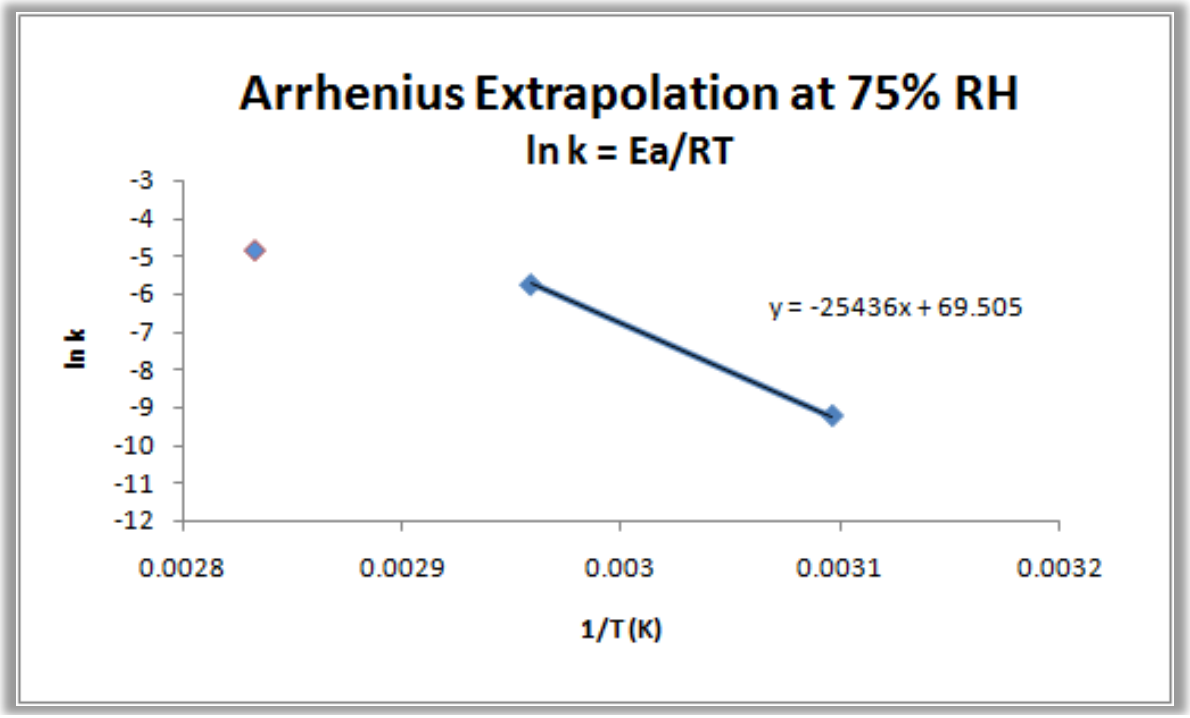

Figure 30. Arrhenius plot for 75%RH at 80°C, 65°C and 50°C TAM experiments.

Extrapolating to 25°C yields a rate constant value of 1.31×10^{-7}. Rearranging the Avrami equation for 5% crystallization gives $t10_{\%} = [- \ln(1 - 0.1) / k]^{1/2}$, which yields a 10% crystallization time of 897 days (~ 2.5 years) for ASDs of AMG 517 in HPMC-AS stored at

25°C/75%RH. This result is consistent with the traditional solid state stability data for ASDs stored at 25°C/60%RH, which indicated 6.1% crystallization for ASD6 (82% AMG 517 in HPMC-AS) by ^{19}F SSNMR over a storage period of 19 months, and < 10% crystallization by ^{19}F SSNMR over a storage period of 19 months for lower drug load ASDs. Although all the ASDs do crystallize at stressed conditions, Arrhenius predictions indicate that for ASDs of AMG 517 in HPMC-AS, the polymer inhibits crystallization to less than 10% in 2.5 years when stored at 25°C/75%RH. This result suggests that at 82% drug load, an amorphous solid dispersion of AMG 517 in HPMC-AS is on the borderline of acceptability, if a 2 year storage time is required.

Conclusions

TAM isothermal microcalorimeter is useful in observing crystallization at or above the T_g of a material at a given set of temperature and relative humidity conditions. TAM can detect crystallization events when heat flow is > 1μW. At conditions below the T_g, crystallization is much slower, resulting in heat signal so low that it is difficult to identify a single crystallization event. However, SS-NMR confirms partial crystallization of HPMC-AS ASDs even for slow crystallizations below T_g.

Crystallization of ASDs of AMG 517 in HPMC-AS follows the expected trends in terms of temperature and humidity (i.e. faster crystallization at higher temperature and humidity conditions). HPMC-AS kinetically slows crystallization of ASDs with AMG 517.

Adding polymer to AMG 517 significantly slows the crystallization of the drug, with both HPMC-AS and PVP. PVP is not as good as HPMC-AS at stabilizing ASDs. PVP picks up more water than HPMC-AS, causing the ASDs to have lower T_g values at the same crystallization conditions. Also, AMG 517 crystallizes out of PVP in a crystal form which is different from the starting material.

Isothermal microcalorimetry can provide important kinetic data for crystallization of ASDs. A dual mechanism observed for crystallization of ASDs indicating phase separation. Rate constants calculated for ASD crystallizations aid selecting drug load for maximizing stability while minimizing polymer used in the formulation. Finally, Arrhenius extrapolation is used to predict stability 10% crystallization predicted in 2.5 years at 25°C/75%RH, which is consistent with results from traditional solid state stability at 25°C/60%RH.

References – Chapter 4

1. Gordon M, Taylor JS. Ideal copolymers and the second-order transitions of synthetic rubbers. I. Noncrystalline copolymers. J Appl Chem1952;2:493-500.
2. Yoshioka M, Hancock BC, Zografi G. Crystallization of indomethacin from the amorphous state below and above its glass transition temperature. Journal of Pharmaceutical Sciences1994;83(12):1700-5.
3. Kennedy M, Hu J, Gao P, Li L, Ali-Reynolds A, Chal B, et al. Enhanced Bioavailability of a Poorly Soluble VR1 Antagonist Using an Amorphous Solid Dispersion Approach: A Case Study. Mol Pharmaceutics2008;5(6):981-93.

Chapter 5 – Conclusions and Suggestions for Further Study

Conclusions

In this project, it is shown that amorphous solid dispersions (ASDs) of AMG 517 in HPMC-AS manufactured by spray drying from ethyl acetate are initially phase mixed amorphous materials. The residual solvent affects the glass transition temperature (T_g) of ASDs and should be dried to < 0.2% ethyl acetate to stabilize the T_g. Compared to Gordon-Taylor predictions, significant depression of the T_g of ASDs of AMG 517 in HPMC-AS is observed. Negative deviation from Gordon-Taylor prediction indicates a thermodynamically unstable ASD system.

Crystallization studies show the presence of polymer (HPMC-AS or PVP) in ASDs slows the crystallization rate of amorphous AMG 517. Isothermal microcalorimetry is a useful technique for observing the crystallization of pure AMG 517, with clear temperature and relative humidity trends. Isothermal microcalorimetry can also be used to observe crystallization of ASDs of AMG 517 in HPMC-AS and in PVP. Crystallization is much slower for ASDs, resulting in low heat signals. At conditions below the T_g of each ASD, the isothermal microcalorimetry signal is so low that it gets lost in the noise signal. Overall, crystallization of ASDs of AMG 517 in polymer is observed to be faster at higher temperature and humidity conditions.

Crystallization rate constants, calculated using isothermal microcalorimetry crystallization time and % crystallinity from de-convolution of ^{19}F SSNMR measurements, can be used to map the crystallization of AMG 517 ASD system. ^{19}F SSNMR is a powerful tool to quantify the % crystalline AMG 517 in each partially crystallized ASD. Even for crystallizations that are slow and have low heat signal, ^{19}F SSNMR shows some crystallized AMG 517, confirming that the

kinetically stabilized ASD system does undergo a crystallization process, even at conditions well below the T_g. Compared to PVP, HPMC-AS is a better polymer for kinetically stabilizing ASD systems of AMG 517.

Suggestions for Further Study

There are several opportunities for further investigation, including the evaluation of alternative drug and polymer systems for crystallization rate prediction using isothermal microcalorimetry. It appears that AMG 517 is a relatively stable drug and a less stable drug would be expected to crystallize faster with potentially higher heat signal, allowing more straight-forward microcalorimetry analysis. Any number of alternative drugs and alternative polymers could be evaluated. In each case, T_g predictions could be correlated with crystallization stability conditions.

There may be value in determining exactly where the ASD interaction is taking place on the molecules. ^{13}C SSNMR could be used to identify which carbons on the AMG 517 are interacting with the polymer for the phase mixed ASDs. Molecular modeling could be useful to understand the interaction, but is beyond the scope of this work.